4. Results and Discussion

In recent years, nanotechnologies have developed from a multidisciplinary research concept to a primary scientific field. The rapid growth of new technologies has led to the development of new biomimetic materials, nanoscale components, and advanced sensors. In addition to chemical and physical approaches, a new, simple, and cheaper strategy for synthesizing metallic nanoparticles uses biological entities such as bacteria, yeast, fungi, and plants. Most of the research has examined the *ex vivo* synthesis of nanoparticles in plants. It has shown that this method is very inexpensive and therefore can be used as a valuable alternative for large-scale production of metal nanoparticles. Therefore, this research mainly focusses on the simple process that uses aqueous extract from the *Curcuma zanthorrhiza* (CZ) and *Curcuma aromatica* (CA) rhizome for the biosynthesis of silver nanoparticles (AgNPs), characterization of the synthesized nanoparticles, catalytic and pharmaceutical applications of silver nanoparticles. The results obtained are summarized and discussed below.

4.1 Collection of Plant materials

The rhizomes of *Curcuma zanthorrhiza* and *Curcuma aromatica* were collected and multiplied for the preparation of aqueous rhizome extracts for preliminary phytochemical analysis and synthesis of silver nanoparticles (Fig. 4.1).

4.2 Preparation of Rhizome extract

Aqueous rhizome extracts were prepared according to the method described in section 3.2. The colour of the rhizome extracts of CZ and CA were dark yellow and pale yellow respectively. The rhizome extracts were used in the identification of phytochemicals and in the synthesis of silver nanoparticles.

The simple decoction method is widely used for the preparation of aqueous rhizome extracts. The filtrate thus formed is utilized in the identification of the phytochemicals. The plants rich in phytochemicals could be used as a green source for nanoparticle synthesis (Dhamecha, Jalalpure, & Jadhav, 2016).
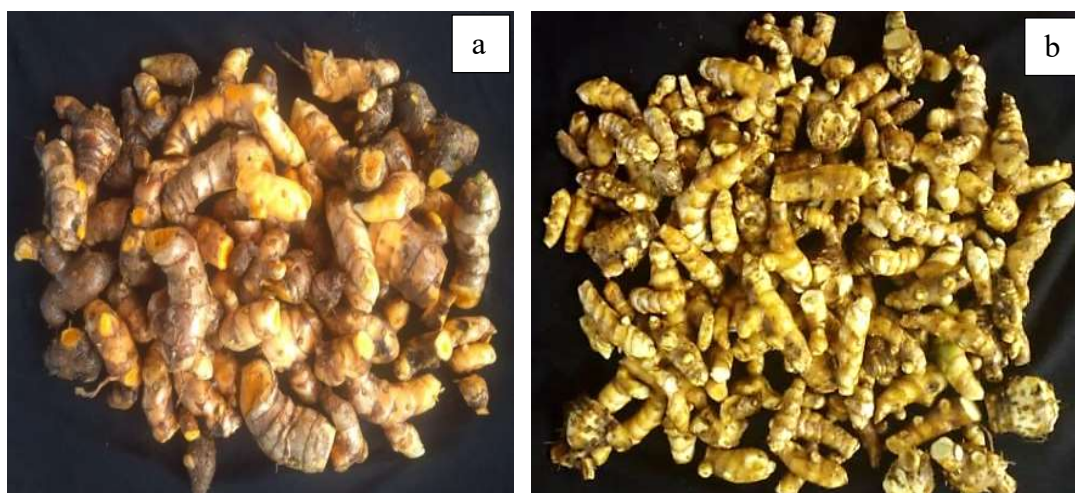

Fig. 4.1 Fresh rhizomes of (a) *Curcuma zanthorrhiza* Roxb. (b) *Curcuma aromatica* Salisb.

4.3 Phytochemical analysis of rhizome extracts

Preliminary qualitative, quantitative and HR-LCMS analysis were done using the aqueous rhizome extract of both *Curcuma zanthorrhiza* and *Curcuma aromatica*. The identification of active biomolecules in the rhizome extract is vital as they are involved in the nanoparticle capping resulting in their catalytic and medicinal application. Hence, the phytochemical analysis was performed in the aqueous rhizome extracts of both the plants and the results are as follows.

4.3.1 Qualitative analysis of Phytoconstituents

Secondary metabolites have been reported to have many biological and therapeutic properties. These compounds find their importance among the scientific community due to their therapeutic performance and low toxicity. Based on the

therapeutic potential of secondary metabolites, the phytochemical characteristics of the *Curcuma zanthorrhiza* and *Curcuma aromatica* rhizome were examined and presented in Table 4.1. Qualitative phytochemical analysis of aqueous extract of the *Curcuma zanthorrhiza* rhizome contained carbohydrates, proteins, terpenoids, flavonoids, alkaloids, coumarins, phenols. Tannins, steroids, glycosides and anthraquinones were absent.

In the aqueous rhizome extract of *Curcuma aromatica*, the phytochemical analysis revealed the presence of carbohydrates, proteins, terpenoids, flavonoids, steroids, alkaloids, coumarins, phenols and saponins while tannins, glycosides and anthraquinones were not present.

The qualitative phytochemical analysis revealed the presence of carbohydrates, free acids and proteins, terpenoids, flavonoids, alkaloids, coumarins, phenols in both *C. aromatica* and *C. zanthorrhiza*. The results summarized in Table 4.1 suggest that both the aqueous rhizome extracts could be used in the synthesis of silver nanoparticles because of the rich antioxidant phytochemicals present in them. In corroboration with our results, the qualitative analysis of CA and CZ by Anjusha and Gangaprasad (Anjusha & Gangaprasad, 2014) have also reported the presence of flavonoids, tannins, saponins, carbohydrates, terpenoids, sterols, protein and phenols in the aqueous extract and the absence of reducing sugars and quinine. Similarly the plant extracts of *Nepenthes khasiana* (Dhamecha *et al*., 2016), *Coriandrum sativum* (P. Sathishkumar *et al*., 2016), *Alternanthera sessilis* (Niraimathi, Sudha, Lavanya, & Brindha, 2013), *Zizipus oeoplia* (Soman & Ray, 2016) have been reported to have rich antioxidant phytochemicals and hence used as source for the synthesis of nanoparticles.

Table 4.1 Qualitative analysis of aqueous rhizome extract of *Curcuma zanthorrhiza* and *Curcuma aromatica*

Sl. No.	Metabolites	*Curcuma zanthorrhiza* rhizome extract	*Curcuma aromatica* rhizome extract
1.	Carbohydrates	+	+
2.	Proteins	+	+
3.	Terpenoids	++	++
4.	Flavanoids	+	+
5.	Steroids	–	+
6.	Alkaloids	+	+
7.	Coumarins	+	+
8.	Phenols	+	+
9.	Saponins	+	+
10.	Tannins	–	–
11.	Glycosides	–	–
12.	Anthraquinones	–	–

"+" indicates presence of the compounds; "++" indicates the high concentration and "-" indicates absence of the compounds

4.3.2 Quantitative analysis – Total phenolic content

The total phenolic content present in the aqueous rhizome extract of both CZ and CA were quantitatively analyzed by Folins'-Ciocalteau Reagent (FCR) Assay. The standard used was gallic acid and the quantity of the total phenolic content expressed as mg / g equivalent gallic acid. Significant amount of total phenol were present in the aqueous rhizome extract of CZ (46.25 ± 0.23 mg / g gallic acid equivalent) and CA (45.64 ± 1.02 mg / g gallic acid equivalent).

One of the important plant components with redox properties are phenolic compounds. The redox properties of the phenolic compounds constitute its antioxidant activity (Aryal *et al*., 2019). The dissolution of the endogenous plant compounds depends on the solvent and the extraction process. Earlier reports have shown that the methanolic extracts due to the presence of hydroxyl groups were rich in phenolic compounds. Total phenolic content of 56.8 ± 5.9 µg GAE / g fresh weight

of *A. sessilis* was reported by Lee *et al*., (Lee, Choo, Watawana, Jayawardena, & Waisundara, 2015) and 851.9 ± 10.698 µg / ml of GAE / g of aqueous extract of *Nepenthes khasiana* was reported by Dhamecha *et al* (Dhamecha *et al*., 2016). However, in comparison to the previous studies, in our study the total phenolic content in aqueous extract was 46.52 ± 0.23 mg / GAE for CZ and 45.64 ± 1.02 mg / GAE for CA. Therefore the observed values further substantiate the use of both CZ and CA as a green source for the synthesis of silver nanoparticles.

4.3.3 Identification of bioactive compounds in CZ and CA rhizome extract by HR LCMS analysis

The bioactive compounds were identified based upon the spectral similarity with the MS library (NIST MS Search 2.0), the Human Metabolome Database and Knapsack family database.

The spectrometric data of the bioactive compounds including retention time, molecular mass, molecular formula, adduct ions formed in the ion source and peak area percentage are listed in Table 4.2. The HR-LCMS analysis revealed the presence of eleven biomolecules in the aqueous rhizome extract of CZ (Fig. 4.2). The bioactive molecules identified by HR-LCMS analysis were norcotinine (peak 1, m/z = 185.0672), N-(1-deoxy -1- fructosyl), valine (peak 2, m/z = 262.1308), ethyl 3 – methyl- 9H- carbazole - 9- carboxylic acid (peak 3, m/z = 276.1463), feruperine (peak 4, m/z = 310.1306), gibberellic acid 19 (peak 5, m/z = 367.1526), harmanine (peak 6, m/z = 181.0779), gibberellic acid 3 (peak 7, m/z = 369.1358), obliquin (peak 8, m/z = 254.0829), pteryxin (peak 9, m/z = 369.1359), glechomafuran (peak 10, m/z = 231.14) and sinapoylspermine (peak 11, 391.2872) which belonged to the organic class of compounds namely, pyridine derivatives, fructose aminoacids, carbozoles,

methoxy phenols, plant hormone, β carboline alkaloids, plant hormone, coumarins, germacrane furano sesquiterpenoids and hydroxycinnamic acid derivatives respectively.

The highest peak was identified to be of harminine, a β carboline alkaloid with a peak area of 35.33 %, followed by obliquin, glechomafuran, ethyl 3 – methyl- 9H- carbazole - 9- carboxylic acid, pteryxin, N-(1-deoxy -1- fructosyl) Valine, gibberellic acid 3, feruperine, sinapoylspermine, gibberellic acid 19 with peak area of 20 %, 8.57 %, 6.78 %, 5.33 %, 3.67 %, 3.44 %, 3.13 %, 1.1 % and 0.77 % respectively. Norcotinine, a pyrimidine derivative was quantified to be the least abundant component present in the aqueous rhizome extract with an intensity of 0.37 %. Major properties of bioactive compounds are given in Table 4.3. Furthermore, the coumarins, obliquin and pteryxin were identified for the first time in the aqueous rhizome extract of *C. zanthorrhiza*.

Table 4.2. Bioactive compounds in the aqueous rhizome extract of *Curcuma zanthorrhiza* identified from the HR-LCMS Chromatogram presented in Fig. 4.2.

Peak No.	Retention time	Molecular mass (g/mol)	m/z	Formula	Adduct	Compound name	Peak Area (%)
1.	0.762	162.0772	185.0672	$C_9H_{10}N_2O$	(M+Na)	Norcotinine (Pyridine derivatives)	0.37
2.	1.147	279.134	262.1308	$C_{11}H_{21}NO_7$	(M+H-H$_2$O)	N-(1-deoxy -1-fructosyl)Valine (Fructose aminoacid)	3.67
3.	1.537	253.1571	276.1463	$C_{16}H_{15}NO_2$	(M+Na)	Ethyl 3 –methyl-9H-carbazole -9-carboxylic acid (Alkaloid)	6.78
4.	1.896	287.1414	310.1306	$C_{17}H_{21}NO_3$	(M+Na)	Feruperine (Methoxyphenols)	3.13
5.	2.997	362.1739	367.1526	$C_{20}H_{26}O_6$	(M+Na-H$_2$O)	Gibberellic acid 19 (Hormone)	0.77
6.	3.227	198.0812	181.0779	$C_{12}H_{10}N_2O$	(M+H-H$_2$O)	Harmanine (Alkaloid)	35.33
7.	8.818	346.1472	369.1358	$C_{19}H_{22}O_6$	M+Na	Gibberellic acid 3 (Hormone)	3.44
8.	11.256	244.0757	245.0829	$C_{14}H_{12}O_4$	M+H	Obliquin (Coumarins)	20.00

Contd.

9.	11.703	386.1393	369.1359	$C_{21}H_{22}O_7$	M+H-H_2O	Pteryxin (Coumarins)	5.33
10.	12.705	248.1433	231.14	$C_{12}H_{20}O_3$	M+H-H_2O	Glechomafuran (Germacrane sesquiterpenoids)	8.57
11.	19.626	408.2905	391.2872	$C_{21}H_{36}N_4O_2$	M++H-H_2O	Sinapoylspermine (Hydroxycinnamic acid derivatives)	1.10

The phytoconstituents were identified based upon spectral similarity with the MS library (NIST MS Search 2.0) and the Human Metabolome Database
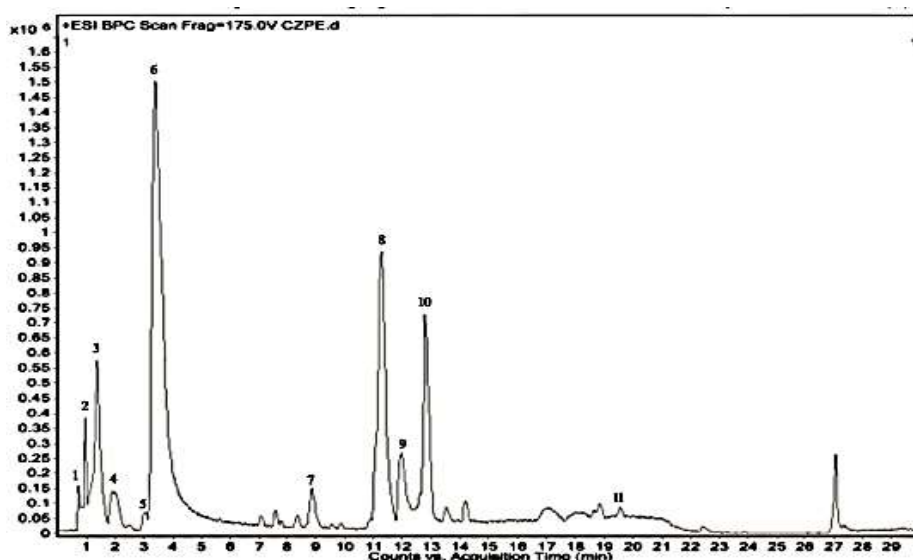
Fig. 4.2 HR-LCMS chromatogram of the aqueous rhizome extract of *C. zanthorrhiza*

Table 4.3 Biological properties of the compounds identified in the rhizome extract of CZ by HR-LCMS

Bioactive Compounds	Properties	References
Norcotinine	Neuropharmalogical property	(Crooks, Li, & Dwoskin, 1997)
Feruperine	Antioxidant activity	(Nakatani, Inatani, Ohta, & Nishioka, 1986)
Harmanine	Insecticidal property	(Almadiy, Nenaah, & Shawer, 2018)
Obliquin	Anti-depressive activity	(Poumale, Hamm, Zang, Shiono, & Kuete, 2013)
Pteryxin	Vasorelaxant, hepatoprotective, treatment of Alzheimer's disease	(Orhan, Senol, Shekfeh, Skalicka-Wozniak, & Banoglu, 2017)
Glechomafuran	Antioxidant, Anticancer activity	(Quassinti *et al*., 2013)
Sinapoylspermine	Anti-inflammatory, Neuroprotective, Antioxidant, Anticancer, Antimicrobial, Cosmetic	(Roumani *et al*., 2020)
Zedorone	Antioxidant, Anticancer, Antimicrobial, Carminative,Analgesic, Insecticide	(Soonwera, Wongnet, & Sittichok, 2018)

Thirteen bioactive compounds were identified in the aqueous rhizome extract of CA using the HR-LCMS analysis (Fig. 4.3). The identified compounds were santonin - sesquiterpenoid (peak 1, m/z = 299.1248), zedoarondiol – terpene (peak 2, m/z = 235.1715), procurcumadiol - sesquiterpenoid (peak 3, m/z = 233.1555), glechomafuran – germacrene sesquiterpenoid (peak 4, m/z = 231.1402), zedoarolide – terpenoid (peak 5, m/z = 265.1456), amiloxate – carboxylic acid cinnamates (peak 6, m/z = 231.1396), zedolactone c – terpenoid (peak 7, m/z = 249.1507), 5 β cyprinosulphate – organic hydroxy compounds (peak 8, m/z = 515.3046), curcumenolactone – sesquiterpenoid (peak 9, m/z = 247.1346), ar- turmenone – sesquiterpenoid (peak 10, m/z = 217.1606), curdione - terpene (peak 11, m/z = 237.1869), costunolide – sesquiterpenoid (peak 12, m/z = 215.1449) and vitamin D3 – steroid (peak 13, m/z = 465.3039). The retention times, molecular mass, molecular formula, adduct ions formed in ion source and peak area percentage of the bioactive molecules of CA is listed in Table 4.4.

Ar- turmenone was identified to be the major compound present in the aqueous rhizome extract of CA with peak area of 29.90 %. The peak area of curdione, glechomafuran, costunolide, 5 β cyprinosulphate, procurcumadiol, amiloxate, santonin, curcumenolactone, zedoarolide, vitamin D3, zedoarondiol, zedolactone c were 14.69 %, 13.20 %, 9.56 %, 3.07 %, 3.36 %, 3.19 %, 1.93 %, 1.54 %, 1.54 %, 1.25 %, 1.01 % and 0.69 % respectively. The bioactive properties of the identified compounds are tabulated (Table 4.5).

The Tables 4.2 and 4.4 establishes the presence of various phytoconstituents like terpenoids, alkaloids, coumarins, carboxylic acid cinnamates, methoxy phenols of CZ and CA determined from the HR-LCMS analysis. The phytoconstituents reported

for *C. aromatica* rhizomes were eucalyptol, linalool, neocurdine, camphor, α terpeniol, germacrone, α vertirenene, androstan – 17 - one, 3 ethyl 3 hydroxy 5 a aromadendrene, camphene 1,8 cineole, boraneol and β elemene. The aqueous rhizome extract of *C. zanthorrhiza* gave characteristic peaks for xanthorrhizol, β curcumene, ar- curcumene, camphor, γ curcumene, γ bisabolene and β farnesene (Rajkumari & Sanatombi, 2018). In consistent with our results the presence of curdione and ar – turmenone was reported for CA by Biren Shah *et al.,* (Shah, Modi, & Bhuva, 2010). The absence of some of the phytoconstituents in the HR-LCMS analysis might be attributed to the difference in the method utilized for the extract preparation.

It was reported that the fractionated extracts of *Cocos nucifera* containing alkaloids, terpenoids, carbohydrates, phenolic compounds, tannins and saponins were used to synthesize nanoparticles (Mariselvam, Ranjitsingh, Thamaraiselvi, & Ignacimuthu, 2019). Another study indicated that the presence of phytochemicals such as tannins, flavonoids and glycosides in *Chrysanthemum indicum* were responsible for the reduction of silver nitrate to silver nanoparticles (Arokiyaraj *et al*., 2017). However, in the present study HR-LCMS analysis revealed the presence of high amounts of terpenoids in the dry extracts of CZ and CA. The high amount of terpenoids along with the other plant metabolites could be the major source for the synthesis of silver nanoparticles. Our results corroborate with that of Magdalena *et al* (Parlinska-Wojtan, Kus-Liskiewicz, Depciuch, & Sadik, 2016), wherein camomile terpenoids were used in the synthesis of silver nanoparticles that also acted as capping and reducing agents.

Table 4.4. Bioactive compunds in the aqueous rhizome extract of *Curcuma aromatica* identified from the HR-LCMS Chromatogram presented in Fig. 4.3.

Peak No.	Retention time	Molecular mass (g / mol)	m/z	Formula	Adduct	Compound name	Peak Area (%)
1.	4.096	246.128	299.1248	$C_{15}H_{18}O_3$	(M+H-H_2O)	Santonin (Sesquiterpenoid)	1.93
2.	5.167	252.1748	235.1715	$C_{15}H_{24}O_3$	(M+H-H_2O)	Zedoarondiol (Terpene)	1.01
3.	5.377, 9.132	250.1587	233.1555	$C_{15}H_{22}O_3$	(M+H-H_2O)	Procurcumadiol (Sesquiterpenoid)	3.36
4.	5.495	248.1433	231.1402	$C_{15}H_{20}O_3$	(M+H-H_2O)	Glechomafuran (Germacrane sesquiterpenoids)	13.20
5.	6.176	282.1488	265.1456	$C_{15}H_{22}O_5$	(M+H-H_2O)	Zedoarolide (Terpenoid)	1.54
6.	6.448	248.1429	231.1396	$C_{15}H_{20}O_3$	(M+H-H_2O)	Amiloxate (carboxylic acid cinnamates)	3.19
7.	8.37	266.154	249.1507	$C_{15}H_{20}O_4$	(M+H-H_2O)	Zedolactone c (Terpenoid)	0.69
8.	8.667	532.3081	515.3046	$C_{27}H_{48}O_8S$	(M+H-H_2O)	5 β cyprinosulphate (Organic hydroxy compounds)	3.36

Contd.

9.	10.076	264.1379	247.1346	$C_{15}H_{20}O_4$	(M+H-H_2O)	Curcumenolactone (Sesquiterpenoid)	1.54
10.	11.111	216.1534	217.1606	$C_{15}H_{20}O$	(M+H)	Ar - turmenone (Sesquiterpenoid)	29.90
11.	11.851, 12.162	236.1796	237.1869	$C_{15}H_{24}O_2$	(M+H)	Curdione (Terpene)	14.69
12.	12.778	232.1482	215.1449	$C_{15}H_{20}O_2$	(M+H-H_2O)	Costunolide (Sesquiterpenoid)	9.56
13.	15.72	464.2969	465.3039	$C_{27}H_{44}O_4S$	(M+H)	Vitamin D3 (Steroid)	1.25

The phytoconstituents were identified based upon spectral similarity with the MS library (NIST MS Search 2.0) and the Human Metabolome Database
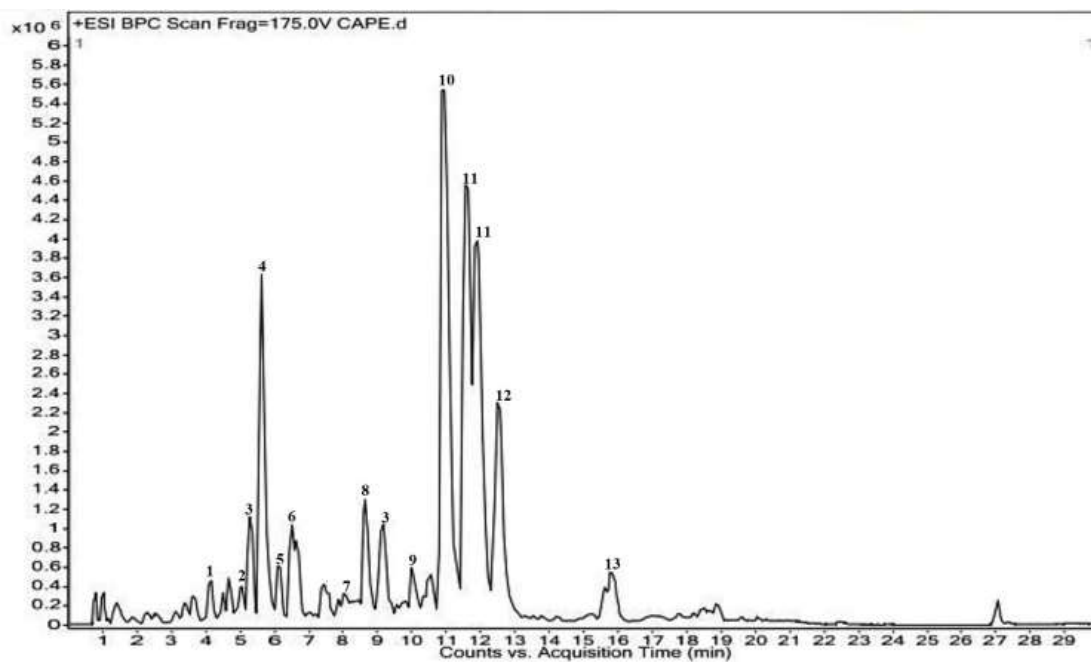
Fig. 4.3 HR-LCMS chromatogram of the aqueous rhizome extract of *C. aromatica*

Table 4.5 Biological properties of the compounds identified in the rhizome extract of CA by HR-LCMS

Bioactive Compounds	Properties	References
Santonin	Antipyretic, antiparasitic, antibacterial activity	(Prasad, Kambala, & Naidu, 2013)
Zedoarondiol	Anti- inflammatory, antioxidants	(Sulaiman *et al*., 2015)
Procurcumadiol	Antioxidant	(Sankar *et al*., 2017)
Glechomafuran	Antioxidant, Anticancer activity	(Al-Saif, Awad, & Siddiqui, 2018)
Zedoarolide	Antioxidant , anti-inflammatory	(Nguyen *et al*., 2019)
Amiloxate	Anti-inflammatory	(Shameli *et al*., 2014)
Zedolactone c	Anti-inflammatory	(Balachandar *et al*., 2019)
5 β cyprinosulphate	Anti-inflammatory	(Sathishkumar, Sneha, & Yun, 2010)

Contd.

Curcumenolactone	Anti-inflammatory	(Sathishkumar *et al*., 2010),(Mohammed, Lawrance, Sampath, Sunderam, & Madhavan, 2021)
Ar - turmenone	Antivenom	(Venkatadri *et al*., 2020)
Curdione	Neuroprotectant	(Sankar *et al*., 2014)
Costunolide	Anticancer	(Sathishkumar *et al*., 2010)(Kora & Sashidhar, 2018)
Vitamin D3	Immunomodulator	(Sharma *et al*., 2014)

4.4 Synthesis and Characterization of silver nanoparticles

Nanoparticles find major application in medicine and also in the environmental remediation processes. Physical, chemical and biological methods are involved in the synthesis of nanoparticles. Out of the various methods involved, synthesis of metal nanoparticles using biological materials has gained importance due to their cost effectiveness and eco-friendly nature. Characterization plays a major role after the synthesis, because the application of the synthesized nanoparticles relies on the properties of the synthesized nanoparticles.

4.4.1 Synthesis of silver nanoparticles (AgNPs) using rhizome extracts

The addition of aqueous rhizome extract of CZ to 1 mM silver nitrate solution caused an immediate change in the color of the solution. The color change from yellow to light brown and to dark brown was observed as the reaction progressed under sunlight for 1 h (Fig. 4.4). The color change indicated the formation of silver nanoparticles at pH = 5.65.

Upon addition of the aqueous rhizome extract of CA to silver nitrate solution (1mM) an immediate change in the colour of reaction mixture was observed. The bioreduction of silver nitrate to silver nanoparticles was inferred from this colour change from pale yellow to reddish-brown after 30 min irradiation under sunlight, at pH 5.65 (Fig.4.5). The colour change also attributes to the excitation of surface vibration plasmon in the silver nanoparticles.
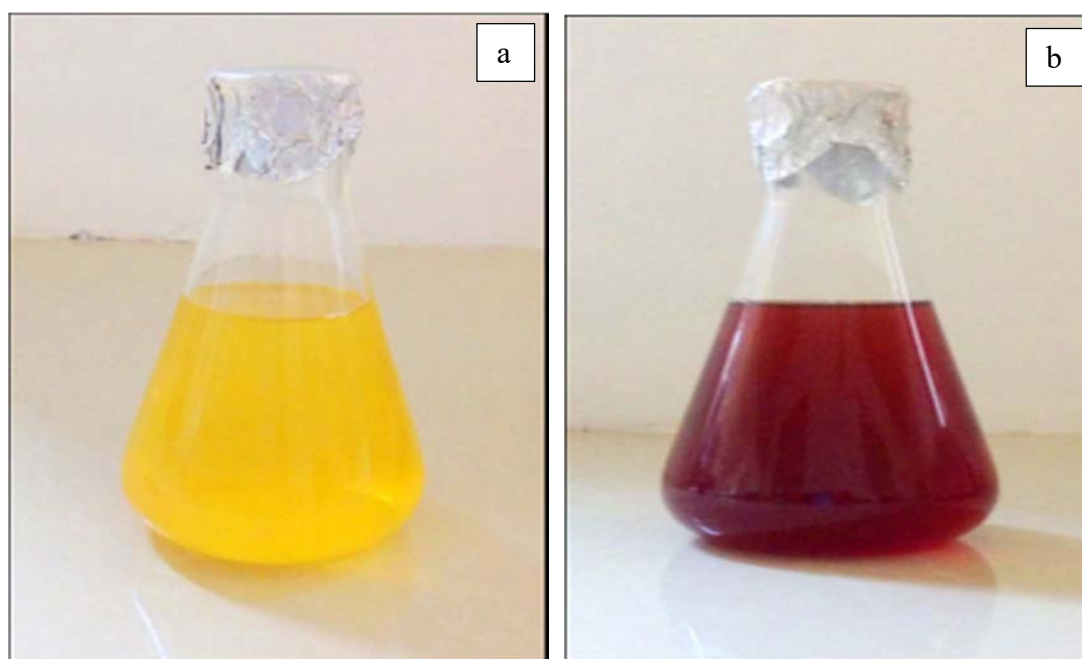

Fig. 4.4 Color change in reaction mixture from yellow to reddish brown indicated formation of AgNPs (a) aqueous rhizome extract (yellow); (b) biosynthesized CZAgNP suspension (reddish brown)
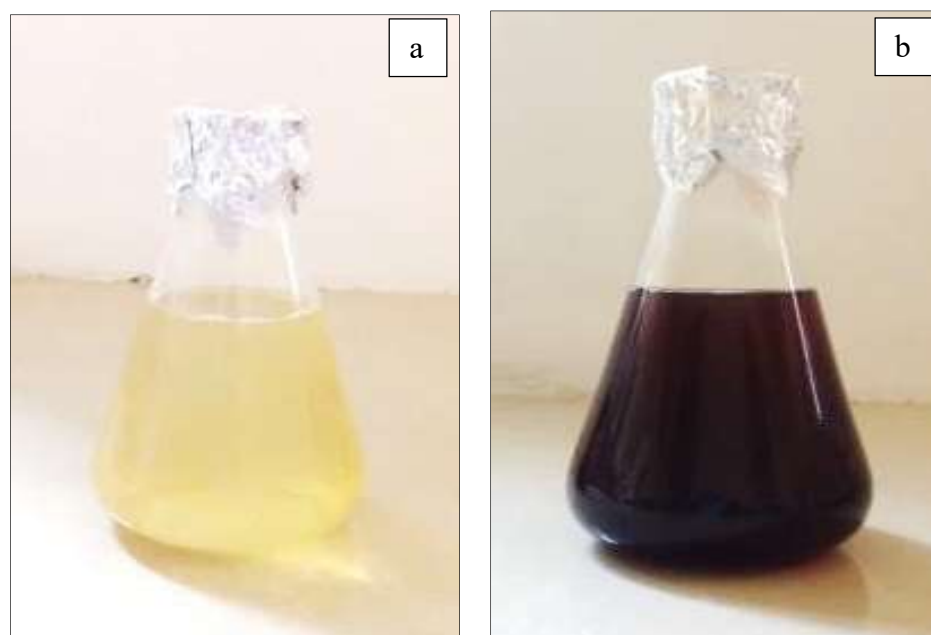
Fig. 4.5 Color change in reaction mixture from yellow to reddish brown indicated formation of AgNPs (a) aqueous rhizome extract (pale yellow); (b) biosynthesized CAAgNP suspension (reddish brown)

A preview of the literature suggested that the nanoparticles were often formed depending upon the reaction conditions. Generally, the silver nanoparticle formation required incubation of the reaction mixture at room temperature and thermal decomposition for 15 h, 24 h and 180 min respectively (Hosseinpour-mashkani & Ramezani, 2014; Muthukrishnan, Vellingiri, & Murugesan, 2018) (Prakash, Gnanaprakasam, Emmanuel, Arokiyaraj, & Saravanan, 2013). Nevertheless in the current study, the formation of silver nanoparticles using the aqueous rhizome extracts of CZ and CA was observed in 60 min, which indicated the rapid and facile mode of synthesis.

4.4.2 Characterization of silver nanoparticles

4.4.2.1 UV-Visible Spectroscopy

The formation of silver nanoparticles was primarily analyzed by UV-Visible spectroscopy. From the UV-Visible spectrum, the Surface Plasmon Resonance (SPR)

peak of the silver nanoparticles synthesized using the aqueous rhizome extract of CZ was observed at 416 nm (Fig. 4.6a). A maximum absorption at 413.5 nm was observed in the UV-Visible spectrum for the reaction mixture containing CA rhizome extract and silver nitrate (Fig. 4.6b). Both the spectra had a single, broad SPR band revealing the spherical shape of synthesized silver nanoparticles. The broadening of the peak also indicated the poly disperse nature of the silver nanoparticles.
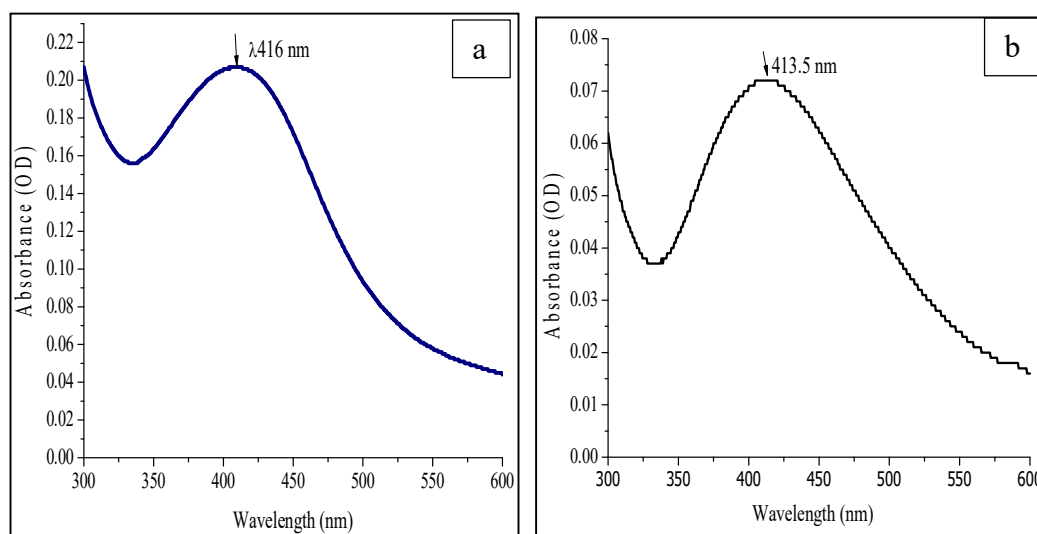

Fig 4.6 The UV–Vis absorption spectrum of (a) CZAgNPs, (b) CAAgNPs

In general, UV-Visible spectroscopy is a technique widely used in the preliminary identification of the synthesized nanoparticles. In the present study the yellow (CZ) and pale yellow (CA) coloured rhizome extracts transformed into dark brown colour upon the addition of silver nitrate followed by exposure to sunlight. The absorption spectra of the solution upon irradiation with sunlight for 60 min gave absorption peak at 416 nm (CZ) and 413.5 nm (CA). According to Mie's theory it is reported that the spherical nanoparticles have a single surface plasmon resonance (SPR) band. From the UV-Visible spectrum it can be inferred that the synthesized silver nanoparticles were spherical in shape due to the formation of single SPR band (Sasidharan, Namitha, Johnson, Jose, & Mathew, 2020)(Ojha, Sett, & Bora, 2017).

Moreover, the brown colour of the reaction mixture resulted due to the interaction of electromagnetic field with free conduction electrons (Kanagamani, Muthukrishnan, Ilayaraja, Shankar, & Kathiresan, 2018). The broadening of the peak could be attributed to the formation of polydispersed nanoparticles (Banerjee, Satapathy, Mukhopahayay, & Das, 2014).

4.4.2.2 Fourier Transform Infrared Spectroscopy (FTIR)

FTIR analysis was performed to identify the various functional groups of plant extract attached to the silver nanoparticles which were responsible for the synthesis and stabilization of the nanoparticles. The FTIR spectra of both the plant rhizome extract and the CZAgNPs are displayed in Fig. 4.7a. The IR spectrum of the plant rhizome extract showed absorption bands at 3467.55 cm^{-1}, 2075.13 cm^{-1}, 1643.13 cm^{-1}, 1074.20 cm^{-1} and 557.25 cm^{-1}. These bands could be assigned to phenolic OH group, $C = O$ stretching vibrations, NH bond of amine group, CO stretching, and CH bending of alkynes respectively. The characteristic absorption bands of CZAgNPs were observed at 3448.27 cm^{-1}, 2057.78 cm^{-1}, 1637.35 cm^{-1}, 1049.14 cm^{-1} and 541.92 cm^{-1}. The shift observed in the absorption bands of the CZAgNPs from 3467.55 cm^{-1} to 3448.27 cm^{-1}, 2075.13 cm^{-1} to 2057.78 cm^{-1}, 1643.13 cm^{-1} to 1637.35 cm^{-1}, 1074.20 cm^{-1} to 1049.14 cm^{-1} and 557.25 cm^{-1} to 541.92 cm^{-1} indicated the involvement of hydroxyl groups, carboxyl amines, amino acid residues and alkyne derivatives which corresponds to carbohydrates, proteins and phenols respectively.

The FTIR spectroscopic peaks showed the active functional groups in the rhizome extract of CA. Prominent peaks were observed at frequencies 3469.58 cm^{-1}, 2074.60 cm^{-1}, 1639.05 cm^{-1}, 1322.25 cm^{-1} and 557.65 cm^{-1} for the aqueous rhizome of CA. The characteristic absorption bands with prominent frequencies were observed

for CAAgNPs at 3437.25 cm^{-1}, 2046.11 cm^{-1}, 1638.68 cm^{-1}, 1456.03 cm^{-1}, and 531.63 cm^{-1} (Fig 4.7b). The spectrum showed the intense and broad absorption peak at 3437.25 cm^{-1} denoting N-H stretching. A peak at 2046.11 cm^{-1} represents C $=$ O stretching vibrations. A strong and sharp absorption band at 1638.68 cm^{-1} can be assigned to the stretching vibration of (NH) C=O group. Furthermore, the peaks at 1456.03 cm^{-1} and 531.63 cm^{-1} indicated the C=C due to aromatic compound in plant extract and C-Br stretching respectively.

From the IR spectrum the role of secondary metabolites involved in the reduction of silver nitrate to silver nanoparticles was ascertained. Similar variations in the peak position of the hydroxyl and other groups have been reported in the synthesis silver nanoparticles using gum kodangu (Vinod, Saravanan, Sreedhar, Devi, & Sashidhar, 2011). The amide linkage of proteins form a coat over the silver nanoparticles, stabilizing them in the aqueous medium (Uddin, Siddique, Rahman, Ullah, & Khan, 2020). It is known that the protein can bind to nanoparticle through cysteine residue or free amine groups in the protein (Arulkumar & Sabesan, 2010). Hence the amide linkage brings about the stability of the synthesized silver nanoparticles (Uddin *et al*., 2020). Therefore the capping of the active molecules on to the synthesized nanoparticles not only masks the extreme toxicity shown by the synthetic nanoparticles but also enhances the synergetic activity of plant metabolites and nanoparticles.
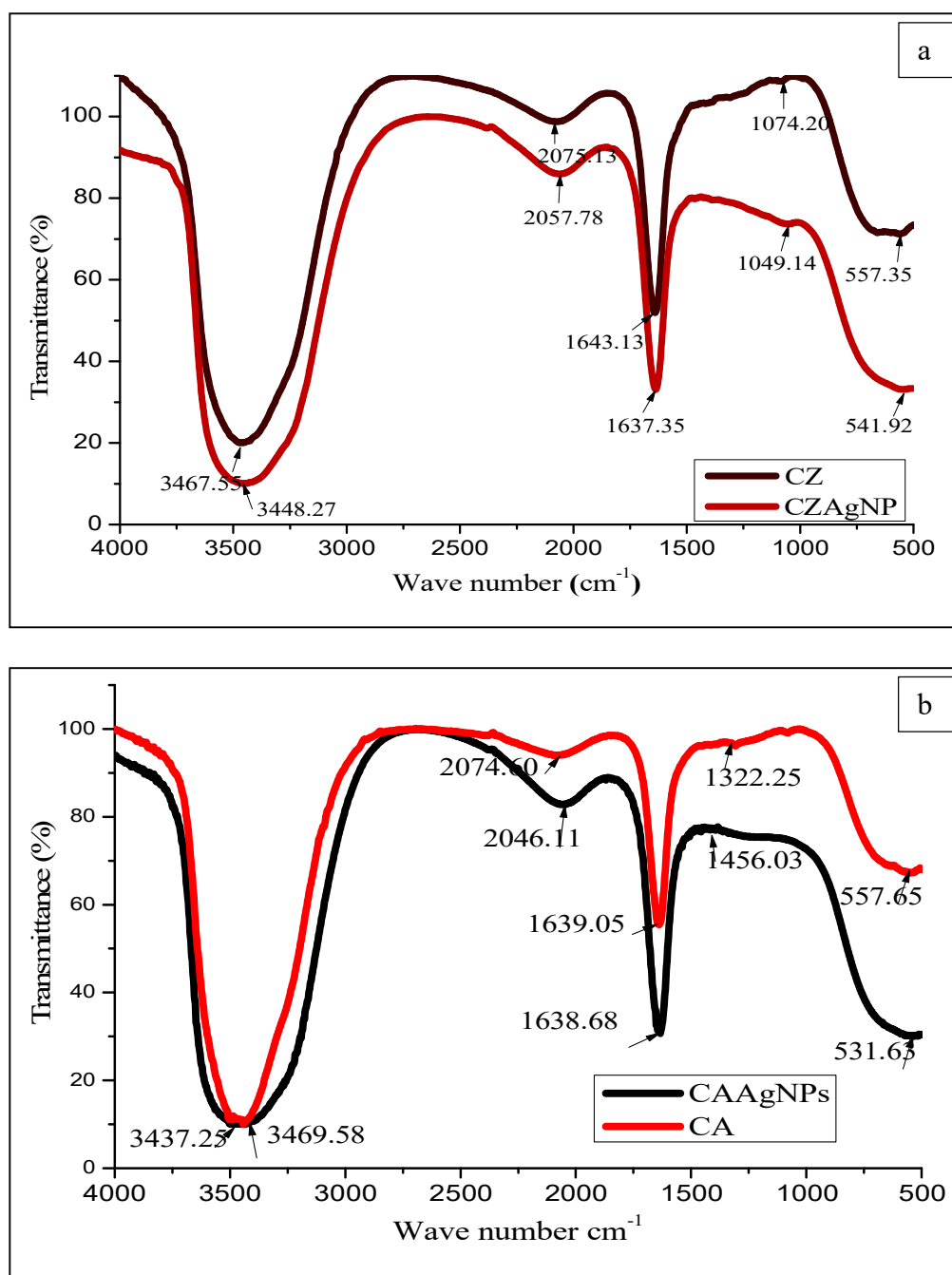
Fig 4.7 The FTIR spectrum of (a) CZAgNPs, (b) CAAgNPs

4.4.2.3 Powder X-Ray Diffraction Studies (PXRD)

The PXRD technique was used to determine and confirm the crystalline structure of synthesized silver nanoparticles. The PXRD pattern of CZAgNPs is depicted in Fig. 4.8a. The well-defined characteristic Bragg's reflection peaks of face centered cubic structure of the metallic silver were observed at 2θ values 38.14°,

46.19°, 64.53° and 77.44° corresponding to the Miller Indices of (111), (200), (222) and (311) planes respectively. The obtained results were found to be in good agreement with JCPDS No. 00-004-0783 indicating the formation of face centred cubic silver. In contrast to the other planes, the intense peak at (111) plane could specify the direction of growth of the synthesized silver nanoparticles. The crystallite size of the silver nanoparticles was determined using Scherrer equation and the average crystallite size of the CZAgNPs was found to be 17.278 nm. In addition, four weak peaks corresponding to the silver oxide nanoparticles were observed at 32.23°, 46.10°, 54.57° and 57.39° (JCPDS No. 76-1393). Another peak at 27.82° could be correlated to the silver chloride nanoparticle (JCPDS No. 31-1238).

Well defined characteristic diffraction peaks at 38.02°, 46.151°, 67.38° and 76.64° corresponding to (111), (200), (222) and (311) planes respectively were identified, attributing to face centred (fcc) crystal structure of metallic AgNPs, according to standard JCPDS file No. 00-004-0783. Additionally, two peaks were observed at 32.133°, 54.71° corresponding to the silver oxide nanoparticles (JCPDS No. 76-1393). The average crystallite size of the CAAgNPs was calculated using the Scherrer equation and was found to be 37.59 nm (Fig. 4.8b).

The obtained results agrees with the earlier reports of (Alsammarraie, Wang, Zhou, Mustapha, & Lin, 2018; Nyabola, Kareru, Madivoli, Wanakai, & Maina, 2020; Velayutham, Ramanibai, & Umadevi, 2016). The pattern of AgNPs synthesized by (S. P. Singh, Mishra, Shyanti, Singh, & Acharya, 2020) coincides with the results of the as-synthesized AgNPs using CZ and CA. It also indicated that the broadening of the Bragg's peak around the bases are due to the formation of small sized silver nanoparticles (Smitha, Philip, & Gopchandran, 2009). The XRD pattern of both

CZAgNPs and CAAgNPs confirm that the (111) lattice plane is the preferred orientation of the synthesized silver nanoparticles. These results highlight their antibacterial activity (Kora, Sashidhar, & Arunachalam, 2012).
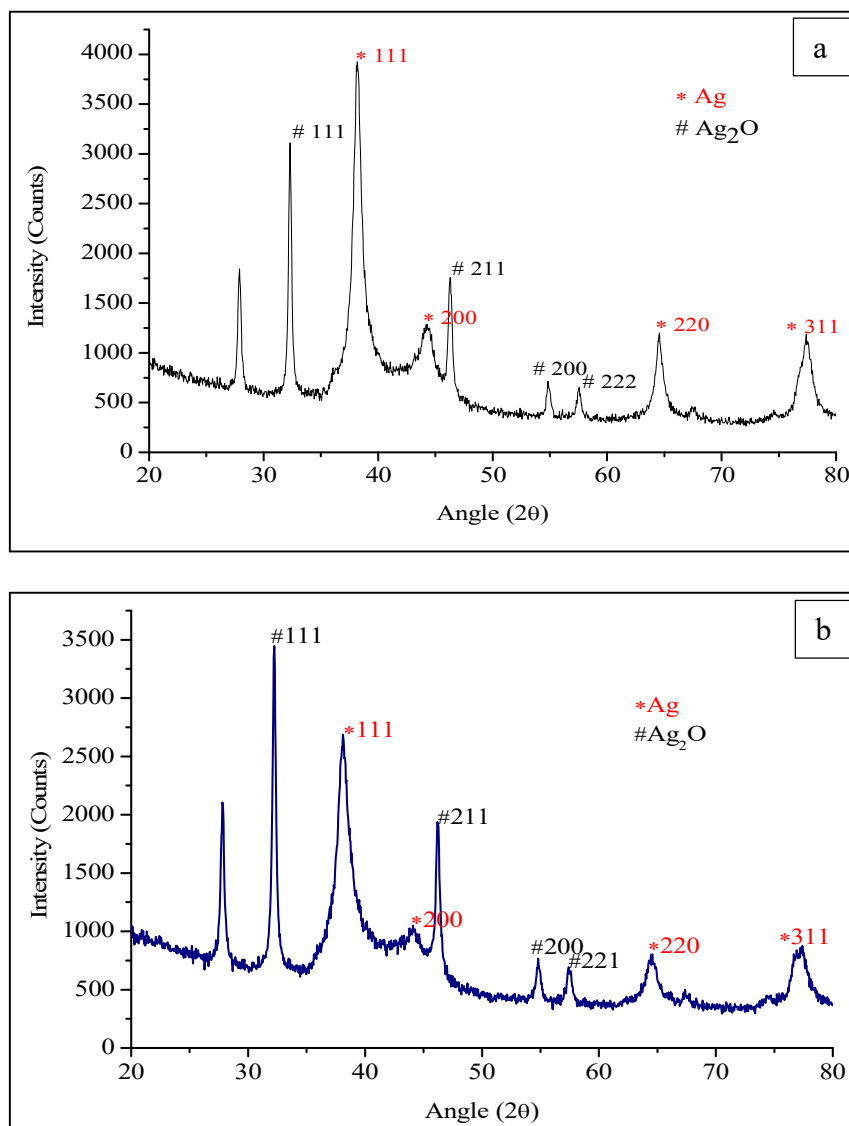
Fig 4.8 The PXRD spectrum of (a) CZAgNPs, (b) CAAgNPs

4.4.2.4 High Resolution Transmission Electron Microscopy (HR TEM)

The size and morphology of the as-synthesized nanoparticles were determined from HR- TEM images. The HR-TEM micrographs revealed the spherical nature of the biosynthesized CZAgNPs. The images obtained were in agreement with the UV data. The SAED pattern with bright circular spots indicated (111), (211), (220) and

(311) planes of face centered cubic (fcc) silver. The bright spots revealed the polycrystalline nature of nanoparticles, which was consistent with the XRD results obtained (Fig. 4.9a, 4.9b). The d spacing value of 0.2359 nm observed is in agreement with the (111) lattice spacing of fcc silver (d_{111}= 0.24) (Kora & Sashidhar, 2018). The size of spherical CZAgNPs had diameter ranging 17.98 nm to 46.73 nm.
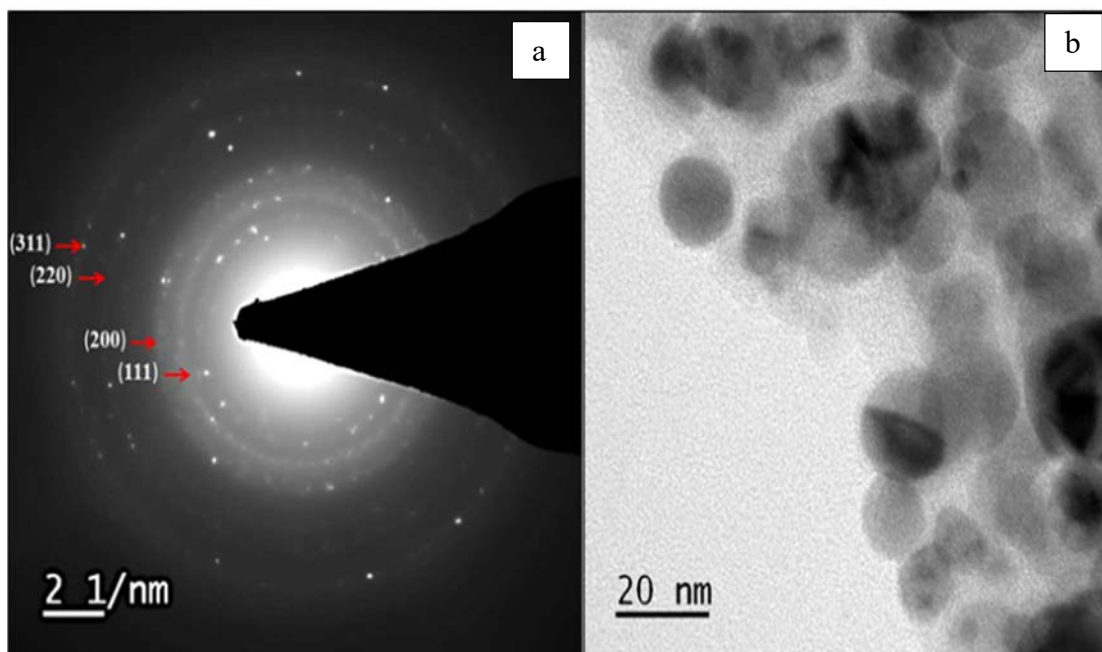

Fig 4.9 (a) SAED pattern of CZAgNPs, (b) HR TEM micrograph of CZAgNPs

The surface morphology of CAAgNPs was also of spherical nature as seen in the TEM micrographs. The SAED pattern with bright circular spots indicated the polycrystalline nature of nanoparticles. The HR-TEM SAED pattern indicated (111), (200), (211) and (222) planes of fcc silver. The HR TEM micrographs confirmed that the synthesized CAAgNPs were spherical with a diameter ranging from 16.73 nm to 39.2 nm (Fig 4.9c, 4.9d). The d spacing value of 0.278 nm observed for CAAgNPs is in agreement with the (111) lattice spacing of fcc silver (d_{111}= 0.24).
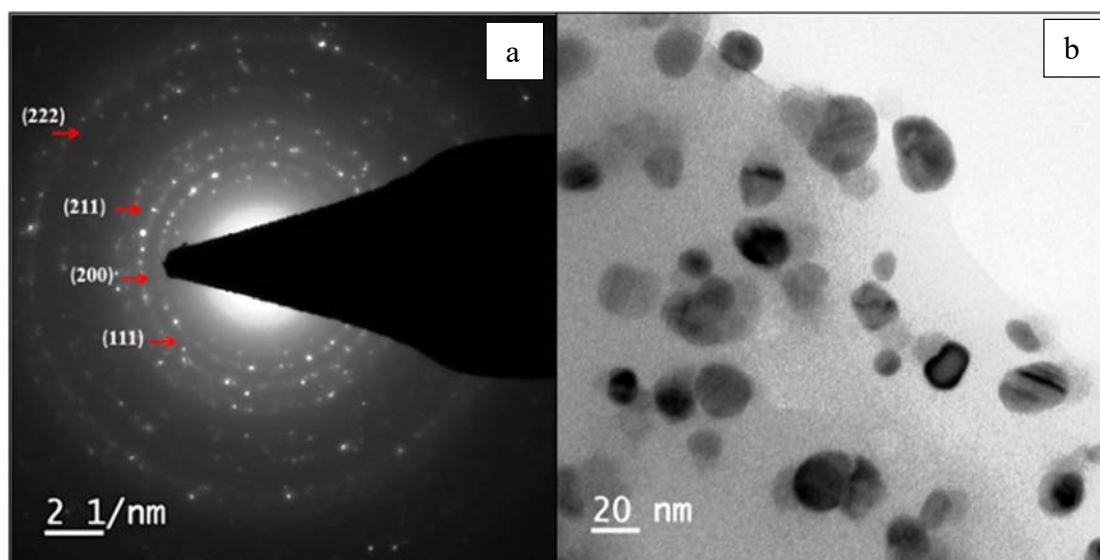
Fig 4.9 (c) SAED pattern of CAAgNPs, (d) HR TEM image of CAAgNPs

These studies closely resemble to the previously biosynthesized silver nanoparticles (Kora & Sashidhar, 2018; Lee & Nagajyothi, 2011; Singh *et al*., 2020). The d spacing value of 0.236 nm for CZAgNPs and 0.278 nm for CAAgNPs closely resemble the d spacing value of 0.235 nm for silver nanoparticles synthesized by Soman and Ray (Soman & Ray, 2016). The small size obtained for the synthesized silver nanoparticles might be due to the suitable reaction conditions employed in the study. However, the varied size of the synthesized AgNPs could be corroborated to the presence of more than one reducing agent in CZ and CA (Seifipour, Nozari, & Pishkar, 2020).

4.4.2.5 Field Emission Scanning Electron Microscopy (FESEM) – Energy Dispersive Absorption X-rays (EDAX)

FESEM-EDAX was carried out to understand the topology and elemental composition of the synthesized silver nanoparticles. The FESEM micrographs of silver nanoparticles synthesized from the aqueous rhizome extracts of CZ and CA revealed the spherical nature of the synthesized silver nanoparticles. The CZAgNPs

and CAAgNPs were found to be scattered in the FESEM micrograph with size ranging from 10 nm to 50 nm and 30 nm to 44 nm respectively (Fig. 4.10a, 4.10b). The larger size shown for CAAgNPs might be due to the clumping of the nanoparticles.
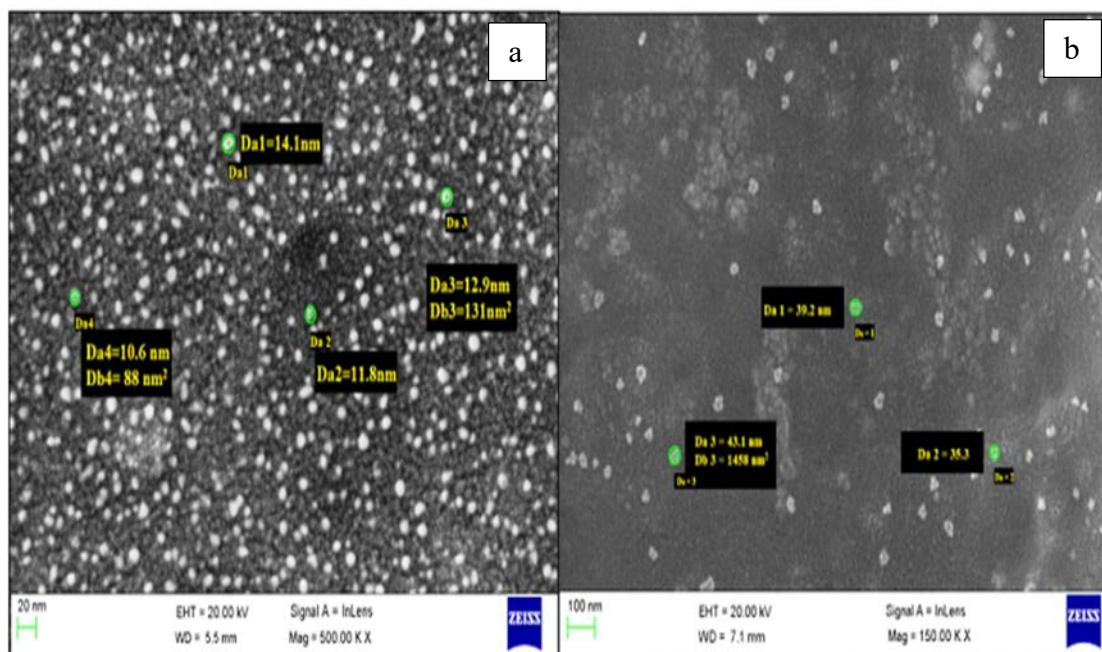

Fig 4.10 FESEM image of (a) CZAgNPs, (b) CAAgNPs

EDAX attached to FESEM assists in finding out the elemental composition of the synthesized nanoparticles (Fig. 4.10c, 4.10d). The EDAX spectrum of both CZAgNPs and CAAgNPs displayed the presence of carbon, oxygen, silicon, chlorine and silver. A weight percentage of 64.24 % silver and 60.46 % silver were obtained for CZAgNPs and CAAgNPs respectively (Table 4.6). The absence of elemental nitrogen confirms the reduction of silver nitrate to silver nanoparticles. The presence of sharp and intense band peak at 3 keV is typical of the existence of metallic silver. Presence of weak signals for carbon in the spectrum might be due to the biomolecules of rhizome extracts that had been related with the synthesis of CZAgNPs. Trace amount of silicon could be due to the impurities while taking micrographs.
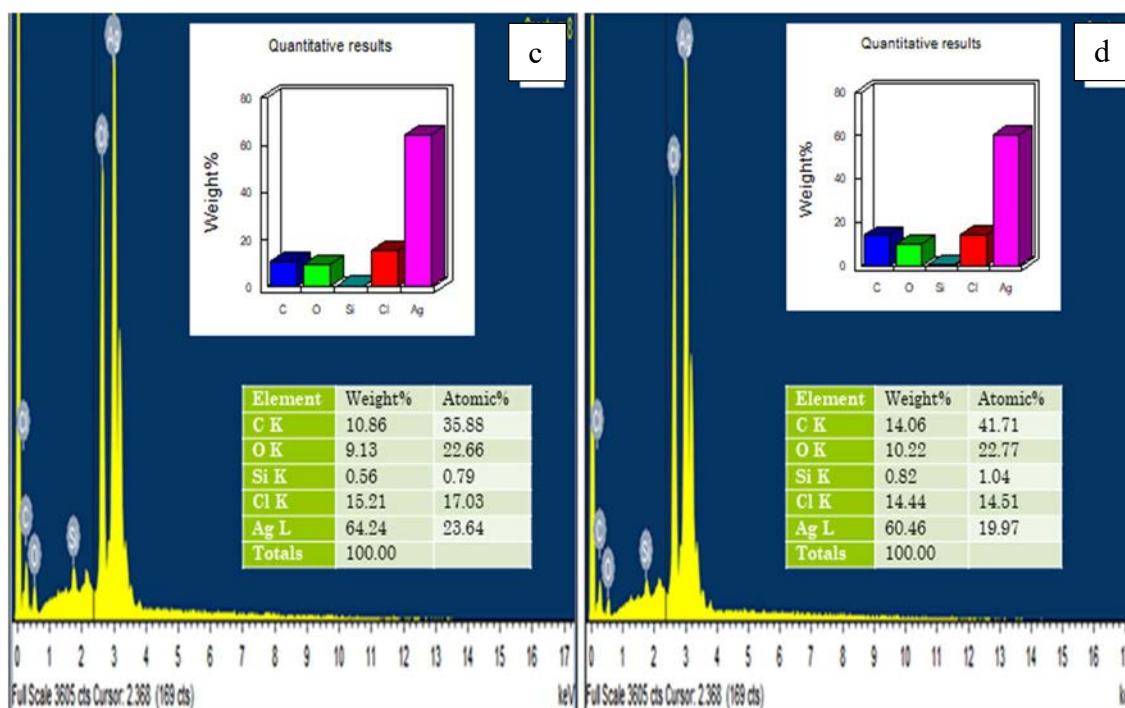
Fig 4.10 EDAX image of (c) CZAgNPs, (d) CAAgNPs

The increase in size of the synthesized silver nanoparticles might be due to the agglomeration. The existence of aggregates could relate to the capping of phytochemicals on to the synthesized silver nanoparticles (Nyabola *et al*., 2020). The EDAX analysis is used to confirm the composition of elements in the synthesized nanoparticles (Kumar *et al*., 2020; Shwetha, Latha, Rajith Kumar, Kiran, & Betageri, 2020). The typical absorption peak at 3 keV shown by the metallic silver nanoparticles is due to the surface plasmon resonance (Jagtap & Bapat, 2013). Similar results with typical characteristic feature showing strong signals for the metallic silver were obtained earlier using Eucalyptus wood (Shivakumar *et al*., 2017), *Bacillus flexus* (Priyadarshini, Gopinath, Meera Priyadharsshini, MubarakAli, & Velusamy, 2013), *Dioscorea alata* (Pugazhendhi, Sathya, Palanisamy, & Gopalakrishnan, 2016).

Table 4.6. Elemental analysis of CZAgNPs and CAAgNPs

Elements	CZAgNPs		CAAgNPs	
	Weight %	Atomic %	Weight %	Atomic %
C K	10.86	35.88	14.06	41.71
O K	9.13	22.66	10.22	22.77
Si K	0.56	0.79	0.82	1.04
Cl K	15.21	17.03	14.44	14.51
Ag L	64.24	23.64	60.46	19.97
Total	100.00		100.00	

4.4.2.6 Dynamic Light Scattering Analysis (DLS)

The DLS analysis was done to measure the hydrodynamic particle size of the synthesized silver nanoparticles. The results obtained for CZAgNPs and CAAgNPs are shown in Fig. 4.11a, 4.11b. The size distribution of CZAgNPs ranged from 20 nm to 145 nm whereas, the size distribution of CAAgNPs ranged from 50 nm to 200 nm. The Z-average for CZAgNPs and CAAgNPs is 111.2 nm and 124.5 nm respectively with a polydispersity index of 0.348. The size of the silver nanoparticles obtained from DLS is larger compared to the electron microscopic analysis. This difference in the size of the synthesized silver nanoparticles might be attributed to the influence of Brownian motion. Moreover, this disparity in size could also be possible due to the capping of plant derived biomolecules and adsorption of water on to the as-synthesized silver nanoparticles.
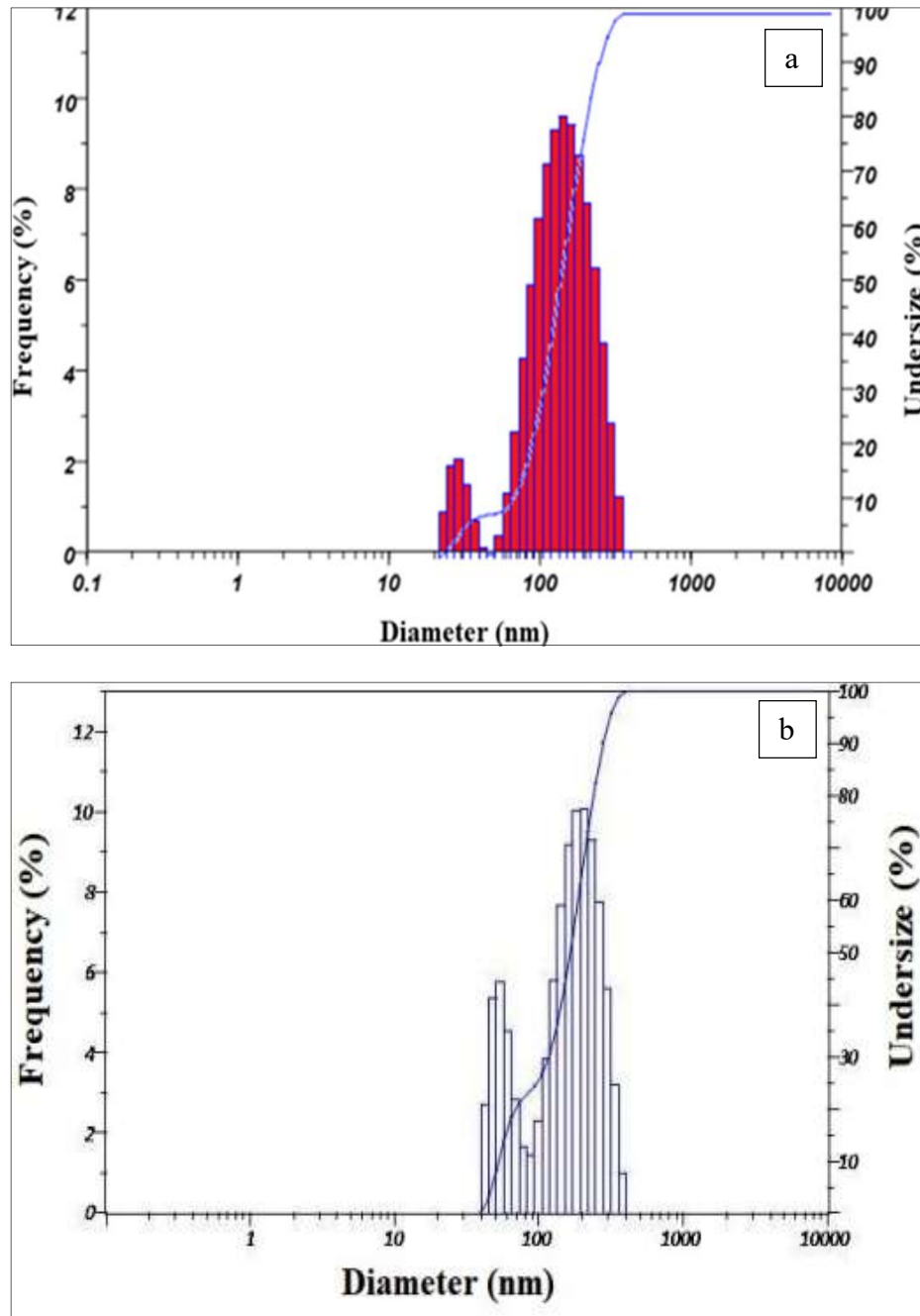
Fig 4.11 DLS image of (a) CZAgNPs, (b) CAAgNPs

The hydrodynamic diameter implies the diameter of the particle along with the ions or molecules attached to the surface and moves with the solution (Madivoli *et al.*, 2020). The measurement of nanoparticles size distribution in the range of 2-500 nm could be measured using DLS (Ghojavand, Madani, & Karimi, 2020; Nyabola *et al.*, 2020). The large size of the particles might also be due to the natural nucleation of

small particles. Due to Ostwald ripening process the small particles might further grow into larger particles with low surface energy (Soman & Ray, 2016).

4.4.2.7 Brunauer Emmett Teller (BET) Surface Analysis

The specific surface area of the synthesized silver nanoparticles was analyzed using BET surface analyzer. The Nitrogen adsorption - desorption isotherm of CZAgNPs and CAAgNPs were measured using volumetric gas adsorption analyzer. The Nitrogen sorption isotherms of CZAgNPs and CAAgNPs are depicted in Fig. 4.12a, 4.12b. The isotherms revealed that the synthesized silver nanoparticles present typical IV adsorption. It is evident from the figure, at relatively low pressure, the isotherm are flat, which describes the adsorption of CZAgNPs and CAAgNPs mostly occurs in the mesopores. Due to the capillary agglomeration phenomenon, a rapid increase in isotherms and formation of lag loop at relatively high pressure is noted (Wei *et al*., 2009).

From the multipoint BET equation, the calculated specific surface area of CZAgNPs is 2.683 m^2 / g and monolayer adsorption volume is 0.614cm^3 / g (Fig. 4.12c). For the CAAgNPs the calculated surface area is 8.9081 m^2 / g and monolayer adsorption volume is 0.2047 cm^3 / g (Fig. 4.12d). The cumulative pore volume and pore diameter were estimated from the BJH size distribution. The total pore volume is 2.634 cm^3 and 3.998 cm^3 for CZAgNPs and CAAgNPs respectively. A cumulative pore diameter of 2.43 nm was observed for both CZAgNPs and CAAgNPs. These results ascertained that the as-synthesized silver nanoparticles are porous with mesoporous nature.
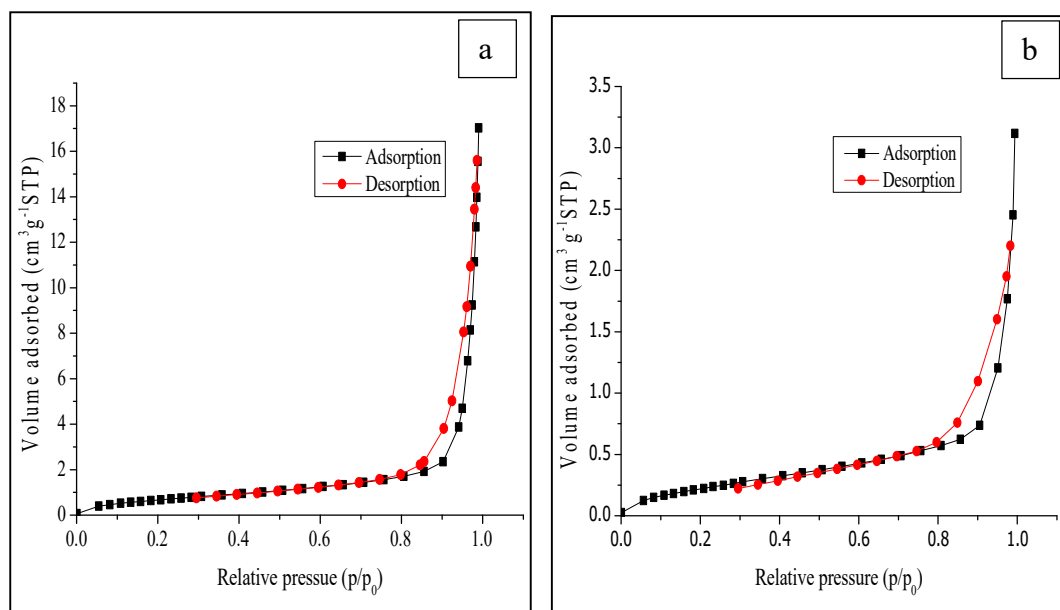
Fig 4.12 Nitrogen sorption isotherms of (a) CZAgNPs and (b) CAAgNPs
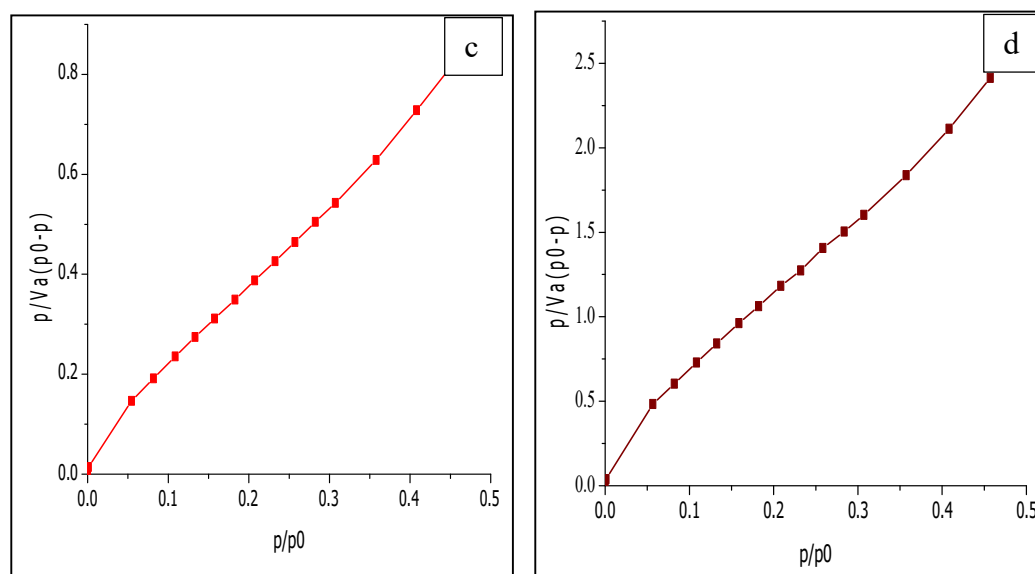
Fig.4.12 BET plots of (c) CZAgNPs and (d) CAAgNPs

4.4.2.8 High Resolution Liquid Chromatography Mass Spectroscopy (HR LCMS)

The presence of six bioactive molecules was ascertained in the CZAgNPs aqueous suspensions using the HR-LCMS analysis (Fig. 4.13a). The observed compounds were comparable with the HR-LCMS data of the aqueous rhizome extract (Fig. 4.2). The bioactive molecules bound to CZAgNPs were zedorone (peak 2, m/z = 229.1244), glechomafuran (peak 4, m/z = 231.1398) which belonged to germacrene

sesquiterpenoids, an aminoalcohol dihydrosphingosine (peak 5, m/z = 284.2973), two lipid molecules namely palmitoyl glycerol (1-hexadecanoyl – sn - glycerol) (peak 3, m/z = 313.2763), stearoyl glycerol (1- octadecanoyl – rac - glycerol) (peak 6, m/z = 341.3073) and tripeptide Val- His- Arg (peak 1, m/z = 415.217) and were quantified to 15.04 %, 8.79 %, 8.17 %, 10.55 %, 14.28 % and 3.51 % respectively. The retention time, adduct ions formed in ion source, molecular mass, molecular formula and peak area percentage of the bioactive molecules are listed in Table 4.7.

Table 4.7. Bioactive macromolecules coated on CZAgNPs identified from the HR-LCMS Chromatogram presented in Fig. 4.13 a.

Peak No.	Retention time	Molecular mass (g/mol)	m/z	Formula	Adduct	Compound name	Peak Area (%)
1.	11.8	410.236	415.217	$C_{17}H_{30}N_8O_4$	(M+Na-H_2O)	Val- His- Arg (tripeptide)	3.51
2.	12.245	246.129	229.124	$C_{15}H_{18}O_3$	(M+H-H_2O)	Zedorone (Germacrane sesquiterpenoids)	15.04
3.	17.332	330.279	313.276	$C_{19}H_{38}O_4$	(M+H-H_2O)	1-hexadecanoyl – sn-glycerol	10.55
4.	17.734	248.143	248.297	$C_{15}H_{20}O_3$	(M+H-H_2O)	Glechomafuran (Germacrane sesquiterpenoids)	8.79
5.	18.641	301.300	284.297	$C_{18}H_{39}NO_2$	(M+H-H_2O)	Dihydrosphingosine (aminoalcohol)	8.17
6.	18.82	358.310	341.307	$C_{21}H_{42}O_4$	(M+H-H_2O)	1- octadecanoyl – rac-glycerol	14.28

The phytoconstituents were identified based upon spectral similarity with the MS library (NIST MS Search 2.0) and the Human Metabolome Database
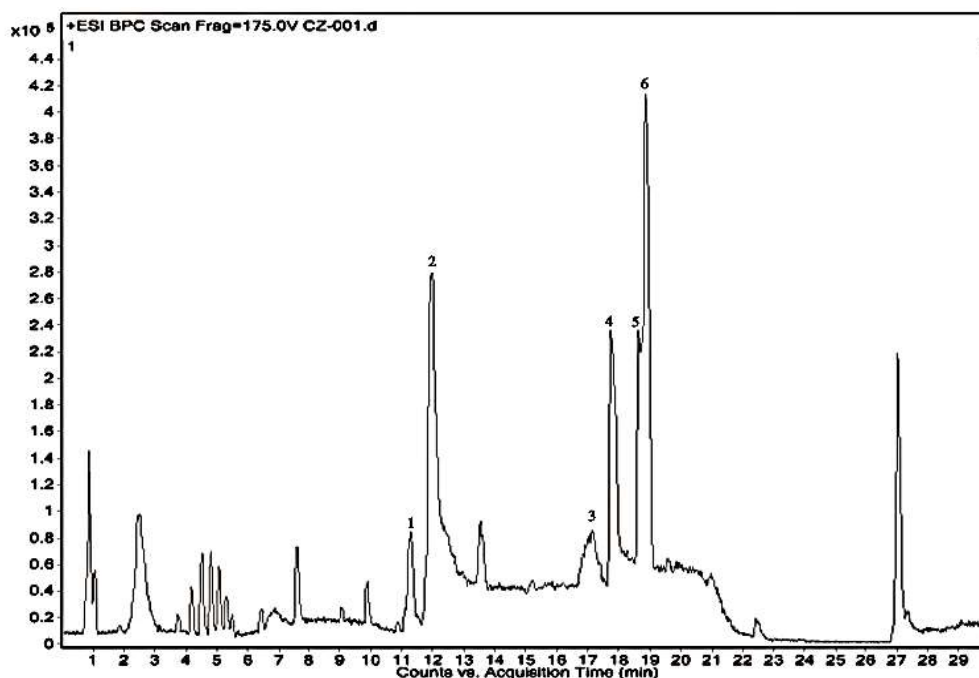
Fig. 4.13 (a) HRLCMS chromatogram of CZAgNPs showing the bound bioactive molecules

A total of ten bioactive compounds were identified from the HR-LCMS spectrum of CAAgNPs suspension (Fig. 4.13b). Zedoarolide B, Curcumenolactone C, Santonin, 5-epicurzeronone, glechomafuran, procurcumadiol, ar-turmenone, costunolide, zedoarondiol and curdione were the bioactive compounds of aqueous rhizome extract of CA that was bound to the CAAgNPs. The retention time, molecular mass, molecular formula, adducts ions formed in ion source, and peak area percentage of the bioactive compounds are listed in Table 4.8.

The result ascertains bioactive molecules are bound to the biosynthesized silver nanoparticles and this corroborates with the FTIR results.

Table 4.8. Bioactive macromolecules coated on CAAgNPs identified from the HR-LCMS Chromatogram presented in Fig. 4.13b.

Peak No.	Retention time	Molecular mass (g / mol)	m/z	Formula	Adduct	Compound name	Peak Area (%)
1.	4.45	282.1486	283.1558	$C_{15}H_{22}O_5$	(M+H+)	Zedoarolide (Terpenoid)	22.4
2.	5.02	264.138	265.1452	$C_{15}H_{20}O_4$	(M+H+)	Curcumenolactone (Sesquiterpenoid)	4.2
3.	6.633	248.1431	249.1503	$C_{15}H_{18}O_3$	(M+H+)	Santonin (Sesquiterpenoid) Procurcumadiol (Sesquiterpenoid)	9.8
4.	7.684	232.148	233.1552	$C_{15}H_{18}O_2$	(M+H+)	5 - epicurzerenone	5.1
5.	8.527	246.1277	247.1349	$C_{15}H_{20}O_3$	(M+H+)	Glechomafuran (Germacrane sesquiterpenoids)	6.5
6.	8.7	250.1588	251.1661	$C_{15}H_{22}O_3$	(M+H+)	Procurcumadiol (Sesquiterpenoids)	3.3
7.	9.938	230.1324	231.1397	$C_{15}H_{20}O$	(M+H+)	Ar - turmenone (Sesquiterpenoid)	6.6
8.	10.24	216.1528	217.16	$C_{15}H_{20}O_2$	(M+H+)	Costunolide (Sesquiterpenoid)	6.4
9.	11.181	252.1745	275.1636	$C_{15}H_{24}O_3$	(M+Na+)	Zedoarondiol (Terpene)	2.9
10.	13.04	236.1791	237.1863	$C_{15}H_{24}O_2$	(M+H+)	Curdione (Terpene)	17.8

The phytoconstituents were identified based upon spectral similarity with the MS library (NIST MS Search 2.0) and the Human Metabolome Database
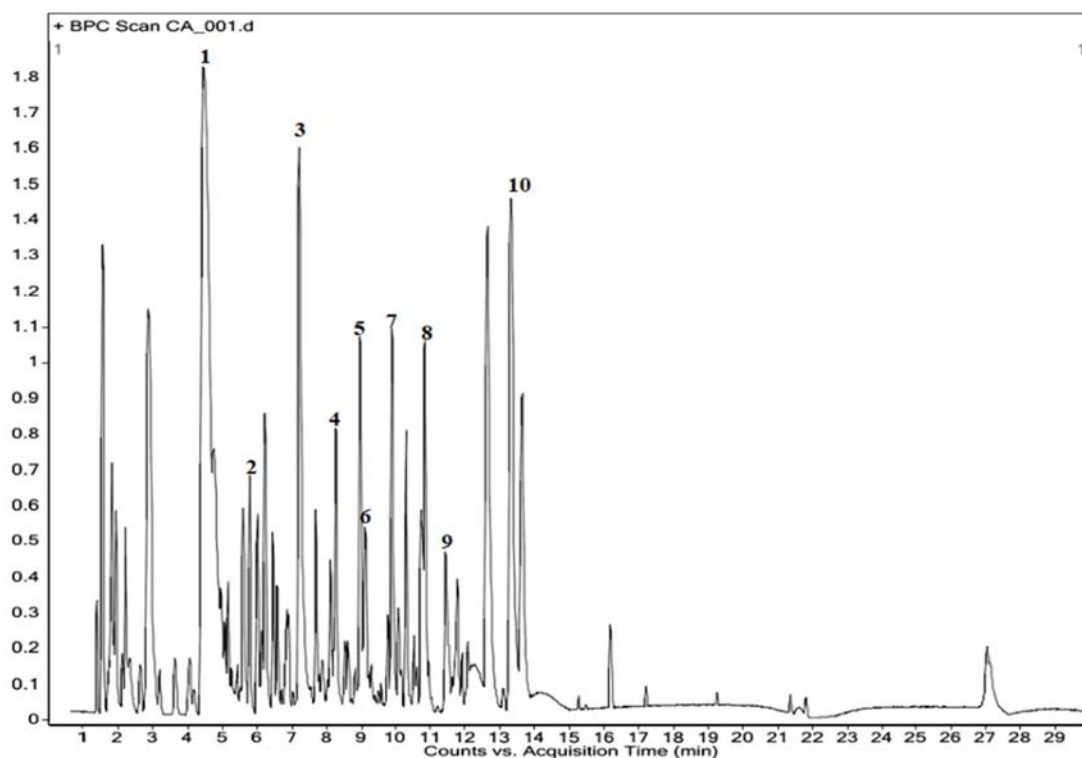
Fig. 4.13 (b) HRLCMS chromatogram of CAAgNPs showing the bound bioactive molecules

4.5 Determination of catalytic property of AgNPs

In the present scenario, the removal of dyes is of major need as dyes contribute to major cause of environmental pollution. Nanoparticles could be used in the degradation of toxic dyes. Here photocatalaytic and non – photocatalytic activity of CZAgNPs and CAAgNPs were studied. Malachite green (cationic dye) and Coomassie brilliant blue (anionic dye) was selected for photocatalytic degradation studies and azo dyes (Orange G, Eriochrome Black T, Methyl Orange and Congo red) were chosen for the non – photocatalytic degradation studies. In light mediated degradation studies, effects of both sunlight and UV light were analyzed. The non – photocatalytic studies were carried out using sodium borohydride as the reducing agent. The results obtained are discussed below.

4.5.1 Photocatalytic degradation of ionic dyes

The drop in the characteristic absorption peak of MG at 615 nm was used as an indicator for examining the degradation of the dye catalyzed by CZAgNPs and CAAgNPs. There was a gradual decrease in the main absorption peak of MG with the increase in exposure time to sunlight and UV light (Fig. 4.14a, 4.14b, 4.14c,4.14d). The sunlight exposed dye-nanoparticle suspension had quick de-colorization (4 h) compared to UV light (24 h) exposed suspension. The percentage of degradation of MG was 94.7 % and 65.79 % under sunlight for CZAgNPs and CAAgNPs respectively. Upon UV irradiation, the percentage of MG degradation was 22.83 % when treated with CZAgNPs and 57.10 % of degradation was observed when treated with CAAgNPs.

The degradation product of the reaction which showed comparatively maximum degradation was subjected to HR-LCMS analysis. The possible intermediates formed during the breakdown of MG are given in Fig. 4.14e. The retention time of the control dye MG is at 11.585, which was different from the retention time of all the degraded products in the range of 1.02 to 11.447. The HR-LCMS analysis of MG and degradation products confirmed the efficacy of bioactive molecule coated CZAgNPs as good photocatalysts in the effective removal of the model dye. The reaction showed no progress in the absence of nanocatalysts (control). The HR-LCMS analysis of reaction product of MG - nanoparticle suspension showed the presence of compounds 4 - aminobenzoic acid, phenylacetic acid, N, N' diacetyl 1, 4 phenylene diamine, methyl 3, 4 di aminobenzoate, 4 - methyl aminobenzoic acid, 4, 4' diamino benzophenone, 4 - amino benzophenone and 4, 4' methylene bis (N,N' dimethyl) benzamine with molecular weights 137.04, 136.03, 192.09, 166.07, 151.06,

212.09, 197.08 and 254.18 m/z respectively (Fig. 4.14f) The molecular weight of MG dye is 330.20 m/z. Out of the eight intermediates formed during the breakdown of MG, N, N' diacetyl 1, 4 phenylene diamine was quantified to be the most abundant degradation product (11.46 %), followed by 4 - methyl aminobenzoic acid (11.43 %), 4, 4' methylene bis (N,N'dimethyl) benzamine (11.09 %), phenylacetic acid (7.99 %), 4, 4' diamino benzophenone (4.85 %), 4 - aminobenzoic acid (1.08 %) and 4- amino benzophenone (0.75 %).
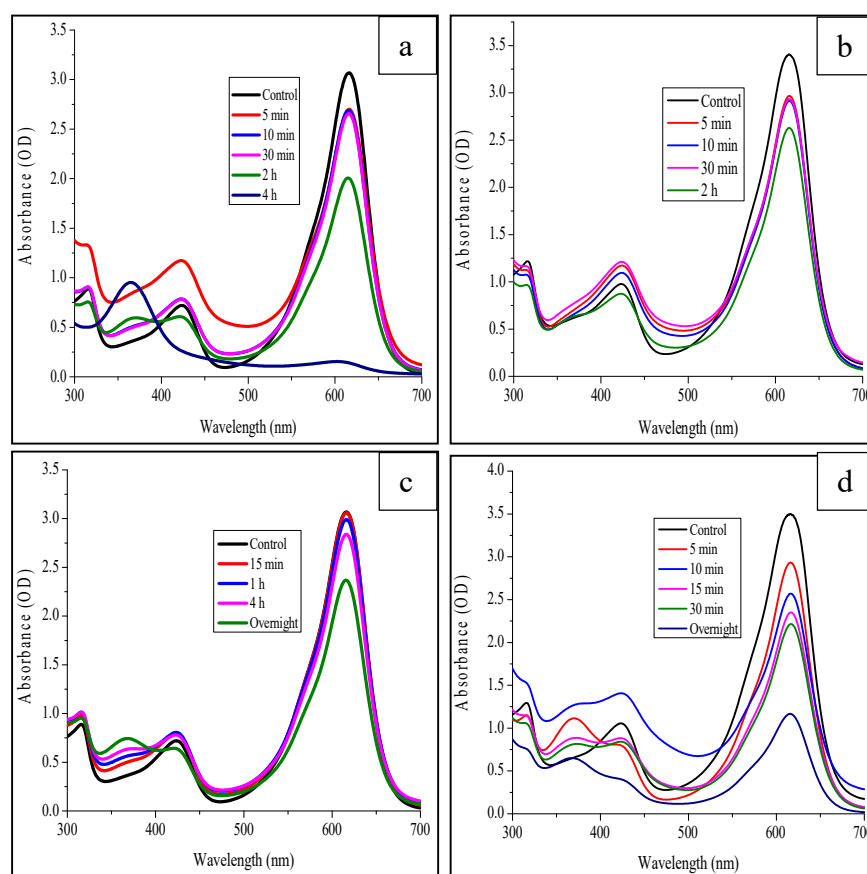
Fig. 4.14 Photocatalytic degradation of MG under sunlight (a) CZAgNPs (b) CAAgNPs; under UV light (c) CZAgNPs (d) CAAgNPs
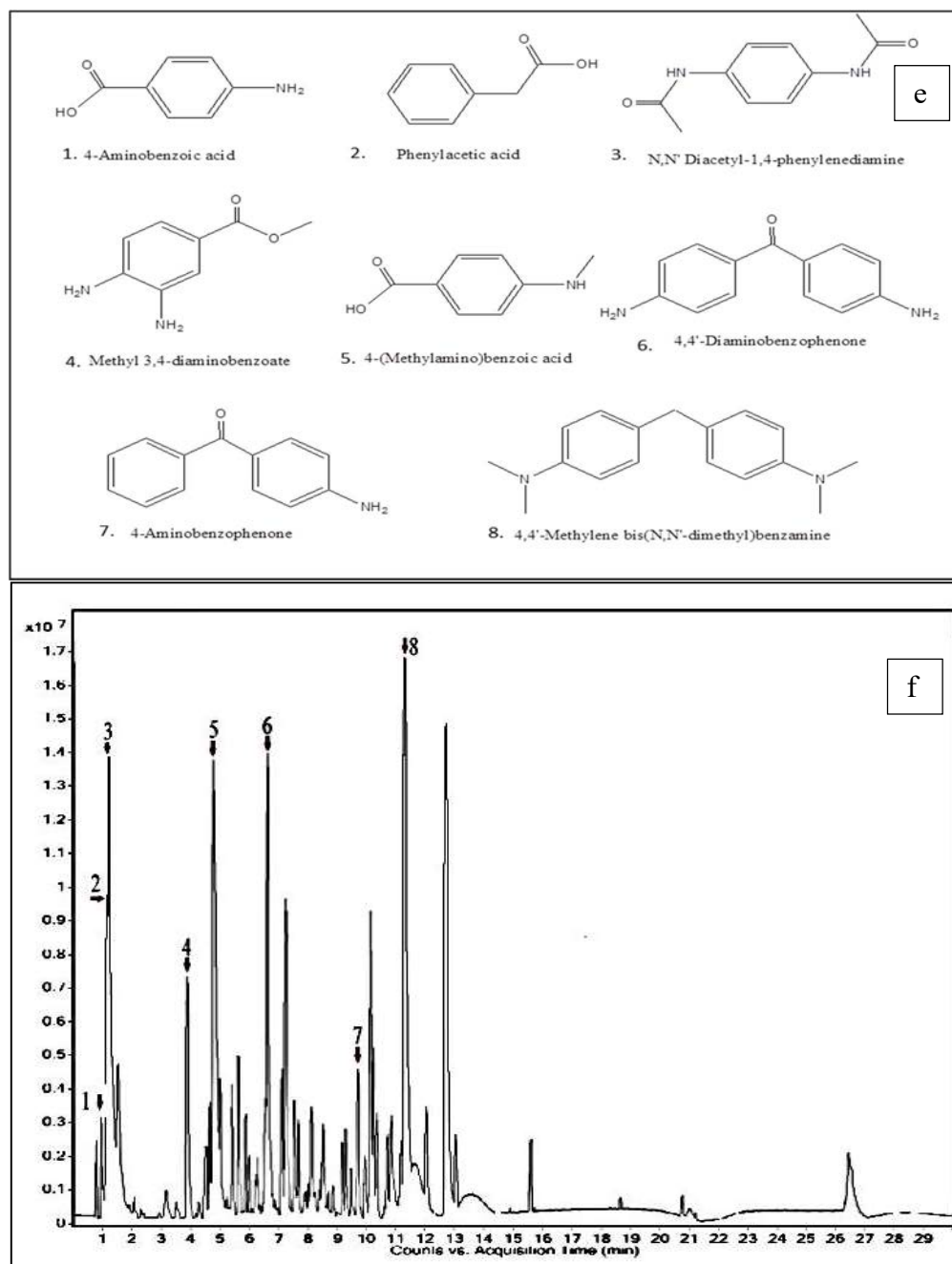
Fig. 14.4 (e) Possible intermediates formed after degradation of MG (f) HR LCMS chromatogram of photocatalytic degradation product of MG by CZAgNPs

The formation of benzophenone derivatives by N-demethylation of MG have been reported as one of the major reaction involved in photo-oxidative process (Pérez-Estrada, Agüera, Hernando, Malato, & Fernández-Alba, 2008). This is in agreement with our obtained results, since most of the products identified after degradation was

derivatives of benzophenone. The possible mechanism of degradation may be due to the generation of hydroxyl radicals by the highly energetic electrons released when the photons struck the valence electrons of the molecule capped CZAgNPs (Wang, Lu, Liu, Wu, & Wu, 2018). These low molecular weight structures being mostly benzene derivatives may further be decomposed to form small organic molecules which eventually breaks down into CO_2 and H_2O (Ju *et al*., 2009). Moreover, the formation of highly toxic leucomalachite green, a reduced form of MG was not detected in our study ascertaining the non-toxic dye removal process by bioactive molecule coated CZAgNPs, rendering unhazardous products to the environment (Sutar *et al*., 2019).

The characteristic absorption peak at 555 nm was used for examining the photocatalytic degradation of CBB. There was a gradual decrease in the main absorption peak of CBB with the lengthening of exposure time, implying the degradation of CBB. The percentage of degradation after overnight exposure to UV light was 98.7% for CAAgNPs. The reaction mixture treated with CZAgNPs had only 44.67 % of dye removal. In the absence of nanocatalysts (control) no progress occurred in the reaction mixture (Fig. 4.15a, 4.15b).

Efficient degradation of CBB was evident when the reaction mixture was exposed to UV light. During the irradiation by UV light, the photons are absorbed and as a result electron and hole pairs are generated on the surface of photocatalyst. The migration of charge carriers occurs on the surface of the AgNPs (photocatalyst) in the absence of recombination of electron and hole pairs. The free electrons reduce O_2 and generate superoxide and peroxide radicals. The ROS then oxidises water to OH radicals. The OH radicals being highly reactive and unstable, reacts with the dye and

cause the oxidation of dye to inorganic acids, CO_2 and water (C. R. R. Kumar *et al.*, 2020). This brings about the efficient removal of dyes.
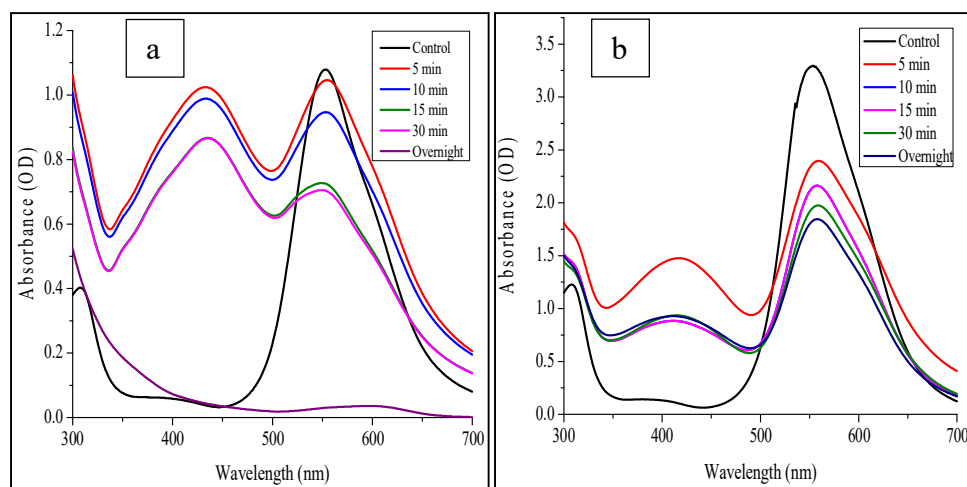

Fig. 4.15 Photocatalytic degradation of CBB exposed to UV light under (a) CAAgNPs (b) CZAgNPs

The results indicated that both the CZAgNPs and CAAgNPs displayed different levels of degradation potencies. The CZAgNPs were effective in degrading the cationic dye - MG whereas, the anionic dye - CBB was effectively removed by the CAAgNPs. This indicated the efficiency of biosynthesized silver nanoparticles as good photocatalyst in the effective degradation of the model dye.

4.5.2 Non – Photocatalytic degradation of Azo dyes

The characteristic absorption peak for OG, CR, EBT, and MO are 486 nm, 498 nm, 550 nm and 468 nm respectively. The drop in the absorption peaks of each dye was used for examining the catalytic degradation. There was a gradual decrease in the main absorption peak in all the three experimental systems as compared to control. The major decrease in absorption peak was found in the system catalyzed by the silver nanoparticles along with sodium borohydride. The percentage degradation of Orange G, Congo Red, Eriochrome Black T and Methyl orange were 92.73 %, 81.55 %, 70.4 %, and 60.17 % respectively for the reaction system catalyzed by CAAgNPs (Fig.

4.16 a -d). The reaction system catalyzed by CZAgNPs also exhibited efficient degradation of azo dyes. The degradation percentages for the reaction system catalyzed by CZAgNPs were 75.68 % (OG), 72.24 % (CR), 72 % (EBT) and 65 % (MO) (Fig. 4.16 e -h). Out of the two nanoparticles synthesized, CAAgNPs were effective in degrading Orange G and Congo Red. Eriochrome Black T and Methyl Orange were efficiently removed in the reaction system catalyzed with CZAgNPs.

From the UV – Visible spectrum, it is evident that experimental system containing the dye and sodium borohydride alone did not show effective degradation process whereas in the experimental system comprising the synthesized silver nanoparticles and sodium borohydride, efficient degradation was noted. The mechanism involved in the process might be due to the ability of the nanoparticles to reduce the activation energy between the dye and sodium borohydride. This accelerates the reduction of azo dyes.

It is reported by Daihua Hu *et al*., (Hu *et al*., 2021) that reduction of azo dyes in the presence of sodium borohydride and AgNPs can be explained using Langmuir – Hinshelwool model. Sodium borohydride acts as hydrogen and electron donor during the reduction process, thereby changing the pH of the solution. Hence the AgNPs becomes positively charged. Then the BH_4^- and azo dyes get adsorbed onto the AgNP's surface. The catalytic process is then initiated by the transfer of electron from the BH_4^- to azo dyes
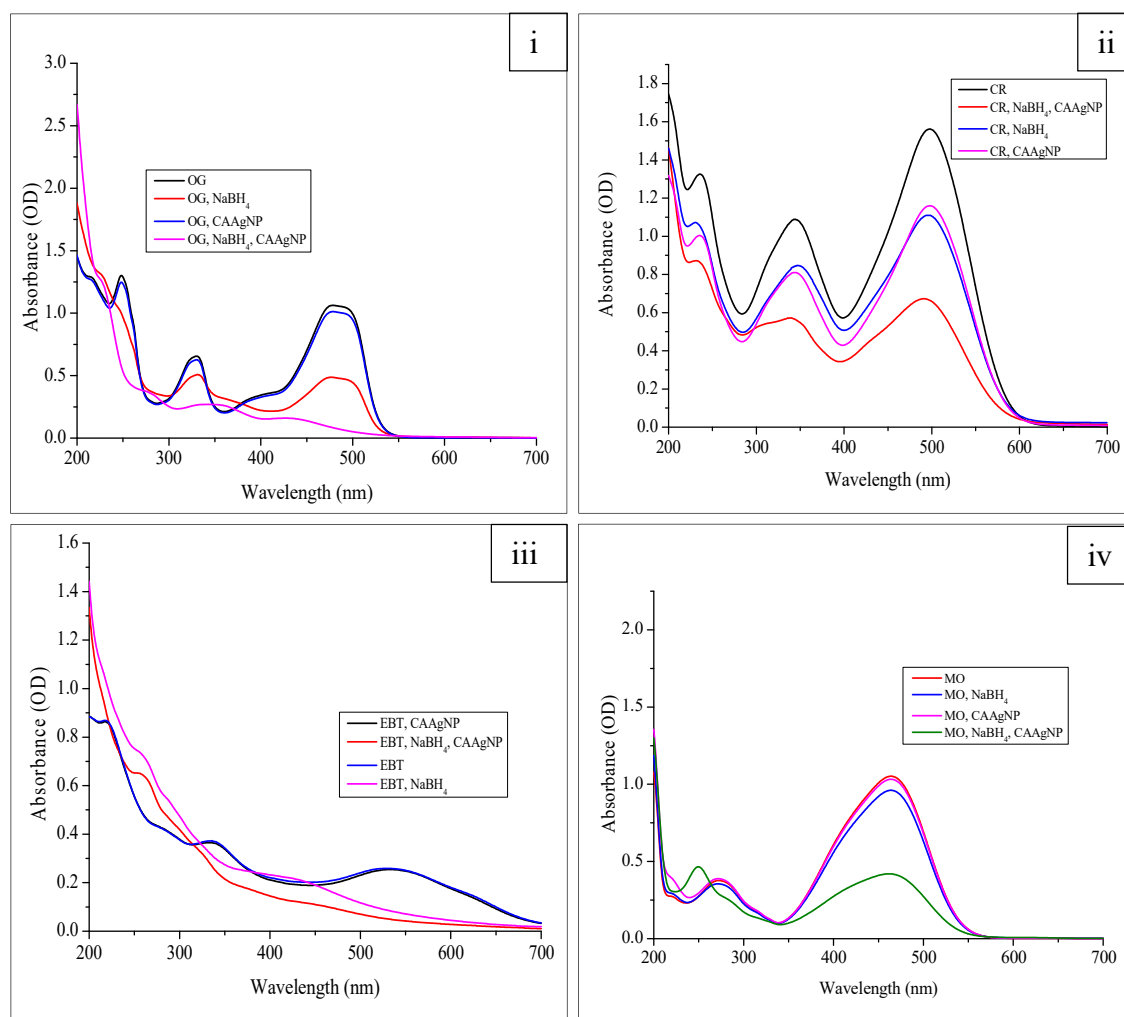
Fig. 4.16aµ Photocatalytic degradation of azo dyes using CZAgNPs (i) OG, (ii) CR, (iii) EBT, (i) MO

through AgNPs. Therefore the AgNPs act as nanocatalyst and help in the process of electron shuttling between the donor (sodium borohydride) and azo dyes (Varadavenkatesan, Selvaraj, & Vinayagam, 2016). It was evident that in the absence of silver nanoparticles, effective degradation of dyes was nil. Hence in all the catalytic reaction studied, the silver nanoparticle served as efficient catalyst accelerating the reduction of azo dyes.
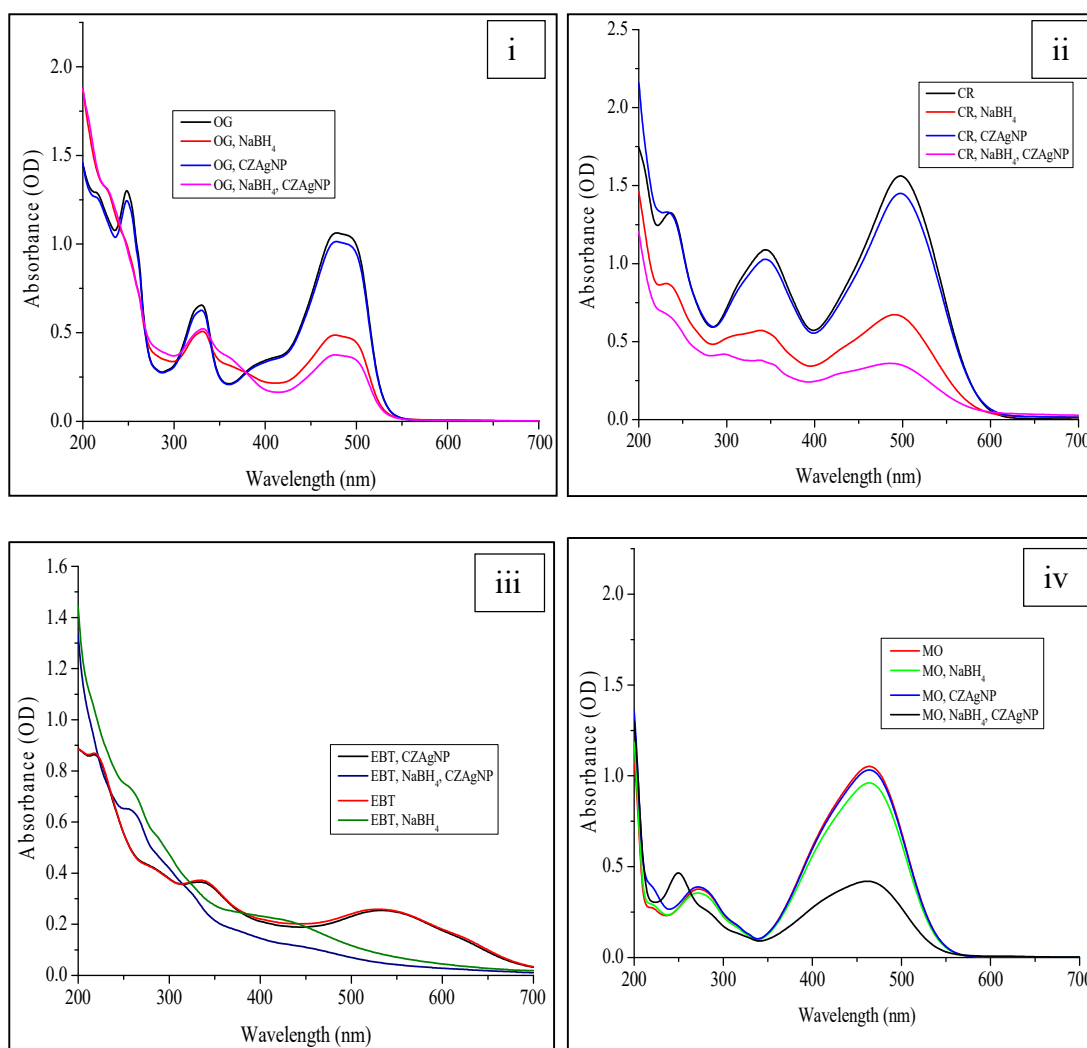
Fig. 4.16b Catalytic degradation of azo dyes using CZAgNPs (i) OG, (ii) CR, (iii) EBT, (i) MO

4.6 Determination of Antibacterial Activity of AgNPs

4.6.1 Disc Diffusion Assay

In disc diffusion assay, the as-synthesized CZAgNPs and CAAgNPs displayed an efficient inhibitory activity towards all the selected bacterial isolates. The highest ZOI observed at 100 µg / ml concentration of CZAgNPs was 13 ± 0.70 mm, 12 ± 0.34 mm and 19 ± 0.34 mm respectively for *P. mirabilis, S. marcescens* and *B. subtilis*. At a concentration of 100 µg / ml, the CAAgNPs displayed highest ZOI of 26 ± 0.6 mm, 10 ± 0.76 mm and 13 ± 0.63 mm for *P. aeruginosa*, *K. pneumoniae* and *S.aureus*

respectively. Both CZAgNPs and CAAgNPs expressed a zone of inhibition of 11 mm against *E. coli*. However, concentrations in the range of 10 µg / ml to 75 µg / ml also showed slight inhibition in bacterial growth. The tetracyclin disc (standard) exhibited 14 ± 0.13 mm, 14 ± 0.64 mm, 12 ± 0.77 mm, 16 ± 0.34 mm and 22 ± 0.45 mm ZOI against *E. coli*, *K. pneumonia*, *S. marcescens, B. subtilis* and *S. aureus* respectively.

As compared to the rhizome extract (CZ and CA) alone, the silver nitrate exhibited inhibitory activity against the selected bacterial strains. The synthesized silver nanoparticles were efficient in inhibiting the growth of *P. aeruginosa* whereas the standard drug Tetracyclin exhibited zero inhibition (Table 4.9; Fig 4.17a).

In accordance with the obtained results for CZAgNPs and CAAgNPs, previous disc diffusion studies have shown that the green synthesized silver nanoparticles from different sources of plants exhibited effective antibacterial activity against gram negative bacteria than gram positive bacteria (Jagtap & Bapat, 2013; Kiran, Betageri, Kumar, Vinay, & Latha, 2020; Nyabola *et al*., 2020).

Table 4.9 Zone of inhibition of various test solutions (100 µg / ml) against bacterial strains (disc diffusion method)

| Drug	Inhibition diameter (mm)						
	E. Coli	*P. aeruginosa*	*K. pneumoniae*	*P. mirabilis*	*S. marcescens*	*B. subtilis*	*S. aureus*
Tetracyclin	14 ± 0.13	0	14 ± 0.64	0	12 ± 0.77	16 ± 0.34	22 ± 0.45
Dist. H_2O	0	0	0	0	0	0	0
CAAgNP	13 ± 0.34	26 ± 0.60	10 ± 0.76	12.5 ± 0.96	11 ± 0.81	17 ± 0.78	13 ± 0.63
CA	7 ± 0.70	0	7 ± 0.66	7 ± 0.56	7 ± 0.11	0	0
CZAgNP	13 ± 0.46	22 ± 0.33	9.5 ± 0.10	13 ± 0.70	12 ± 0.34	19 ± 0.34	12.5 ± 0.44
CZ	7 ± 0.56	0	7 ± 0.34	7 ± 0.23	7 ± 0.26	0	0
$AgNO_3$	10 ± 0.22	22 ± 0.48	9 ± 0.33	11 ± 0.17	11 ± 0.34	16 ± 0.56	11 ± 0.63

Values are expressed as Mean $\pm$ SD; n = 3
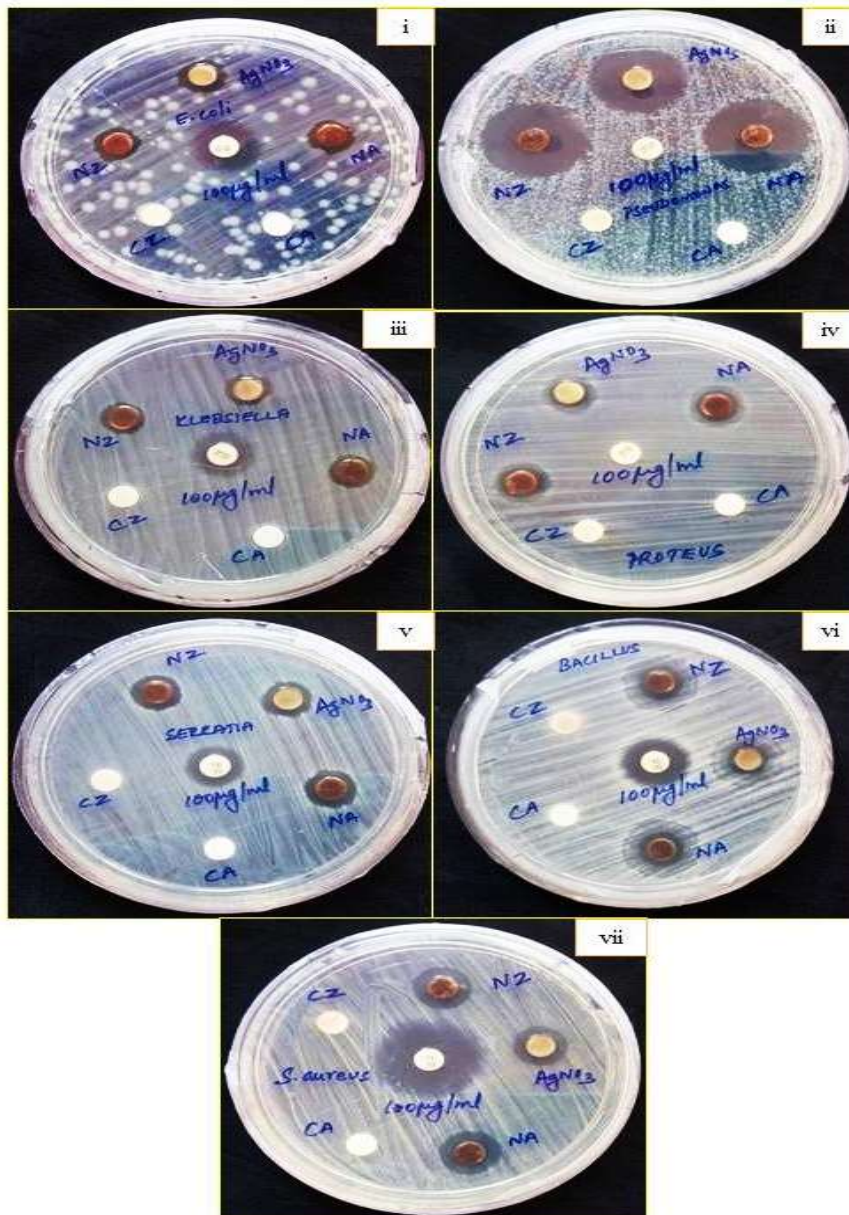
Fig. 4.17 Antibacterial activity of AgNPs (a) Disc diffusion method against (i) *E. coli,* (ii) *P. aeruginosa,* (iii) *K. pneumonia,* (iv) *P. mirabilis,* (v) *S. marcescens* (vi) *B. subtilis* and (vii) *S.aureus* [NA- CAAgNPs, NZ- CZAgNPs]

4.6.2 Broth Microdilution Assay

The Broth microdilution assay explains the MIC of the as-synthesized CZAgNPs against two strains of bacteria. After 24 h of incubation, the wells with no color change were scored for the MIC value and the wells stained with dark red color showed the presence of bacteria. The MIC was found to be 4 µg / ml and 32 µg / ml respectively for ampicillin and CZAgNPs against *S. aureus*. In the case of *E. coli*, the MIC was 16 µg / ml and 64 µg / ml for the antibiotic ampicillin and CZAgNPs. The plant rhizome extract (CZ) showed the least activity against both the bacterial strains in which the MIC was 512 µg / ml. The MIC of silver nitrate solution was 64 µg / ml for both the bacterial isolates (Fig. 4.17b).

The MIC of CAAgNPs against *E. coli* and *S. aureus* was 32 µg / ml and 16 µg / ml respectively. The plant rhizome extract (CA) exhibited the lowest activity with a MIC of 512 µg / ml against both the strains of bacteria (Table 4.10; Fig. 4.17b).

The antibacterial activity exhibited by both CZAgNPs and CAAgNPs could be attributed to their ultra-small size. The possible mechanism involved in the inhibition of the bacterial growth could be the increased surface to volume ratio of the nanoparticles, making the plasma membrane unstable, thereby reducing the adenosine triphosphate levels (ATP) in the bacterial cells. This action destroys the bacterial cell membrane and eventually kills the bacteria. It is reported that the silver nanoparticles damage the inhibitory components of the of the bacteria which are present on the outer membrane resulting in the leaching out of the lipopolysaccharides and purines (Seifipour *et al*., 2020). The penetration of AgNPs into the microbes result in ROS generation and finally intracellular damage (Franci *et al*., 2015). It is also reported that the size, concentration and shape of AgNPs can affect the antimicrobial activity.

Earlier studies showed that *E. coli* responded best to the triangular shaped nanoparticles when compared with the spherical and rod shaped ones, since the triangular shape provides more positive charge to the nanoparticles ensuring greater antimicrobial activity (Pal, Tak, & Song, 2007). Therefore the almost equal ZOI exhibited by CZAgNPs and CAAgNPs (100 μg / ml) and Tetracyclin against *E. coli, S. marcescens, B. subtilis* could be attributed to their spherical shape and lower surface area of synthesized silver nanoparticles which was ascertained from nitrogen physisorption.

The CZAgNPs were found to be more effective against *E. coli* than *S. aureus* whereas CAAgNPs inhibited *S. aureus* more effectively. Better performance of CZAgNPs to inhibit the growth of *E. coli* is in good agreement with the previous reports (Madivoli *et al*., 2020; Priyadarshini *et al*., 2013; Pugazhendhi *et al*., 2016). On the other hand several studies reported greater zone of inhibition for *S. aureus* than *E. coli* using AgNPs (Seifipour *et al*., 2020) which could be correlated with the activity of CAAgNPs of the present study. The decrease in the ZOI exhibited by CZAgNPs for gram positive bacteria is perhaps due to the thick peptidoglycan layer and absence of lipopolysaccharide layer in their cell wall composition, which hinders the anchoring of AgNPs, thereby obstructing the antibacterial activity (Franci *et al*., 2015). The effective inhibition of *S. aureus* shown by CAAgNPs could be due to its high penetration ability affecting both the membrane permeability and DNA replication of the bacteria (Uddin *et al*., 2020).

In contradiction to the presumed activity of aqueous rhizome extracts of CZ and CA, the very low activity or the absence of antibacterial activity is due to the medium of extraction and also the use of low concentration during experimentation.

Eventhough several researchers have reported the potential of the biosynthesized AgNPs as efficient microbicides against various chemical isolates (Uddin *et al*., 2020), novel reports ascertain the resistance of certain bacterial strains to biosynthesized AgNPs. It was reported by Aina *et al*., (Aina, Owolo, Lateef, Aina, & Hakeem, 2019) that the biosynthesized AgNPs did not perform well even at concentration 100 µg / ml against both *S. aureus* and *E. coli*. The resistance in bacterial strains was due to the repeated exposure of AgNPs resulting in the production of flagellin. Flagellin, an adhesive protein, triggers the agglomeration of nanoparticles, reduces their stability and finally bring down the efficacy of AgNPs as bactericides (Panáček *et al*., 2018).

Nevertheless, the obtained results indicated that both CZAgNPs and CAAgNPs were relatively effective against both gram positive and gram negative bacteria.

Table 4.10 Comparison of MIC of Ampicillin, biosynthesised silver nanoparticles, plant rhizome extracts and silver nitrate solution against pathogenic bacterial strain

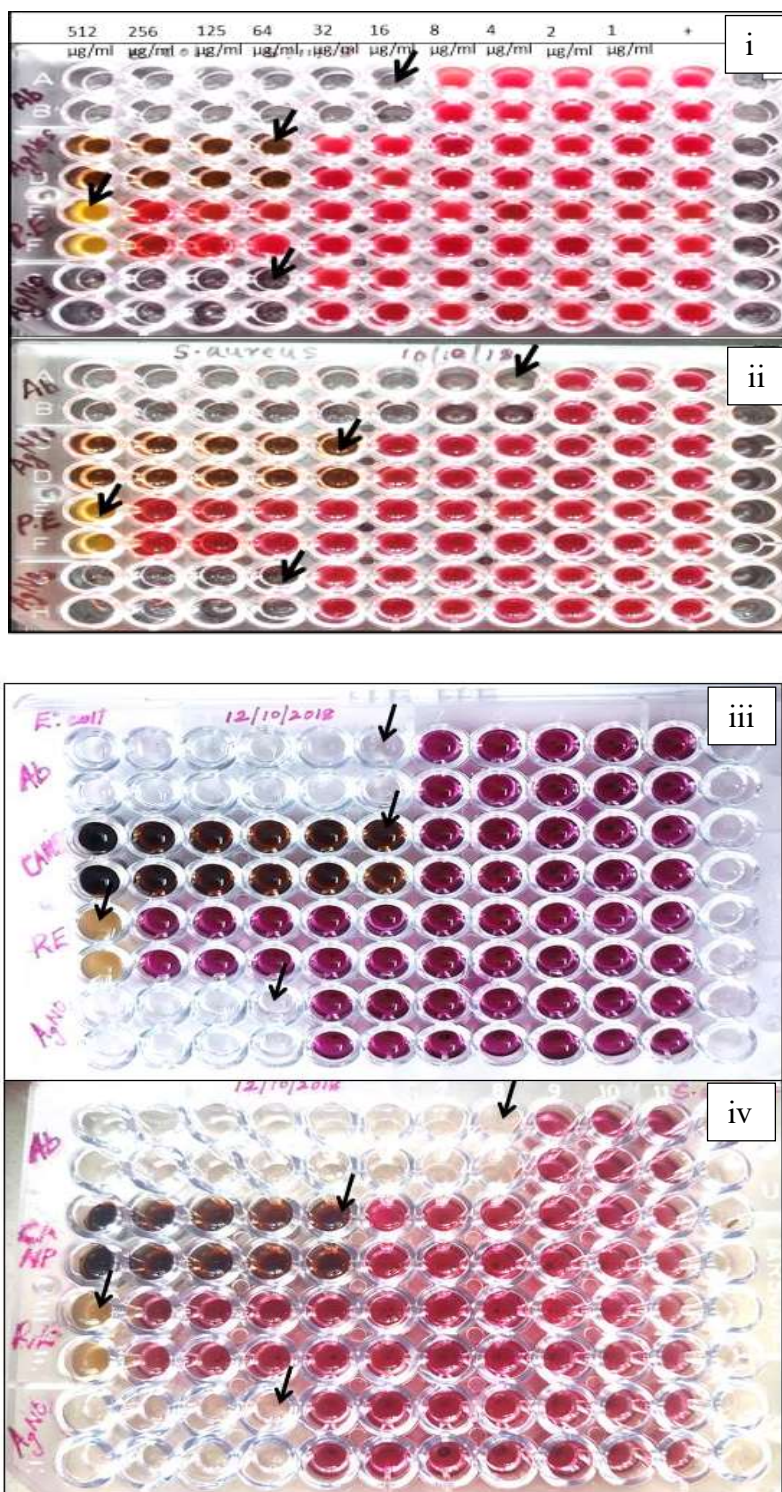| Bacterial strains	MIC (µg/ml)					
	Ampicillin	CZAgNPs	CAAgNPs	CZ	CA	AgNO$_3$ solution
E. coli	16	64	16	512	512	64
S. aureus	4	32	32	512	512	64

Fig. 4.17 (b) Broth microdilution method: Plates showing MIC against (i, iii) *E.coli*, (ii, iv) *S. aureus* [Ab- Ampicillin, AgNPs – CZAgNPs, PE- CZ, AgNO$_3$ – silver nitrate, CANP –CAAgNPs, RE – CA]

4.6.3 In Silico molecular docking

To further understand the antibacterial property of the active biomolecules bound on to the surface of CZAgNPs and CAAgNPs *in silico* molecular docking was performed. The protein targets selected for *E. coli* and *S. aureus* were diaminopimelate epimerase (PDB ID: 5N9M) and α glutamine amidotransferase (PDB ID: 4IJZ) respectively. Thirteen ligands were selected from HRLCMS analysis data of both CZAgNPs and CAAgNPs. The selected ligand molecules were curculone, curcumenolactone C, curdione, curzene, dihydrosphingosine, epicurzerenone, furanogermenone, glechomafuran, glycerolpalmitate, glycerolmonostearate, procurcumadiol, zedoarolide B and zeroarondiol. The molecular properties of the selected ligands are represented in Table 4.11.

The interaction between the selected protein molecules and the 13 ligands were studied using the tool AutoDock 4.2. The result was analyzed based on the binding energy (ΔG) formed between the ligand molecule within the active site of the target protein. The binding energy formed between all the ligand molecule and protein targets diaminopimelate epimerase (PDB ID: 5N9M) and α glutamine amidotransferase (PDB ID: 4IJZ) are given in Table 4.12 and Table 4.13 respectively. Both bonded and non-bonded interactions formed by the lead molecules against the target proteins were analyzed. Out of the 13 ligands the lead molecule identified for the protein 4ijz and 5n9m were Curcumenolactone C and Procurcumadiol respectively. For the protein 4ijz, only two active site residues were selected Cys 73 and Cys 217 which were proton donor and acceptor respectively. The lead molecule Curcumenolactone C formed four H-bond interactions one of which is with the proton donor active site residue Cys 73. Also Cys 217 is involved in forming a *Vander Waals*

interaction with the ligand molecule. The ligand forms a strong binding with the target involving both the active site residues. Procurcumadiol formed six H-bond interactions, three of them with active site residues of the protein 5n9m. Among the H-bonds, three were formed with GLN98.

From the docking studies, it was reported that Acetaminophen and Dexamethasone could bind to the active site of diaminopimelate epimerase, a key enzyme in lysine synthesis of bacteria, confirmed that those molecules could be developed as tight inhibitors, which can be used to treat bacterial infection effectively (H. Singh *et al*., 2021). In concordance with the previous reports it suggests that procurcumadiol bound on the synthesized AgNPs could be exploited as inhibitors in treating bacterial infections.

Table 4.11 The molecular properties of the selected ligands (Data from PubChem)

Compound	Canonical smiles	Molecular Weight (g/mol)	XLog P3-AA / XLog P3	Hydrogen Bond Donor Count	Hydrogen Bond Acceptor Count	Rotatable Bond Count	Exact Mass (g/mol)	Monoisotopic Mass (g/mol)
Zedoarolide B	CC1=C2CC3C(CCC3(C)O)C(CC2(OC1=O)O)(C)O	282.33	-0.1	3	5	0	282.146724	282.146724
Curcumenolactone C	CC1C2=CC3C(C3(CC2(OC1=O)O)C)CCC(=O)C	264.32	0.7	1	4	3	264.136159	264.136159
Curcolone	CC1=C2C(=O)C3=C(CC2(C(CC1)O)C)OC=C3C	246.3	2	1	3	0	246.125594	246.125594
Epicurzerenone	CC1=COC2=C1C(=O)C(C(C2)(C)C=C)C(=C)C	230.3	4	0	2	2	230.13068	230.13068
Glechomafuran	CC1=COC2=C1CC3C(O3)(CC4C(C2)(O4)C)C	248.32	2.3	0	3	0	248.141244	248.141244
Procurcumadiol	CC1=CC(=O)C(=C(C)C)CC2(C1CCC2(C)O)O	250.33	1.3	2	3	0	250.156895	250.156895
Curzerene	CC1=COC2=C1CC(C(C2)(C)	216.32	4.6	0	1	2	216.151415	216.151415

Contd.

Furanogermeno ne	C=C)C(=C)C CC1CCC=C(C C2=C(CC1=O) C(=CO2)C)C	232.32	3	0	2	0	232.14633	232.14633
Zedoarondiol	CC(=C1CC2C (CCC2(C)O)C(CC1=O)(C)O) C	252.35	1.6	2	3	0	252.172545	252.172545
Curdione	CC1CCC=C(C C(=O)C(CC1= O)C(C)C)C	236.35	2.7	0	2	1	236.17763	236.17763
Glycerol palmitate	CCCCCCCCC CCCCCCC(= O)OCC(CO)O	330.5	6.3	2	4	18	330.27701	330.27701
Dihydrosphingo sine	CCCCCCCCC CCCCCC(C(CO)N)O	301.5	5.8	3	3	16	301.298079	301.298079
Glyceryl monostearate	CCCCCCCCC CCCCCCCCC (=O)OCC(CO) O	358.6	7.4	2	4	20	358.30831	358.30831

Table 4.12 The binding energy formed between all the ligand molecule and the protein target- 5N9M

Sl no:	Phytochemical	RUN	Binding energy (kcal/mol)	Inhibition constant
1.	**Procurcumadiol**	**4**	**-8.10**	**1.15 µM**
2.	Zedoarondiol	7	-6.95	8.11µM
3.	Zedoarolide B	5	-6.88	9.00 µM
4.	Epicurzerenone	8	-6.77	10.96 µM
5.	Curdione	7	-6.74	11.46 µM
6.	Curzerene	3	-6.41	20.00 µM
7.	Furanogermenone	1	-6.39	20.87 µM
8.	Curcumenolactone C	10	-6.36	21.70 µM
9.	Curcolone	3	-6.21	28.21 µM
10.	Glechomafuran	7	-5.82	54.07 µM
11.	Glycerylmonostearate	1	-3.23	4.29 mM
12.	Dihydrosphingosine	1	-3.07	5.62 mM
13.	Glycerolpalmitate	5	-1.12	150.33 mM

Table 4.13 The binding energy formed between all the ligand molecule and the protein target- 4IJZ

Sl no:	Phytochemical	Run	Binding Energy (kcal/mol)	Inhibition constant
1.	**Curcumenolactone C**	**6**	**-6.87**	**9.25 µM**
2.	Curcolone	5	-6.61	14.26 µM
3.	Curdione	3	-6.60	14.43 µM
4.	Furanogermenone	5	-6.44	18.94 µM
5.	Zedoarondiol	6	-6.31	23.71 µM
6.	Zedoarolide B	5	-6.23	27.31 µM
7.	Procurcumadiol	7	-6.17	29.78 µM
8.	Curzerene	2	-6.09	34.18 µM
9.	Glechomafuran	8	-5.89	48.44 µM
10.	Dihydrosphingosine	1	-5.86	50.92 µM
11.	Epicurzerenone	1	-5.69	67.30 µM
12.	Glycerylmonostearate	10	-3.11	5.25 mM
13.	Glycerolpalmitate	8	-2.49	14.97 mM

From the interaction diagram (Fig. 4.17c, 4.17d) it is evident that all the lead molecules showed interactions within the active site region, which indicates correct binding pose for the ligand in the binding region that helps the ligand to carry out the designated function. The protein ligand bound complex visualized using Pymol (Fig. 4.17e, 4.17f) also shows the buried ligand in the active site of the targets. The results confirm the inhibitory potential of the selected compounds which can be considered for further analysis.
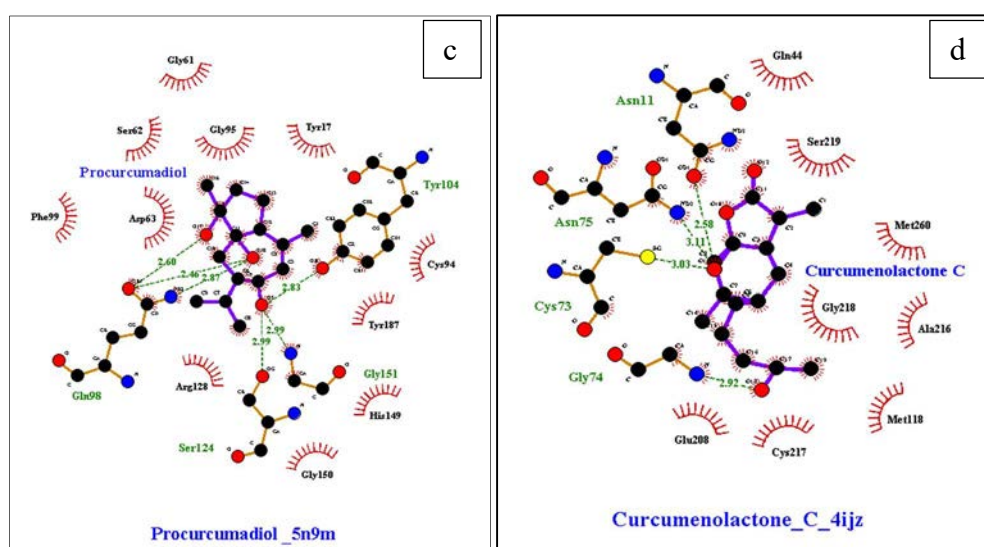

Fig. 4.17 (c) Interaction diagram of procurcumadiol and 5n9m protein (d) interaction diagram of curcumenolactone and 4ijz
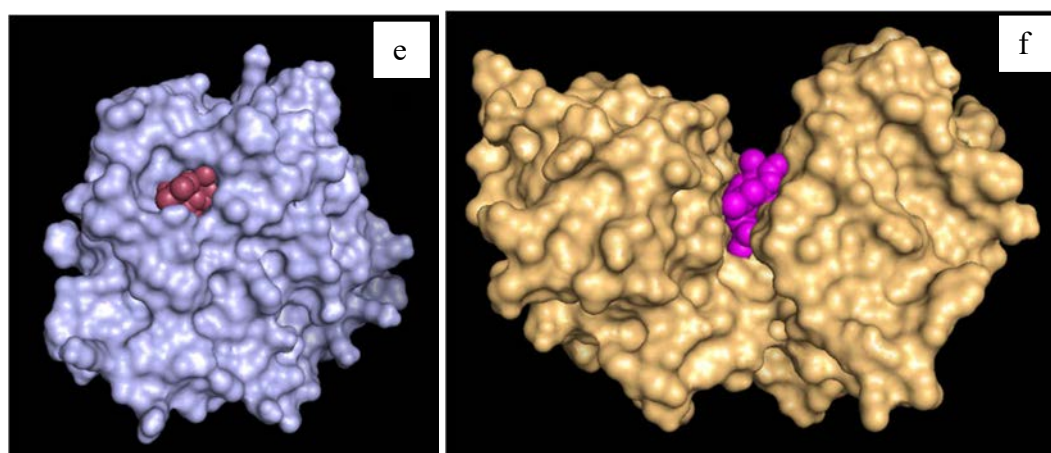

Fig. 4.17 Protein ligand complex of (e) procurcumadiol and 5n9m protein (f) curcumenolactone and 4ijz visualized usong Pymol

4.7 Determination of Antifungal Activity of AgNPs

4.7.1 Poisoned food technique

The antifungal activity of various concentrations of CZAgNPs and CAAgNPs against *A. niger* is presented in Table 4.14. The rate of inhibition of fungal growth was proportional to the concentration of the synthesized silver nanoparticles from both the aqueous rhizome extracts. The standard drug, fluconazole, inhibited 80.96 % of fungal growth. The inhibition percentage of silver nitrate solution was 45 %. The plant rhizome extracts CZ and CA exhibited 24.61 % and 20.00 % inhibition against *A. niger* respectively. The CZAgNPs showed 86.34 % inhibition, whereas 84.12 % inhibition was shown by CAAgNPs at a concentration of 100 μg / ml. Hence, the proliferation of *A. niger* was largely suppressed at 100 μg / ml concentration of CZAgNPs and CAAgNPs. The silver nitrate solution and the plant rhizome extracts (CZ and CA) showed relatively very low inhibition rate under the same concentration. This demonstrates the antifungal activity of as-synthesized silver nanoparticles. The control group did not show any zone of inhibition (Fig. 4.18a).

Table 4.14 Percentage of mycelial growth inhibition by various drugs against fungal pathogen *A. niger*

Drug (concentration)		Mycelial growth (mm)	Percentage of inhibition = C - T/C × 100 (%)
Flucanazole (100 μg / mL)		16.50 ± 0.50	80.96
Distilled water (control)		86.66 ± 0.57	0
(100 μg / mL)	CZAgNPs	11.83 ± 0.76*	86.34
	CAAgNPs	13.76 ± 0.63*	84.12
(75 μg / mL)	CZAgNPs	30.00 ± 1.73	65.38
	CAAgNPs	32.00 ± 2.01	63.07
(50 μg / mL)	CZAgNPs	34.00 ± 1.00	60.76

Contd.

	CAAgNPs	38.50 ± 0.71	55.57
(25 µg / mL)	CZAgNPs	35.66 ± 2.08	58.85
	CAAgNPs	42.73 ± 1.93	50.69
AgNO₃ solution (1mM)		47.66 ± 1.15	45.00
(0.1 g / mL)	CZ	65.33 ± 3.78	24.61
	CA	69.32 ± 2.46	20.00

Values are expressed as Mean ± SD; n = 3 * p-value less than 0.05, significant value

It was evident from the antifungal studies that both the synthesized nanoparticles exhibited a dose dependent inhibition towards the growth of *Aspergillus niger*. The results outline the fact that the synthesized silver nanoparticles were highly effective in inhibiting the growth of *A. niger*. The growth suppression of the plant pathogen by CZAgNPs and CAAgNPs were comparatively higher than the standard fluconazole. The property of the AgNPs to adhere to the hyphal membrane of fungi, inhibiting the normal budding process and thereby destructing the membrane integrity could be the probable mechanism involved in the death of the fungus (Medda, Hajra, Dey, Bose, & Mondal, 2015) (Ghojavand *et al*., 2020). Another mechanism could be the inhibitory action of silver ions on the DNA of the microorganism, inhibiting replication and resulting in the inactivated expression of certain ribosomal proteins and enzymes essential for the ATP production (Medda *et al*., 2015). Therefore our results were in line with the results of Shivakumar *et al*., (Shivakumar *et al*., 2017) confirming the inhibitory role of the synthesized silver nanoparticle. Thus, the as synthesized silver have caused detrimental effects to the infectious filamentous fungi *A. niger* and manifests its efficacy in the development of potential antifungal agent.
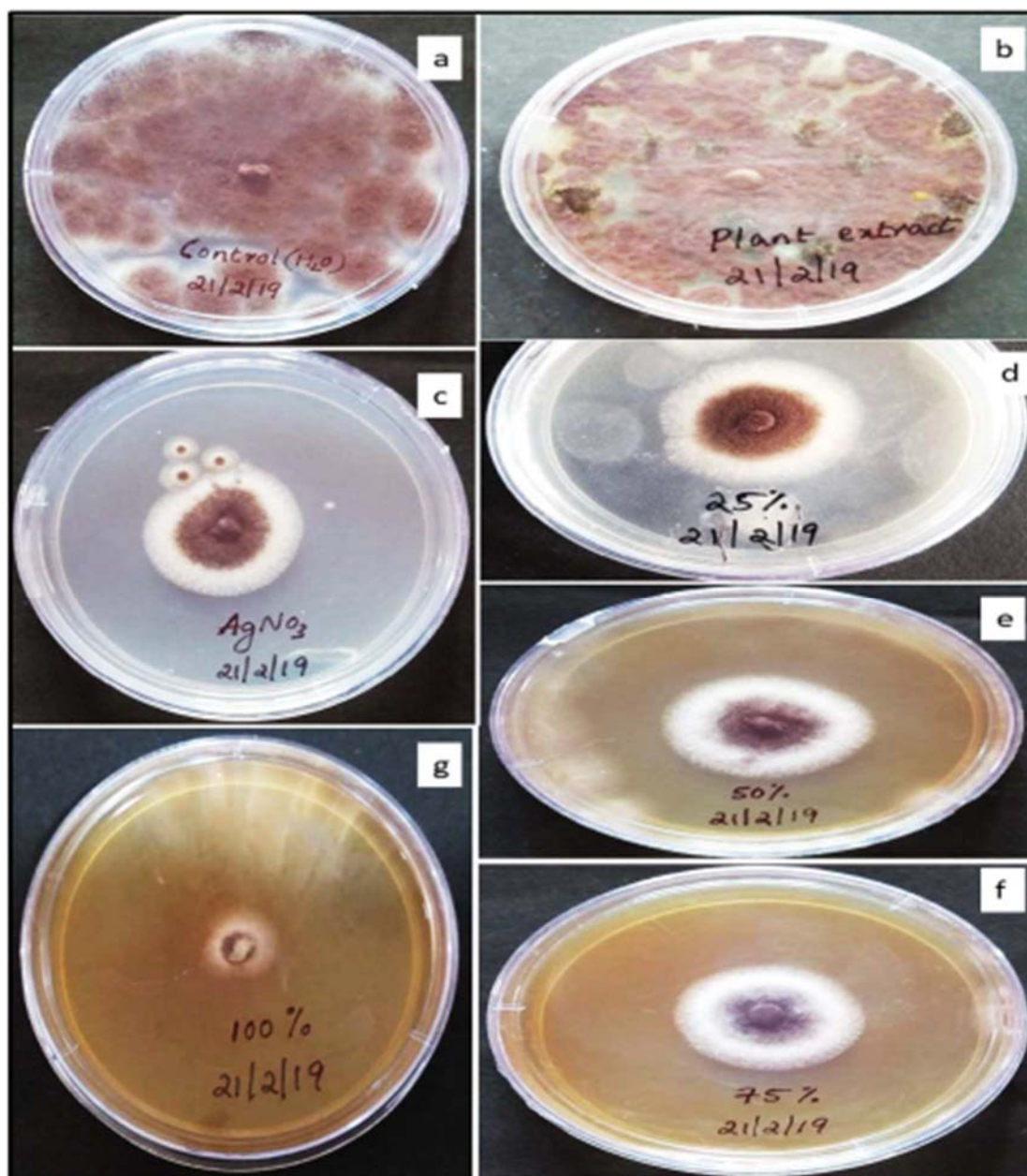
Fig. 4.18a Antifungal activity (a) control, (b) plant extract, (c) silver nitrate , (d-f) various concentrations of synthesized silver nanoparticles

4.7.2 In Silico molecular docking

In silico molecular docking was performed to further substantiate the antifungal activity of the synthesized silver nanoparticles. The 13 ligands were docked against the protein isocitrate lyase (PDB ID: 1dqu). Based on the binding energy formed between the ligands and the target protein molecule the lead ligand was selected. The binding energy and inhibition constant of the 13 ligands with the protein

1DQU is represented in Table 4.15. The lead ligand identified for the protein was Curcumenolactone C. The interaction between 1dqu and Curcumenolactone C showed a single H-bond interaction with ILE 443, which is part of the active site residue complex. Non-bonded Vander Waals interactions were also observed with active site residues. The interaction diagram (Fig. 4.18b) revealed all the interactions were within the active site of the protein indicating correct binding pose for the ligand in the binding region. This helps the ligand to carry out the designated function. The protein ligand bound complex visualized using Pymol (Fig. 4.18c) also shows the buried ligand in the active site of the targets. The results confirm that the selected compounds possess inhibitory potential, which can be considered for further analysis.

Table 4.15 The binding energy formed between all the ligand molecule and the protein target- 1DQU

| Sl No:	Phytochemical	Run	Binding energy (kcal/mol)	Inhibition constant
1.	**Curcumenolactone C**	**3**	**-7.01**	**7.26 µM**
2.	Curdione	1	-6.98	7.59 µM
3.	Curcolone	3	-6.78	10.80 µM
4.	Furanogermenone	4	-6.61	14.33 µM
5.	Zedoarondiol	6	-6.23	26.97 µM
6.	Procurcumadiol	1	-6.17	30.10 µM
7.	Epicurzerenone	4	-6.11	32.97 µM
8.	Glechomafuran	6	-5.85	51.56 µM
9.	Zedoarolide B	1	-5.78	58.17 µM
10.	Curzerene	1	-5.73	63.56 µM
11.	Glycerolpalmitate	9	-4.00	1.17 mM
12.	Dihydrosphingosine	10	-3.51	2.66 mM
13.	Glycerylmonostearate	7	-3.45	2.96 mM
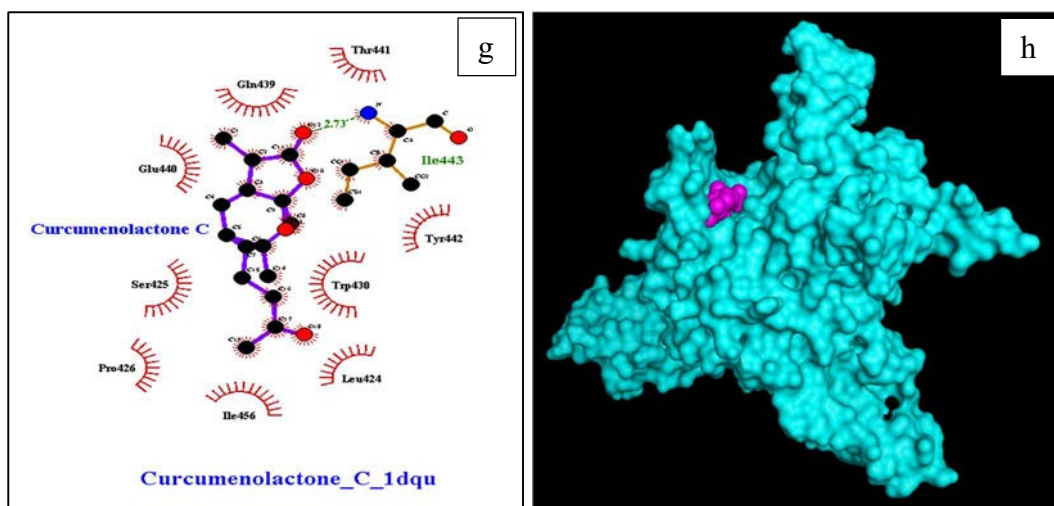
Fig. 4.18 (g) Interaction diagram (h) protein ligand bound complex of Curcumenolactone C and 1dqu

4.8 In Vitro Antioxidant Assay of AgNPs

4.8.1 DPPH free radical scavenging activity

DPPH radical scavenging activity of *Curcuma aromatica* rhizome extract, *Curcuma zathorrhiza* rhizome extract, CAAgNPs, CZAgNPs and standard quercetin are presented in Fig. 4.19. The half inhibition concentration (IC 50) of CA, CZ, CAAgNPs, CZAgNPs and quercetin were 25.49, 45.64, 50.46, 61.11 and 57.95 μg / ml respectively**.** Both the silver nanoparticles exhibited a significant dose dependent inhibition of DPPH activity as compared to their corresponding CA and CZ aqueous extracts. The potential of quercetin to scavenge DPPH radical was directly proportional to the concentrations. The dose dependent increase in the DPPH radical scavenging activity of the synthesized silver nanoparticles was near to the standard quercetin. The DPPH activity of CA and CZ was comparatively low when compared to the standard.

The antioxidant activity in general refers to the inhibition of the oxidation of molecules. The oxidation process is achieved by inhibiting the initiation step of the oxidative chain reactions and formation of non – reactive stable radicals (Kumar *et*

al., 2016). The polyphenols and flavonoid compounds possess strong antioxidant activity and protect the cells against oxidative stress caused by the reactive oxygen species.
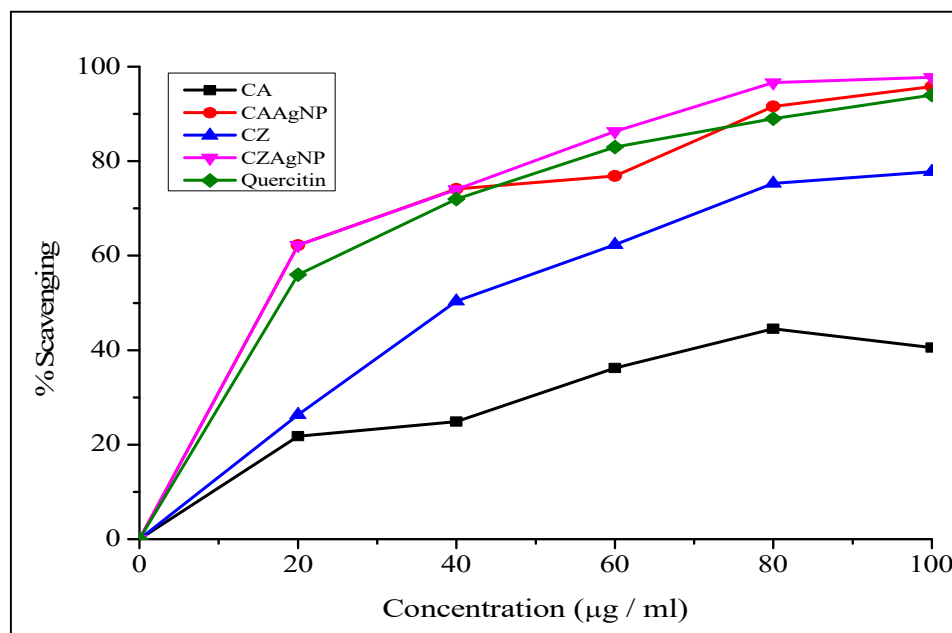

Fig. 4.19 DPPH assay of rhizome extracts and as synthesized silver nanoparticles

The total phenolic content of the CZAgNPs and CAAgNPs were quantified using the Folins'-Ciocalteau method described in section 3.3.2. The total phenolic content of the CZAgNPs and CAAgNPs were 19.51 mg / g GAE and 17.67 mg / g GAE respectively. Moreover, the results substantiates that the synthesized nanoparticles exhibited comparatively higher antioxidant property than their respective rhizome extracts (CZ with 46.25 mg / g GAE and CA with 46.25 mg / g GAE). The antioxidant activity of CZAgNPs and CAAgNPs were comparable to that of the standard quercitin. Hence the higher activity of the synthesized silver nanoparticles can be ascribed to the silver ions and also the phenolic compounds present on the surface of the nanoparticles. This brings about the fact that the synthesized silver nanoparticles are good radical scavengers. Therefore due to their

scavenging property, the CZAgNPS and CAAgNPs as antioxidants can be used in the management of neurogenerative diseases, AIDS and cancer (Antony *et al*., 2013).

4.9 In Vitro Cytotoxicity Assay of AgNPs

4.9.1 Trypan Blue Exclusion Method

The short term *in vitro* cytotoxicity of CZAgNPs and CAAgNPs was studied in both DLA and EAC cell lines and compared with normal cells (spleen cells). The transparent viable cells and stained dead cells were counted using hemocytometer. The percentage cytotoxicity exhibited by the CZAgNPs, CAAgNPs, plant rhizome extracts (CZ and CA) and silver nitrate solution on DLA, EAC and normal cell lines are presented in Table 4.16, 4.17.

The plant rhizome extracts (CZ and CA), CZAgNPs, CAAgNPs and silver nitrate solution exhibited a dose-dependent cell death in both DLA and EAC cell lines. The IC 50 value of the CZ, CA, CZAgNPs, CAAgNPs and silver nitrate solution in DLA cells was determined to be 90.13 ± 0.31 μg / ml, 325.95 ± 0.21 μg / ml, 1.67 ± 1.2 μg / ml, 1.4 ± 0.7 μg / ml and 0.494 ± 0.72 μg / ml respectively. In EAC cell lines the IC 50 value was observed to be 50.23 ± 0.89 μg / ml, 135.02 ± 0.36 μg / ml, 1.84 ± 0.12 μg / ml, 1.634 ± 0.34 μg / ml and 0.513 ±0.19 μg / ml for the CZ, CA, CZAgNPs, CAAgNPs and silver nitrate solution respectively. The CZAgNPs inhibited 93.75 ± 0.12 % of DLA cells and 91.4 ± 0.34 % EAC cells lines at a concentration of 2.5 μg / ml and 3 μg / ml respectively. A percentage of 23.38 ± 0.13 % of DLA cells and 89.66 ± 0.46 % of EAC cells were inhibited by 2.5 μg / ml and 3 μg / ml concentrations of CAAgNPs respectively.

In vitro cytotoxicity assay was conducted in normal cells. The IC 50 value of 0.706 ± 0.23 µg / ml, 8.911 ± 0.51 µg / ml, 4.45 ± 0.07 µg / ml, 8.93 ± 0.31 mg / ml and 6.85 ± 0.61 mg / ml for silver nitrate, CAAgNPs, CZAgNPs, CA and Cz respectively were observed for normal cells.

The short term *in vitro* toxicity of the CZAgNPs and CAAgNPs evaluated using Trypan Blue Exclusion method revealed a dose dependent increase in the inhibition of both DLA and EAC cells. Moreover, the cancer cell lines (DLA and EAC) were more sensitive to CZAgNPs and CAAgNPs than the spleen cell lines. The most striking result to emerge from the data is that compared to CAAgNPs, the CZAgNPs exhibited efficient inhibition towards the growth and proliferation of DLA and EAC cell lines. Whereas, the CAAgNPs showed remarkable activity only towards the EAC cell lines. It has been reported that 200 µg / ml of AgNPs synthesized using extracts of *Ficus hispida*, *Halymenia porphyroids* and *Colpomenia sinusa* inhibited the DLA and EAC cells completely (Dr Vishnu Kiran Manam, 2014; Kanagamani *et al*., 2018). Kanagamani *et al*., (Krishnaswamy Kanagamani *et al*., 2019) reported that 50 µg / ml of curcumin (standard) is required for the inhibition of 98.07 % DLA cell lines. Interestingly, in our study 2.5 µg / ml and 3 µg / ml of CZAgNPs is sufficient to inhibit 97.99 ± % DLA and 91.4 ± % EAC cells respectively. The CAAgNPs inhibited 89.66 % of EAC cells at a concentration of 3 µg / ml. These findings validated that low doses of CZAgNPs and CAAgNPs can effectively inhibit the viability and proliferation of both DLA and EAC cell lines and higher concentrations might induce some toxicity in the normal spleen cells.

Table 4.16 Comparison of percentage cytotoxicity of CZAgNPs, CAAgNPs, CZ, CA and silver nitrate solution against DLA cell lines

Concentration	Percentage cytotoxicity (%)		IC_{50} value	
(μg / ml)			(μg / ml)	
	CZAgNPs	CAAgNPs	CZAgNPs	CAAgNPs
0.2	2.42 ± 0.12	15.2 ± 0.31		
0.6	6.95 ± 0.21	21.56 ± 0.40		
0.8	13.65 ± 0.13	20.39 ± 0.57	1.67 ±1.2	1.4 ± 0.7
1.0	18.74 ± 0.17	27.97 ± 0.20		
1.6	34.17 ± 0.07	29 ± 0		
2.5	93.75 ± 0.12	23.38 ± 0.13		
	CZ	CA	CZ	CA
10	4.42 ± 0.13	7.61 ± 0.27		
25	7.62 ± 0.21	8.46 ± 0.32		
35	19.41 ± 0.31	9.01 ± 0.27	90.13 ± 0.31	325.95 ± .021
55	21.15 ± 0.42	7.54 ± 0.10		
75	42.35 ± 0.56	10.28 ± 0.07		
100	62.5 ± 0.13	13.71 ± 0.07		
	AgNO$_3$			
0.2	6.91 ± 0.31			
0.4	13.34± 0.21			
0.5	53.94 ± 0.46			
0.6	76.74 ± 0.59		0.494 ± 0.72	
0.8	83.2 ± 0.17			
1	95.68 ± 0.07			

Values are expressed as Mean ± SD; n = 3

Table 4.17 Comparison of percentage cytotoxicity of CZAgNPs, CAAgNPs, CZ, CA and silver nitrate solution against EAC cell lines

Concentration (μg / ml)	Percentage cytotoxicity (%)		IC_{50} value (μg / ml)	
	CZAgNPs	CAAgNPs	CZAgNPs	CAAgNPs
1.0	14.39 ± 0.13	24.457 ± 0.21		
1.6	23.48 ± 0.71	48.5 ± 0.32		
1.8	35.28 ± 0.07	55.07 ± 0.16	1.84 ± 0.12	1.634 ± 0.34
2.0	53.30 ± 0.61	67.82 ± 0.21		
2.5	83.87 ± 0.71	76.49 ± 0.34		
3.0	91.4 ± 0.34	89.66 ± 0.46		
	CZ	CA	CZ	CA
10	17.17 ± 0.21	15.2 ± 0.56		
25	15.42 ± 0.34	21.56 ± 0.72		
35	33.78 ± 0.12	25.3 ± 0.16	50.23 ± 0.89	135.02 ± 0.36
55	41.24 ± 0.70	27.97 ± 0.32		
75	79.3 ± 0.06	29 ± 0		
100	96.34 ± 0.12	23.38 ± 0.26		
	$AgNO_3$			
0.2	7.66 ± 0.21			
0.4	49.40 ± 0.32			
0.5	63.10 ± 0.12		0.513 ± 0.29	
0.6	70.46 ± 0.16			
0.8	78.85 ± 0.17			
1	80.34 ± 0.08			

Values are expressed as Mean $\pm$ SD; n = 3

4.9.2 MTT Assay

In vitro cytotoxicity of the synthesized silver nanoparticles (CZAgNPs, CAAgNPs) was screened against MCF -7 cell lines (breast cancer cell lines). The silver nanoparticles were found to reduce the viability of the cells in a dose dependent manner. The IC 50 value of CZAgNPs and CAAgNPs were 42.48 ± 0.53 μg / ml and 41.28 ± 0.68 μg / ml respectively. The viability of the cells was found to decrease in a dose dependent manner. Both the plant extracts (CZ and CA) did not show appreciable cytotoxicity. The plant rhizome extracts did not inhibit the viability of MCF-7 cells. The rhizome extracts CA and CZ inhibited only 26.1 ± 0.38 % and 21.2 ± 0.46 % of MCF -7 cells at a concentration of 100 μg / ml. The percentage of inhibition of MCF -7 cell lines by the treatment with various concentrations of CA, CZ, CAAgNPs, and CZAgNPs are given in Table 4.18. The synthesized silver nanoparticles, CZAgNPs, CAAgNPs (100 μg / ml) inhibited 96.6 ± 0.07 % and 97.7 ± 0.06 % percentage of the MCF -7 cell lines respectively (Fig.4.20a, 4.20b, 4.20c, 4.20d).

Table 4.18 Comparison of percentage inhibition of MCF -7 cell lines by CZAgNPs, CAAgNPs, CZ, CA

Concentration (μg / ml)	Percentage of inhibition (%)			
	CZAgNPs	CAAgNPs	CZ	CA
12.5	31.95 ± 0.52	46.2 ± 0.61	3.8 ± 0.1	2.9 ± 0.13
25	52.85 ± 0.36	53.1 ± 0.32	12.3 ± 0.34	6.3 ± 0.26
50	82.35 ± 0.71	81.1 ± 0.21	14.9 ± 0.27	13.6 ± 0.34
75	90 ± 0.31	95.6 ± 0.10	19.1 ± 0.19	19.7 ± 0.29
100	$96.6 \pm 0.07*$	$97.7 \pm 0.06*$	26.1 ± 0.36	21.2 ± 0.46

Values are expressed as Mean ± SD; n = 3 * p-value less than 0.05, significant value
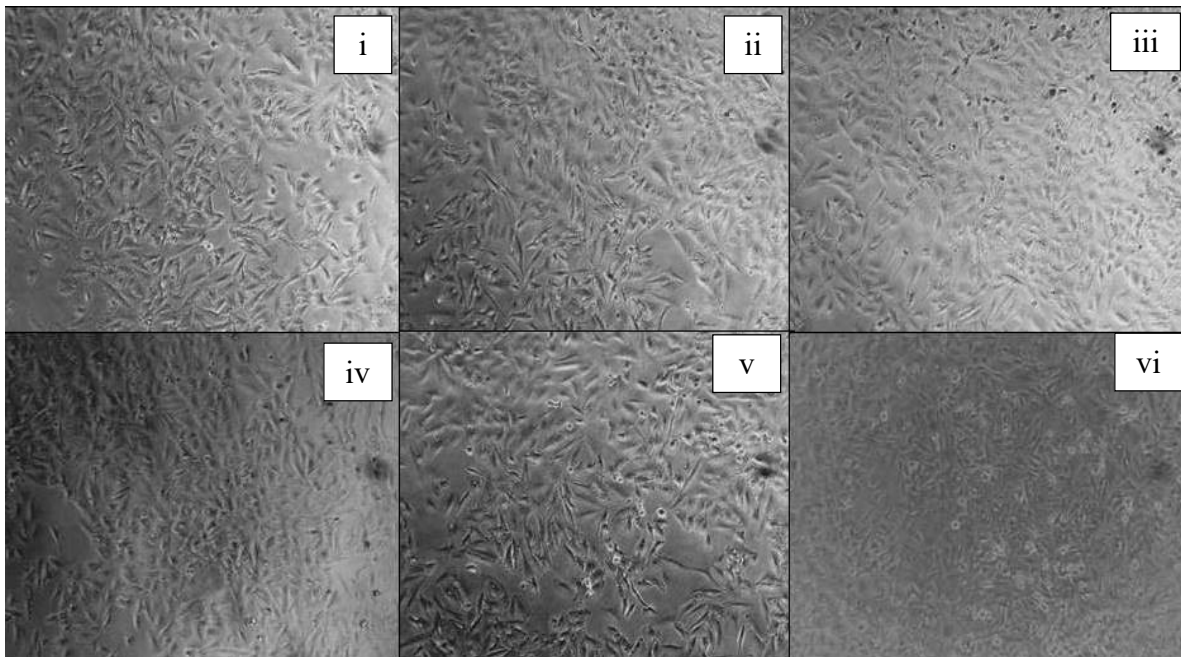

Fig 4.20 (a) MTT assay of MCF -7 cell lines against various concentrations of CZ (i) 12.5 µg / ml (ii) 25 µg / ml (iii) 50 µg / ml (iv) 75 µg / ml (v) 100 µg / ml (vi) control
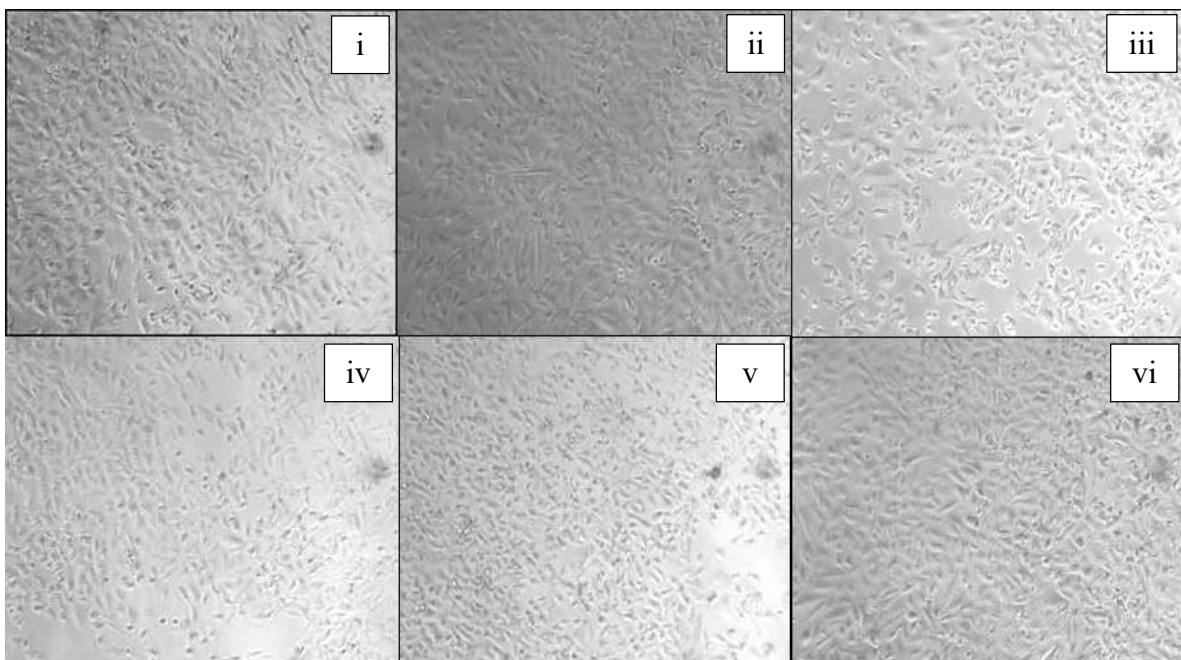

Fig 4.20 (b) MTT assay of MCF -7 cell lines against various concentrations of CA (i) 12.5 µg / ml (ii) 25 µg / ml (iii) 50 µg / ml (iv) 75 µg / ml (v) 100 µg / ml (vi) control

Fig 4.20 (c) MTT assay of MCF -7 cell lines against various concentrations of CZAgNPs (i) 3.125 µg / ml (ii) 6.12 µg / ml (iii) 12.5 µg / ml (iv) 25 µg / ml (v) 50 µg / ml (vi) 75 µg / ml (vii) 100 µg / ml (viii) control
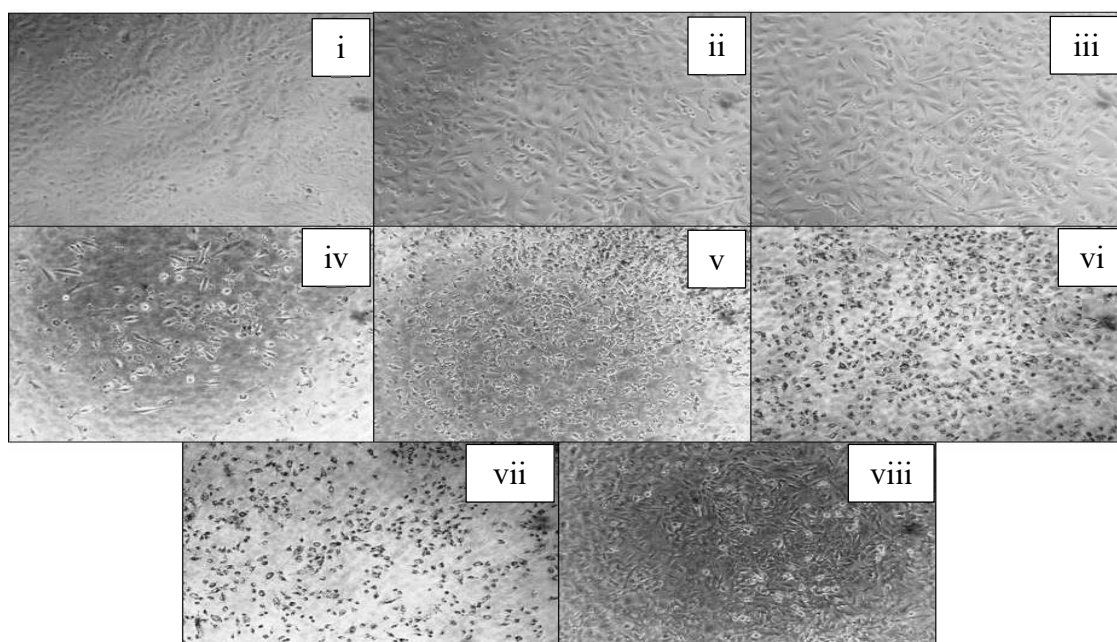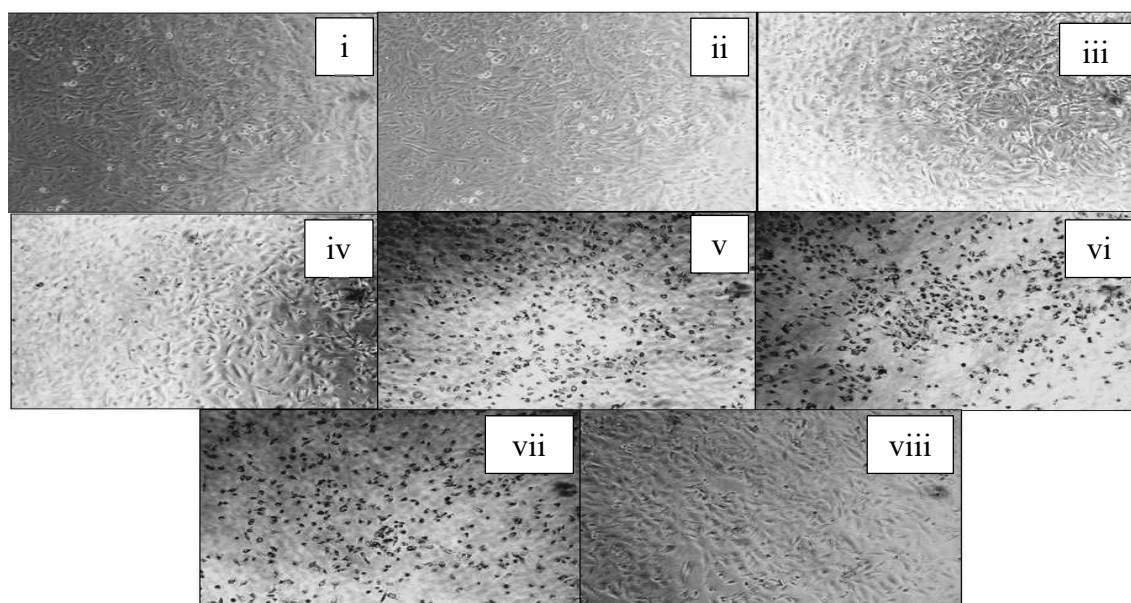

Fig 4.20 (d) MTT assay of MCF -7 cell lines against various concentrations of CAAgNPs (i) 3.125 µg / ml (ii) 6.12 µg / ml (iii) 12.5 µg / ml (iv) 25 µg / ml (v) 50 µg / ml (vi) 75 µg / ml (vii) 100 µg / ml (viii) control

From the study, it is understood that the MCF -7 cells treated with CZAgNPs, CAAgNPs, CZ and CA exhibited morphological changes including rounding off of

the cells, detachment of the cells from the surface and accumulation of cells. Whereas the untreated MCF – 7 cells had intact cell membrane and high confluency. The disruption of mitochondrial respiratory chain, leading to the production of ROS and inhibiting the ATP synthesis might be the mechanism involved in causing DNA damage to the synthesized AgNPs treated MCF cell lines (Sathishkumar *et al*., 2016). In addition, it was reported that the AgNPs inhibits MCF - 7 cell lines by down regulating the mRNA level of anti - apoptotic Bcl 2 and up regulating the expression of tumor suppressor (p53) gene, and subsequently increasing the activity of pro apoptotic proteins like Bax, caspase 3, 9 (Jeong *et al*., 2008).

Many reports showed the AgNPs are effective against various cancer cell lines lines Hep G2 (Sivakumar *et al*., 2020), MCF -7 (Remya, Rajasree, Aranganathan, & Suman, 2015), HeLa cells (Moteriya & Chanda, 2020), etc. The IC 50 value of CZAgNPs and CAAgNPs against MCF-7 cell lines were in good agreement with that of Sathish kumar *et al*., (Sathishkumar *et al*., 2016) in which the IC 50 value was 42.5 µg / ml for AgNPs synthesized using *A. tenella* against MCF-7 cells.

The AgNPs synthesized from fruit of *Piper longum* exhibited effective toxicity against MCF –cell lines, in which the IC 50 value was 67 µg / ml at 24 h (Nakkala, Mata, Raja, Khub Chandra, & Sadras, 2018). Dose dependent cell viability of MCF – 7 cell lines with IC 50 value of 63.257 µg / ml for 48 h was observed when treated with AgNPs synthesized using *Eucalyptus teriticorins* (Kiran *et al*., 2020). Inexplicably the study confirmed that the potential of the CZAgNPs and CAAgNPs had remarkable anticancer activity and can be utilized in cancer therapy.

4.9.2.1 *In Silico* molecular docking of AgNPs

The interaction of the bound bioactive compounds (seen on the synthesized silver nanoparticles) with the receptors of cancer cell line (MCF -7) was studied using tool Auto Dock 4.2. The thirteen ligands capped in the AgNPs were docked against the target proteins of MCF -7. Human tyrosine protein kinase C- SRC (PDB ID: 2SRC) and CDK 2 with EGFR inhibitor compound 8 (PDB ID: 4RJ3). Procurcumadiol was identified as the lead molecule for both the target proteins based on the binding energies. The binding energy of Procurcumadiol to the protein 2SRC and 4RJ3 are ΔG = - 8.13 and ΔG = - 8.10 respectively (Table 4.19 and 4.20). The binding energies were higher for all the other ligand molecules docked. The binding energy was in the range - 4.69 to -8.13 for 2SRC protein interaction and - 4.30 to - 7.79 for 4RJ3 interaction with the selected bound bioactive compounds on AgNPs. Procurcumadiol formed 6 H-bond interactions with 2SRC in which three of them with active site residues.

Table 4.19 The binding energy formed between all the ligand molecule and the protein target- 2SRC

Sl no:	Phytochemical	Run	Binding energy (kcal/mol)	Inhibition constant
1.	**Procurcumadiol**	**2**	**-8.13**	**1.10 μM**
2.	Furanogermenone	2	-7.73	2.17 μ
3.	Curcolone	10	-7.57	2.83 μM
4.	Curdione	1	-7.40	3.78 μM
5.	Curcumenolactone C	1	-7.21	5.20 μM
6.	Zedoarondiol	10	-7.17	5.58 μM
7.	Curzerene	5	-7.06	6.67 μM
8.	Zedoarolide B	1	-6.99	7.54 μM
9.	Epicurzerenone	5	-6.71	12.03 μM
10.	Glechomafuran	9	-6.50	17.12 μM
11.	Dihydrosphingosine	4	-6.13	31.88 μM
12.	Glycerylmonostearate	5	-5.38	113.02 uM
13.	Glycerolpalmitate	8	-4.69	366.78 uM

Table 4.20 The binding energy formed between all the ligand molecule and the protein target- 4RJ3

Sl no:	Phytochemical	Run	Binding Energy (kcal/mol)	Inhibition constant
1.	**Furanogermenone**	**3**	**-7.79**	**1.96 μM**
2.	Zedoarondiol	6	-7.49	3.23 μM
3.	Curcumenolactone C	4	-7.42	3.66 μM
4.	Glechomafuran	3	-7.36	4.00 μM
5.	Curcolone	6	-7.25	4.87 μM
6.	Curdione	6	-7.00	7.43 μM
7.	Zedoarolide B	4	-6.91	8.64 μM
8.	Procurcumadiol	5	-6.70	12.25 μM
9.	Curzerene	5	-6.43	19.44 μM
10.	Epicurzerenone	7	-6.18	29.42 μM
11.	Dihydrosphingosine	1	-5.86	50.92 μM
12.	Glycerolpalmitate	1	-4.64	397.23 μM
13.	Glycerylmonostearate	7	-4.30	706.16 μM
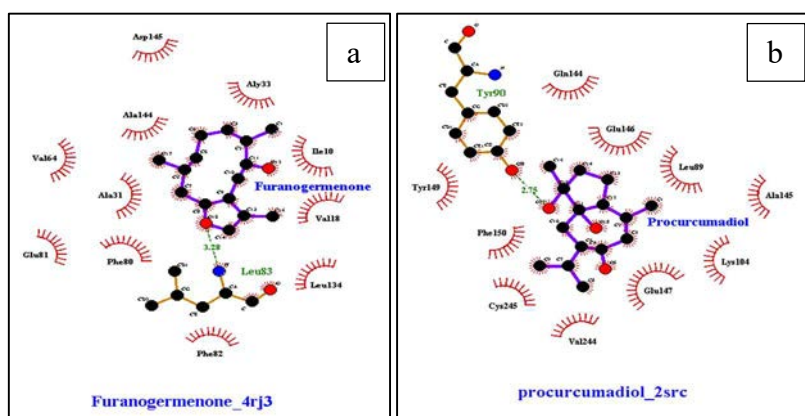
Fig. 4.21 (a) Interaction diagram of furanogermanone and 4rj3 protein (b) interaction diagram of procurcumadiol and 2src

Among the H-bonds, three were formed with GLN98. From docking it was understood that all the interactions of furanogermenone were within the active sites of the protein 4RJ3. This is evident in the interaction diagram shown in Fig. 4.21a, 4.21b. This ensures correct binding pose for the ligand thereby helps the ligand to carry out the designated function. The buried ligand in the active site of the targets of the protein ligand bound complex was also visualized using Pymol (Fig. 4.21c, 4.21d). The results confirm the inhibitory

potential of the selected compounds which can be considered for further analysis.

Fig. 4.21 Protein ligand complex of (c) furanogermanone and 4rj3 protein (d) procurcumadiol and 2src
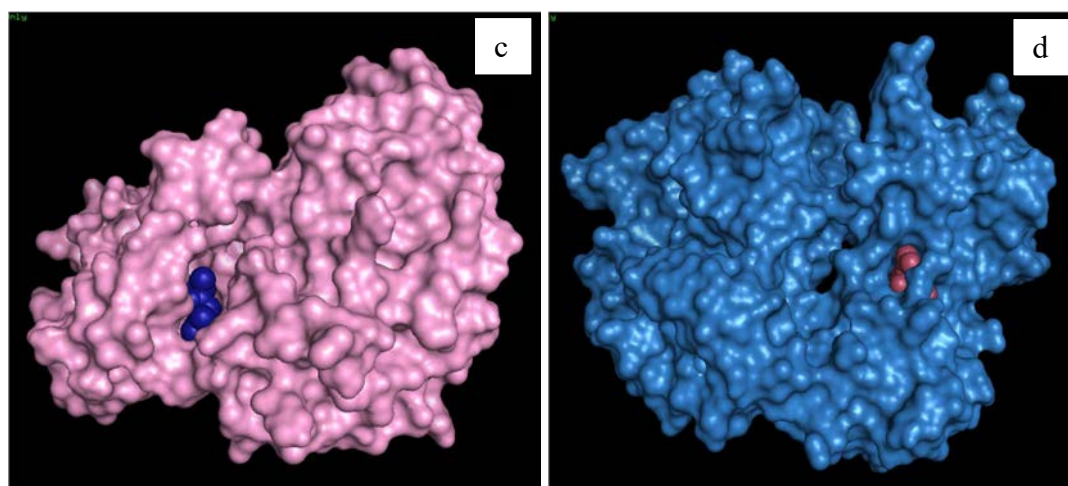
Out of the 13 ligand molecules docked with the selected proteins targeting the MCF - 7 cell lines *i.e.*, 4RJ3 (CDK 2 EGFR inhibitor) and 2 SRC (Human Tyrosine protein kinase), it was observed that furanogermanone and procurcumadiol exhibited strong interactions within the active sites of respective proteins. This was identified from the lowest binding energies exhibited from their interactions. Higher the negative value more the binding affinity (Pushpalatha, Selvamuthukumar, & Kilimozhi, 2017). The binding of furanogermanone to 4RJ3 protein and procurcumadiol to 2SRC might aid in inhibiting the proliferation of breast cancer. Hence the observed inhibition of MCF - 7 cell lines by the synthesized silver nanoparticles could be further substantiated by the fact that the ligand molecule could bind to the active site of the protein thereby inhibiting cell proliferation.

4.10 In Vivo Toxicity Analysis of AgNPs

Based on the *in vitro* cytotoxicity evaluation of both the synthesized silver nanoparticles, CZAgNPs were selected for the *in vivo* studies. Despite the application

of silver nanoparticles as antimicrobial agents and in the cancer treatment, it is important to monitor the oral toxicity of the synthesized silver nanoparticles. This will in turn provide safety information regarding the CZAgNPs and also safe doses for the study. The results regarding the safety evaluation of CZAgNPs after a single and 28 days of consecutive oral administration of the drug are given below.

4.10.1 Acute toxicity

Oral administration of single dose of CZAgNPs (500 mg / kg b. wt) to both the sexes, followed by monitoring animals continuously for 14 days did not show any adverse morphological changes in the treated groups. The animals did not show any toxic signs like, changes in skin and fur, behavioural pattern, diarrohea, breathing difficulty, salivation, coma, tremors and postural abnormalities. Necropsy of the treated animals did not show any changes in the size, colour, and texture of internal organs when compared to control groups in both males and females. The change in body weight, feed consumption and water intake of both the sexes of animals administered with CZAgNPs are given in Table 4.21, 4.22, 4.23.

Table 4.21 Percentage change in body weight of mice in acute oral toxicity test

Acute toxicity - Body weight change (500 mg / kg b. wt)			
Body Weight (g)	Sex	Control	CZAgNP
Initial Weight	Male	28.23 ± 2.1	26.67 ± 1.1
	Female	22.73 ± 0.6	25.1 ± 1.1
Final Weight	Male	31.17 ± 2.3	27.30 ± 0.9
	Female	23.87 ± 0.8	24.97 ± 2.0
% Change in Weight	Male	13.61 ± 4.4	2.4 ± 1.6
	Female	4.98 ± 1.3	-2.85 ± 0.5*

Values are expressed as mean ± SEM (n=5) by two way ANOVA followed by Dunnett's multiple comparisons test. *$p < 0.05$ as significance

Table 4.22 Feed consumption of mice in acute oral toxicity test

Acute toxicity - Feed Consumption (500 mg / kg b.wt)			
Week	Sex	Control	CZAgNP
I	Male	13.23 ± 1.45	7.1 ± 3.55
	Female	12.07 ± 2.42	9.37 ± 1.57
II	Male	16.49 ± 2.15	16.14 ± 5.52
	Female	13.44 ± 4.37	13.14 ± 4.30

Values are expressed as mean ± SEM (n=5) by two way ANOVA followed by Dunnett's multiple comparisons test. *$p < 0.05$ as significance

Table 4.23 Water consumption of mice in acute oral toxicity test

Acute toxicity - Water Consumption (500 mg / kg b. wt)			
Week	Sex	Control	CZAgNP
I	Male	15.86 ± 5.73	13.43 ± 7.25
	Female	12 ± 2.45	8.57 ± 1.62
II	Male	16.14 ± 5.52	21.14 ± 4.56
	Female	8.57 ± 1.62	9.71 ± 6.42

Values are expressed as mean ± SEM (n=5) by two way ANOVA followed by Dunnett's multiple comparisons test. *$p < 0.05$ as significance
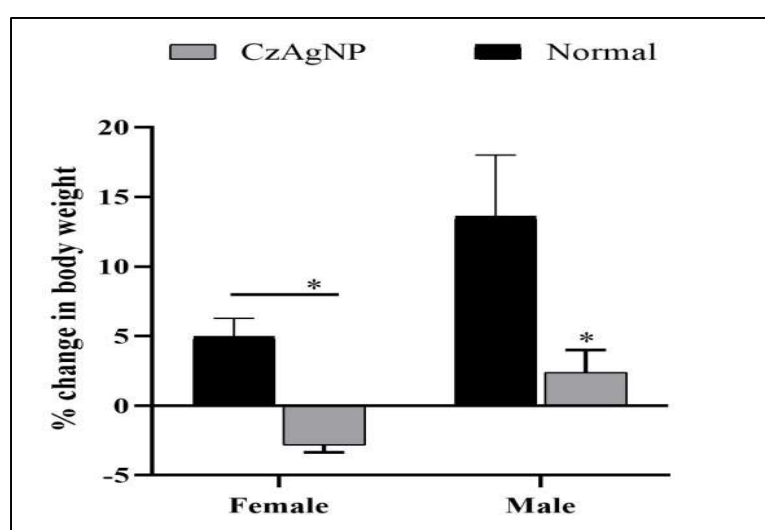

Fig. 4.22 Percentage change in body weight of the animals treated with 500 mg / kg bwt of CZAgNPs. Values are expressed as mean ± SEM (n=5) by two way ANOVA followed by Dunnett's multiple comparisons test. *$p < 0.05$ as significance

There was gradual decrease in body weight of the CZAgNPs treated group as compared to the control group. The percentage changes in body weight of the CZAgNPs treated groups were significantly different as compared with the control mice at $p < 0.05$ in females (Fig. 4.22).
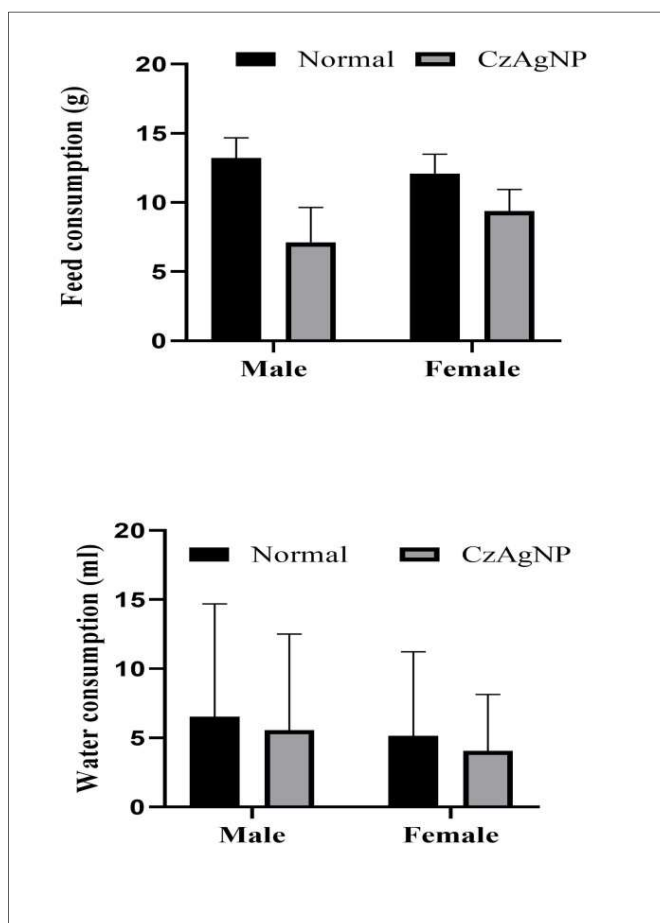
Fig. 4.23 Feed and water consumption of the animals treated with 500 mg / kg bwt of CZAgNPs. Values are expressed as mean ± SEM (n=5) by two way ANOVA followed by Dunnett's multiple comparisons test. *p<0.05 as significance

The food consumption of the CZAgNPs treated groups did not significantly differ in both the sexes as compared to the control group measured throughout the study ($p > 0.05$). Similarly the intake of water in the groups treated with CZAgNPs did not differ significantly as compared to the control group in both the sexes as measured throughout the study ($p > 0.05$). During the first week after the administration of single dose (500 mg / kg b. wt) CZAgNPs there was a decrease in

the intake of feed and water in both females and males as compared to the control group. But this pattern changed during the second week and the feed and water consumption of the treated group was comparable to that of the normal animals. No animals were found dead under the given dose (Fig. 4.23).

4.10.2 Sub – acute toxicity

The general behavior and conditions of the animals treated with three different doses of CZAgNPs [50 mg / kg b. wt (low dose), 75 mg / kg b. wt (medium dose) and 100 mg / kg b. wt (high dose)] did not vary in both the sexes of animals, when compared to the control group. All the treated animals were found to be healthy. The animals did not show any signs of weakness, lethargy, self-isolation and heavy breathing for the entire experimental period (28 days). The necropsy of the drug treated animals done after the treatment did not show any pathological abnormalities in any of the CZAgNP treated groups (Fig 4.24).
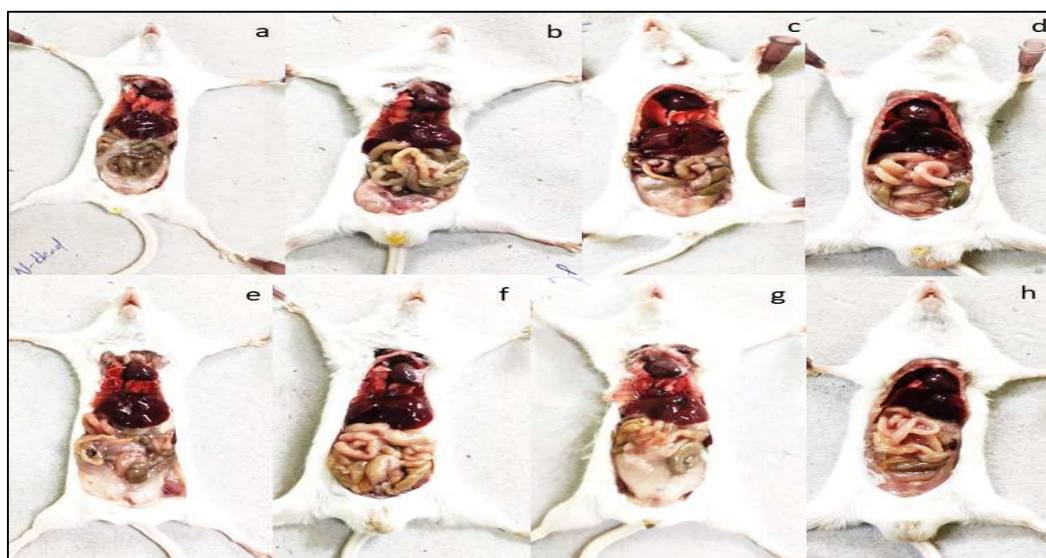

Fig. 4.24 Gross anatomy of swiss albino mice (a) Normal female, (b) Normal male, (c) High dose female, (d) High dose male, (e) Medium dose female, (f) Medium dose male, (g) Low dose female, (h) Low dose male

The water intake and feed consumption of all the animals in the treated groups did not show any significant change when compared with the animals in the untreated groups for the entire experimental period of 28 days. In animals treated with low dose (50 mg / kg b. wt) and medium dose (75 mg / kg b. wt) of CZAgNPs, there was decrease in water and feed intake but the change was non-significant (p > 0.05) when compared to the control group (Table 4.24, 4.25).

Table 4.24 Feed consumption of mice in sub-acute oral toxicity test

Sub-Acute toxicity – Feed Consumption (g)				
Week	Sex	Control	CZAgNP Low Dose (50 mg / kg b. wt)	CZAgNP Medium Dose (75 mg / kg b. wt)	CZAgNP High Dose (100 mg / kg b.wt)
I	Males	13 ± 3.21	11.6 ± 2.02	9 ± 2.15	16.5 ± 5.44
	Females	8.27 ± 1.11	11.6 ± 2.02	10.97± 1.40	8.01 ± 1.12
II	Males	16.53 ± 1.17	11.06 ± 1.28	14.49 ± 3.22	20.17 ± 3.89
	Females	9.73 ± 0.66	11.20 ± 1.97	9.37 ± 1.68	9.87 ± 1.67
III	Males	12.46 ± 2.21	10.40 ± 1.78	9.36 ± 2.24	17.74 ± 2.90
	Females	9.49 ± 1.63	7.81 ± 2.98	13.36 ± 1.83	9.63 ± 0.73
IV	Males	14.21 ± 2.61	9.96 ± 1.87	8.93 ± 1.11	18.60 ± 3.15
	Females	9.16 ± 1.33	7.83 ± 1.69	13.20 ± 1.65	9.10 ± 2.56

Values are expressed as mean ± SEM (n=5) by one way ANOVA followed by Dunnett's multiple comparisons test. *p<0.05 as significance

Table 4.25 Water consumption of mice in sub-acute oral toxicity test

Sub-Acute toxicity - Water Consumption (ml)				
Week	Sex	Control	CZAgNP Low Dose (50 mg / kg b.wt)	CZAgNP Medium Dose (75mg / kg b.wt)	CZAgNP High Dose (100 mg / kg b.wt)
I	Males	13.14 ± 4.49	8.86 ± 3.24	7.71 ± 2.93	11.86 ± 3.89
	Females	8.86 ± 2.12	9 ± 2.08	11.29 ± 1.80	6.29 ± 1.38
II	Males	15.14 ± 1.68	8 ± 2.38	10.29 ± 2.50	15.43 ± 2.07

Contd.

	Females	9 ± 1.29	8.71 ± 1.25	12.29 ± 1.25	7.86 ± 1.77
III	Males	19 ± 5.64	9 ± 2.83	8 ± 2.12	17 ± 4.44
	Females	6.57 ± 1.13	6.57 ± 2.30	11 ± 0.82	6.57 ± 0.79
IV	Males	15 ± 2.98	8 ± 2.58	7 ± 1.15	17 ± 4.31
	Females	8.14 ± 1.86	6.29 ± 1.50	12.43 ± 1.99	7.14 ± 2.27

Values are expressed as mean ± SEM (n=5) by one way ANOVA followed by Dunnett's multiple comparisons test. *p<0.05 as significance

4.10.2.1 Relative Organ Weight

After necropsy, the vital organs of all the animals were taken. The organs included brain, heart, lungs, liver, kidney, stomach, testis and ovary. The organs were weighed and the relative organ weight for all the animals (both treated and untreated) were calculated and tabulated in Table 4.26. There was no change in the organ weight of the vital organs incised from the animals with respect to the body mass of the animals treated orally with low, medium and high dose of CZAgNPs when compared with the normal, untreated animals.

Table 4.26 Relative organ weight of mice in sub-acute oral toxicity test

Sub - Acute toxicity - Relative Organ Weight (g %)					
Organ	Sex	Control	CZAgNP Low Dose (50 mg / kg b. wt)	CZAgNP Medium Dose (75mg / kg b. wt)	CZAgNP High Dose (100 mg / kg b. wt)
Brain	Male	1.24 ± 0.43	1.49 ± 0.25	1.37 ± 0.29	1.07 ± 0.28
	Female	1.57 ± 0.20	1.66 ± 0.05	1.59 ± 0.11	1.54 ± 0.20
Heart	Male	0.45 ± 0.08	0.44 ± 0.02	0.50 ± 0.05	0.48 ± 0.02
	Female	0.45 ± 0.02	0.48 ± 0.04	0.47 ± 0.06	0.46 ± 0.08
Lungs	Male	0.49 ± 0.03	0.66 ± 0.06	0.83 ± 0.13	0.58 ± 0.05
	Female	0.57 ± 0.01	0.94 ± 0.17	0.76 ± 0.18	0.67 ± 0.13
Liver	Male	4.50 ± 0.31	3.57 ± 0.82	3.36 ± 0.44	4.07 ± 0.43
	Female	4.19 ± 0.14	4.22 ± 0.36	4.21 ± 0.39	3.85 ± 0. 24
Kidney	Male	1.23 ± 0.19	1.12 ± 0.32	1.01 ± 0.35	1.12 ± 0.43

Contd.

		Control	Low Dose	Medium Dose	High Dose
	Female	1.04 ± 0.09	1.39 ± 0.58	1.02 ± 0.09	1.04 ± 0.07
Stomach	Male	0.68 ± 0.03	0.87 ± 0.12	0.87 ± 0.09	0.78 ± 0.12
	Female	0.86 ± 0.12	1 ± 0.16	0.80 ± 0.11	0.92 ± 0.05
Testis	Male	0.06 ± 0.00	0.08 ± 0.01	0.10 ± 0.4	0.08 ± 0.02
Ovary	Female	0.05 ± 0.02	0.09 ± 0.03	0.08 ± 0.03	0.08 ± 0.01

Values are expressed as mean ± SEM (n=5) by one way ANOVA followed by Dunnett's multiple comparisons test. *$p<0.05$ as significance

4.10.2.2 Hematological parameters

Various hematological parameters like, Hb, RBC, PLT and TC was measured in males and females treated with low, medium and high dose of CZAgNPs (Table 4.27). The hematological parameters were compared with that of the control group. There was no significant change in the Hb of all the treated animals.

Table 4.27 Hematological parameters of mice in sub-acute oral toxicity test

Sub-Acute toxicity - Hematological parameters					
Parameters	Sex	Control	CZAgNP Low Dose (50 mg / kg b.wt)	CZAgNP Medium Dose (75mg / kg b.wt)	CZAgNP High Dose (100 mg / kg b.wt)
Hb	Males	15.1 ± 0.61	13.8 ± 0.70	14.6 ± 0.84	12.75 ± 1.48
(g /dl)	Females	14.8 ± 0.78	15.5 ± 0.57	14.25 ±1.20	14.35 ± 0.07
RBC	Males	7.7 ± 0.70	7.25 ± 0.70	8 ± 0.70	7.35 ± 1.06
(10^6)	Females	7.8 ± 0.86	8.9 ± 0.14	8.05 ± 0.92	8.05 ± 0.21
PLT	Males	7.5 ± 0.32	8.8 ± 1.55	8.55 ± 0.49	11.4 ± 0.56
(10^6)	Females	10.5 ± 0.75	10.25 ± 1.63	11.8 ± 0.85	13.2 ± 0.14
TC	Males	6500 ± 0.70	8700 ± 0	6600 ± 141.42	7750 ± 70.71
(mm^3)	Females	6400 ± 182.3	8400 ± 989.95	9050 ± 777.82	10100 ± 141.42

Values are expressed as mean ± SEM (n=5) by one way ANOVA followed by Dunnett's multiple comparisons test. *$p<0.05$ as significance

The values obtained were well within the normal range for all 3 groups of both males and females. Similarly, there was no change in the RBC count for all the treatment groups. The RBC count of normal males and females were $7.7 ± 0.70 \times 10^6$ and $7.8 ±$

0.86×10^6 respectively. The platelet count was slightly high for both males and females treated with high dose of CZAgNPs. The values were $13.2 \pm 0.14 \times 10^6$ and $11.4 \pm 0.56 \times 10^6$ respectively. The platelet count of normal females was $10.5 \pm 0.14 \times 10^6$ whereas $7.5 \pm 0.32 \times 10^6$ for normal males. The total count of WBC was found to be higher in females treated with high dose of CZAgNPs (10100 ± 141.42 mm^3), whereas in males the animals treated with low doses of CZAgNPs had 8700 ± 0 mm^3 of total WBC.

4.10.2.3 Determination of Hepatic function

In order to determine the proper functioning of liver, various liver function tests such as SGOT, SGPT, ALP and total bilirubin was carried out (Table 4.28). Total bilirubin was measured for all the animals treated with low, medium and high doses of CZAgNPs and the control group. The total bilirubin in both males and females, treated with various doses of CZAgNPs were in the range 0.3 to 0.4 mg / dl. The value was well within the normal range of the control group. In males the level of SGOT was higher in all the three treatment groups with values 293 ± 1.41 U / l, 281.57 ± 2.12 U / l and 270.5 ± 3.53 U / l respectively for low, medium and high doses of CZAgNPs. The SGOT value of normal group was 226 ± 1.2 U / l. In females, the SGOT level was similar to the normal group for both low dose and medium dose administered groups. But, there was decrease in SGOT value for high dose treated females. The SGOT value of high dose treated females and normal females were 135.5 ± 4.95 U / l and 186 ± 3.02 U / l respectively.

In males, the SGPT level was high (92.5 ± 4.94 U / l) in animals treated with low dose of CZAgNPs, when compared to the normal group (67 ± 0.7 U / l). Both medium and high doses administered animals had only marginal difference in the SGPT values. The SGPT level in treated females was measured to be low when

compared to normal females. The lowest value of SGPT was seen in the animals treated with high dose of CZAgNPs. The values of SGPT for normal females and high dose treated females were 68 ± 0.7 U / l and 54 ± 3.54 U / l respectively.

There was decrease in ALP for all the animals treated with low, medium and high doses of CZAgNPs when compared to the normal groups. The least value (144 ± 4.24 U / l) of ALP was noted in females treated with medium dose of CZAgNPs. The ALP level in normal females was 236 ± 1.24 U / l. The males and females treated with medium dose had low ALP level.

The observed difference in all the hepatological parameters for treated groups (males and females) were not significant ($p > 0.05$) when compared to the normal set of animals.

Table 4.28 Hepatological parameters of mice in sub-acute oral toxicity test

Sub-Acute toxicity - Liver Function Test					
Parameters	Sex	Control	CZAgNP Low Dose (50 mg / kg b. wt)	CZAgNP Medium Dose (75 mg / kg b. wt)	CZAgNP High Dose (100 mg / kg b. wt)
BIL (mg / dl)	Males	0.4 ± 0	0.4 ± 0	0.3 ± 0	0.4 ± 0
	Females	0.4 ± 0	0.3 ± 0	0.35 ± 0.07	0.3 ± 0
SGOT (U / l)	Males	226 ± 1.2	293 ± 1.41	281.5 ± 2.12	270.5 ± 3.53
	Females	186 ± 3.02	184.5 ± 2.12	177 ± 4.24	135.5 ± 4.95
SGPT (U / l)	Males	67 ± 0.70	92.5 ± 4.94	66 ± 1.41	59 ± 2.82
	Females	68 ± 0.70	67.5 ± 0.71	63.5 ± 4.95	54.5 ± 3.54
ALP (U / l)	Males	229 ± 1.02	169.5 ± 0.07	160 ± 1.41	185 ± 2.82
	Females	236 ± 1.24	148 ± 1.41	144 ± 4.24	163 ± 4.24

Values are expressed as mean $\pm$ SEM (n=5) by one way ANOVA followed by Dunnett's multiple comparisons test. *$p<0.05$ as significance

4.10.2.4 Determination Renal function

In order to assess the functioning of the kidneys, renal function tests were carried out in both sexes of treated and untreated groups of animals. Serum urea and serum creatinine were tested. For both males and females, the treated groups had low amount of urea when compared with that of the control group. In males, both high dose and medium dose treated animals had low urea level of 37 ± 0.5 U / l, whereas 58 ± 0.4 U / l for control group males. In females, the medium dose treated animals had 35.5 ± 3.54 U / l of urea while the control group females had 44 ± 0.7 U / l of urea. The change observed in the amount of urea in all the treatment groups, in both males and females were not significant ($p > 0.05$).

The amount of creatinine was almost similar in all the groups that is, both treated and untreated males and females. The results obtained are given in Table 4.29.

Table 4.29 Renal function parameters of mice in sub-acute oral toxicity test

			Sub-Acute toxicity – Renal Function Test		
Parameters	Sex	Control	CZAgNP Low Dose (50 mg / kg b. wt)	CZAgNP Medium Dose (75 mg / kg b.wt)	CZAgNP High Dose (100 mg / kg b.wt)
Urea (U / l)	Males	58 ± 0.4	37.5 ± 0.5	37.5 ± 0.5	38 ± 1
	Females	44 ± 0.70	37 ± 2.83	35.5 ± 3.54	42.5 ± 0.71
Creatinine (mg / dl)	Males	0.54 ± 0	0.525 ± 0.005	0.51 ± 0.02	0.495 ± 0.02
	Females	0.58 ± 0.01	0.56 ± 0.02	0.59 ± 0.01	0.55 ± 0.02

Values are expressed as mean ± SEM (n=5) by one way ANOVA followed by Dunnett's multiple comparisons test. *p<0.05 as significance

4.10.2.5 Analysis of Lipid Profile

The lipid profile of treated and untreated groups was monitored. The various parameters checked were cholesterol, triglycerides, high density lipoprotein, low density lipoprotein and very low density lipoprotein.

Cholesterol levels were low in treatment groups of both males and femlaes. When compared to normal males (122 ± 0.02 mg /dl), the cholesterol level in medium dose treated group was 113 ± 2 mg /dl. In females, low cholesterol was found in animals treated with low dose of CZAgNPs (102.5 ± 0.71 mg /dl) whereas; the normal females the cholesterol level was 142 ± 1.21 mg /dl.

The amount of triglycerides in all the treatment groups was lesser compared to their corresponding control group of males and females. Medium dose treated males had the lowest amount of triglycerides (69 ± 1 mg /dl) when compared to all the other treatment groups. Only the females treated with high dose of CZAgNPs had almost similar amount of triglycerides (167.5 ± 0.71 mg /dl) when compared to normal females (166 ± 1.20 mg /dl).

Table 4.30 Lipid profile of mice in sub-acute oral toxicity test

Sub-Acute toxicity – Lipid profile					
Parameters	Sex	Control	CZAgNP Low Dose (50 mg / kg b. wt)	CZAgNP Medium Dose (75 mg / kg b. wt)	CZAgNP High Dose (100 mg / kg b. wt)
Cholesterol	Males	122 ± 0.02	127 ± 0	113 ± 2	125.5 ± 0.5
(mg / dl)	Females	142 ± 1.21	102.5 ± 0.71	124.5 ± 2.12	123 ± 2.83
Triglycerides	Males	142 ± 0.71	103 ± 1	69± 1	85 ± 1
(mg / dl)	Females	166 ±1.20	109.5 ± 2.12	153 ± 1.41	167.5 ± 0.71
HDL	Males	41 ± 0.4	40.5 ± 0.5	37.5 ± 0.5	41 ± 1
(mg / dl)	Females	43 ±0.70	38.5 ± 0.71	42.5 ± 3.54	42 ± 0
LDL	Males	53 ± 0.5	97.5 ± 0.5	53± 1	71 ± 2
(mg / dl)	Females	76 ± 1.21	43.5 ± 2.12	74.5 ± 2.12	52.5 ± 3.54
VLDL	Males	28 ± 1	19 ± 1	27.75 ± 0.25	18 ± 1
(mg / dl)	Females	23 ± 1.41	20.5 ± 2.12	29 ± 1.41	28.5 ± 0.71

Values are expressed as mean ± SEM (n=5) by one way ANOVA followed by Dunnett's multiple comparisons test. *$p < 0.05$ as significance

The level of HDL in normal males and females were 41 ± 0.4 mg /dl and 43 ± 0.70 mg /dl. All the treatment groups (both males and females) had HDL similar to their corresponding normal animals. LDL was found to be high in low dose treated male mice (97.5 ± 0.5 mg /dl), whereas the normal males has 53 ± 0.5 mg /dl of LDL. Least amount of LDL was observed in female mice treated with low dose of CZAgNPs. The LDL level in low dose treated females was 43.5 ± 2.12 mg /dl, whereas for the normal females the LDL level was 76 ± 1.21 mg /dl. The amount of VLDL was almost same in all the groups (both males and females). Very slight deviation was observed in males treated with high dose of CZAgNPs. All the data representing the lipid profile of both males and females are given in Table 4.30.

4.10.2.6 Histological Analysis

In order to confirm the biochemical findings and to understand the structural changes in the vital organs of the male and female mice, administered with CZAgNPs, histological evaluation was conducted. Light microscopic examination of heart, lungs, liver, kidney, stomach, small intestine, testis and ovary of the mice in all the treated and untreated groups was performed. The result revealed the treatment groups did not show any gross pathological conditions (Fig 4.25a, 4.25b, 4.25c, 4.25d).

In normal and low dose treated males, the brain section showed glial tissue with focal aggregates of oligodendrocytes in a neurophil rich stroma. Scattered neuronal bodies were also noted. Whereas, the high and medium dose treated males showed glial tissue with neurophil rich stroma.

The Histological section of the heart of males showed myocardial tissue with widened and intact myocardial fibres, and elongated nucleus in normal, high and low

dose treated males, whereas myocardial fibres with mild disarray was noted in males treated with medium dose of CZAgNPs.

The sections of lungs showed parenchyma with focally widened alveolar septa for all the treatment and control group of males.

Hepatic parenchyma with preserved architecture, central and portal triad having intact morphology with unremarkable interstitium was seen in section of liver tissue treated with high dose and also in normal group. In medium and low dose treated groups hepatic parenchyma with dialated central vein and intact portal triads were observed.

Renal parenchyma with intact glomerulin, tubules and blood vessels were observed in the histological section of kidney of both treated and untreated group of males.

The section of stomach showed gastric parenchyma with preserved epithelium and gastric pits in animals treated with all three doses of CZAgNPs as well as in the control group.

Intestinal tissue with intact villi and crypts of preserved morphology was observed. Aggregates of paneth cells were noted in all the groups which underwent CZAgNPs administration and also in normal set of animals.

Testicular and epididymal parenchyma, preserved seminiferous tubules and interstitium were noted in the section of testis. This pattern was observed in control group and groups that were administered with various doses of CZAgNPs.

The histology section showed the ovary had ovarian parenchyma with ampulla and the sequential maturation up to terminal follicle was intact in both treated and untreated females.

Mild congestion was noted in liver, kidney and lungs of all the treated group and normal group of males. This could be spontaneous one and might not be related with treatment of drug.

Therefore, the histological study of the vital organs did not show any evident anatomical lesions that might be related to the oral administration of CZAgNPs to the mice.
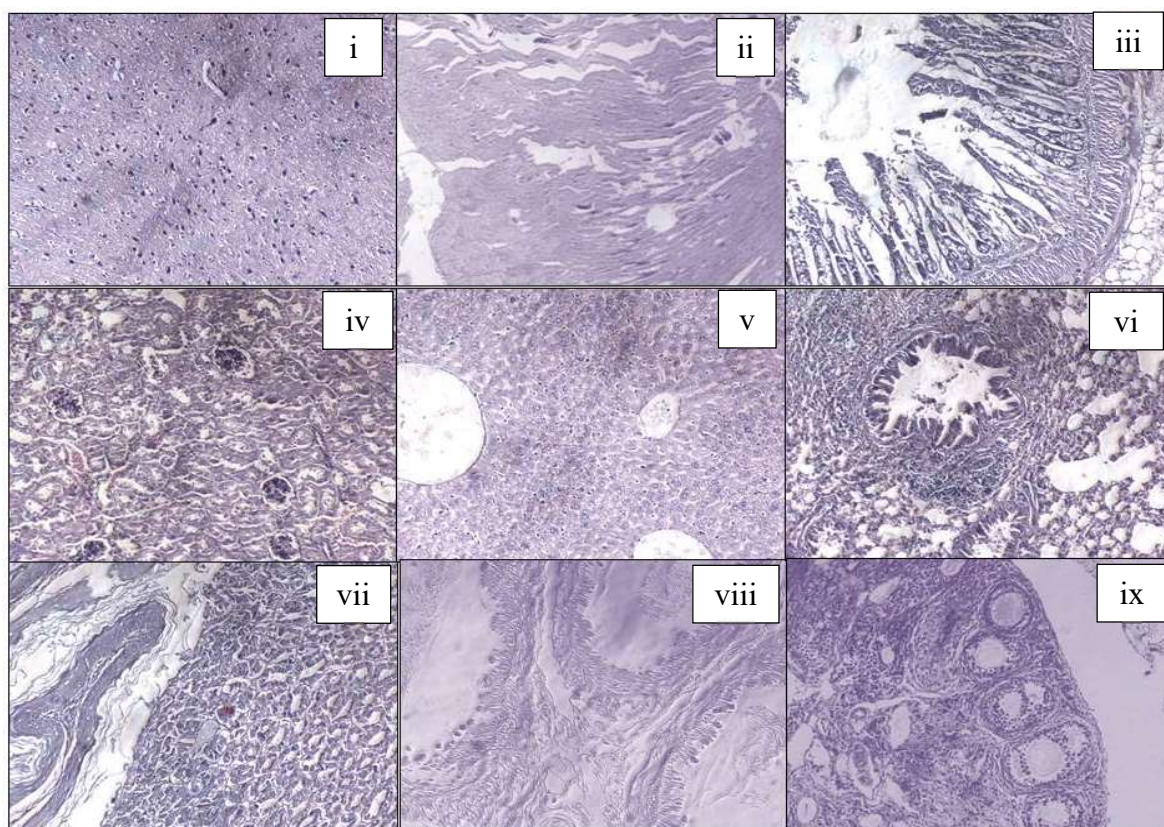
Fig. 4.25 a Histological section of mice treated with high dose of CZAgNPs (i) Brain, (ii) Heart, (iii) Intestine, (iv) Kidney, (v) Liver, (vi) Lungs, (vii) Stomach, (viii) Testis, (ix) Ovary
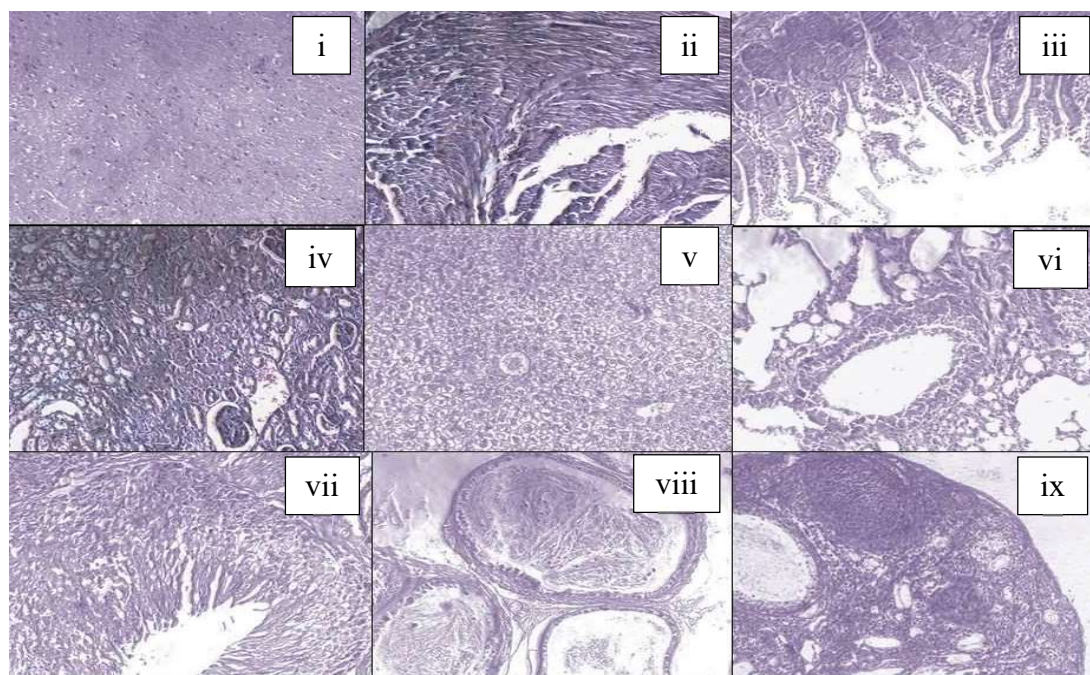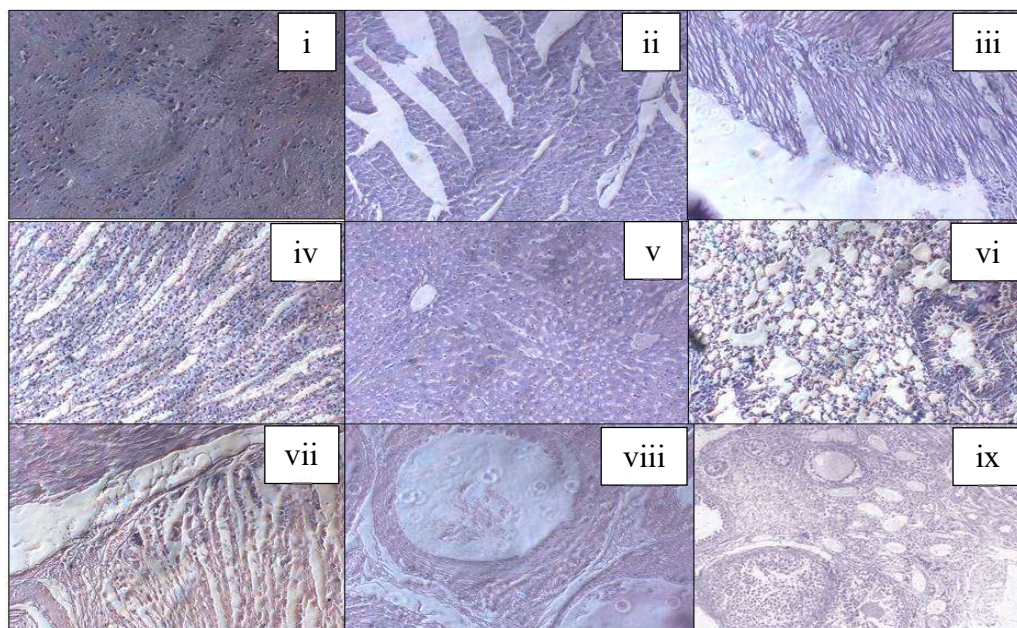
Fig. 4.25 b Histological section of mice treated with medium dose of CZAgNPs (i) Brain, (ii) Heart, (iii) Intestine, (iv) Kidney, (v) Liver, (vi) Lungs, (vii) Stomach, (viii) Testis, (ix) Ovary
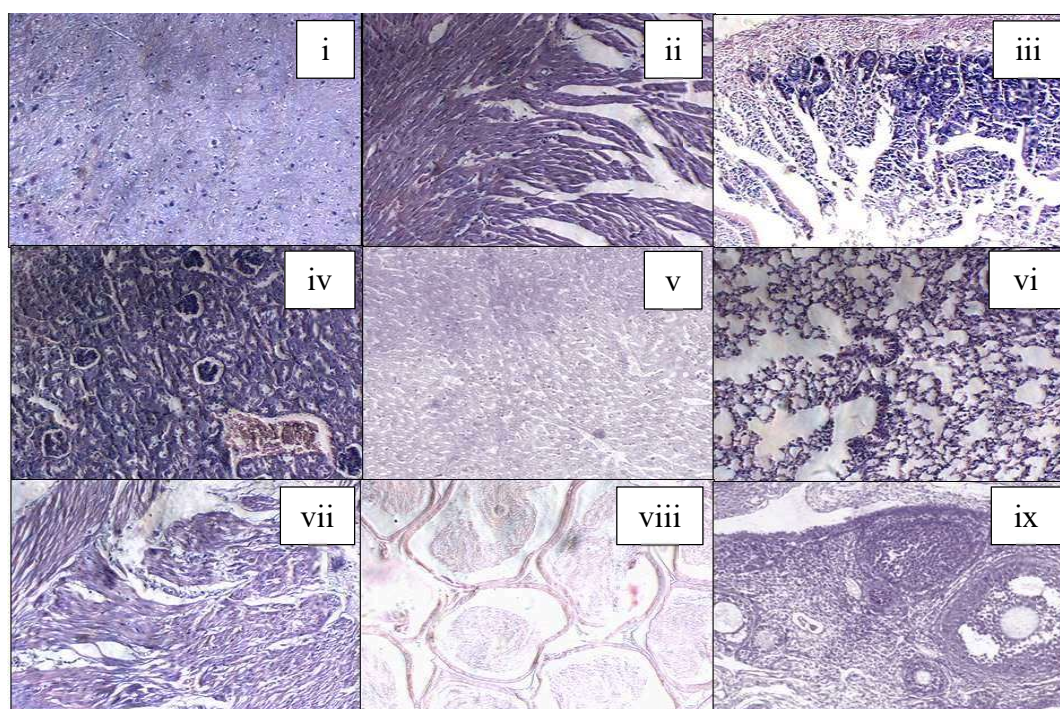
Fig. 4.25 c Histological section of mice treated with low dose of CZAgNPs (i) Brain, (ii) Heart, (iii) Intestine, (iv) Kidney, (v) Liver, (vi) Lungs, (vii) Stomach, (viii) Testis, (ix) Ovary

Fig. 4.25d Histological section of untreated normal mice (i) Brain, (ii) Heart, (iii) Intestine, (iv) Kidney, (v) Liver, (vi) Lungs, (vii) Stomach, (viii) Testis, (ix) Ovary

Nanoparticles are increasingly being used in biomedical applications. However, our understanding on the effects of these nanoparticles on living cells or biochemical indices is still lacking. It is therefore critical to stimulate research aimed at determining the biochemical assessments of silver nanoparticles. The LD 50 of AgNPs was previously reported to be > 5000 mg / kg b. wt in rat (Maneewattanapinyo, Banlunara, Thammacharoen, Ekgasit, & Kaewamatawong, 2011) however the current work measured it at substantially lower dose of 500 mg / kg b. wt in Swiss albino mice.

A significant decrease in body weight was observed in CZAgNPs treated groups indicating some level of toxicity at 500 mg / kg b. wt. Studies report that significant alterations in the body weight and organ weight can be linked to toxicity of the administered drug (Sulaiman *et al*., 2015). This demonstrated the acute LD 50 of CZAgNPs was above 500 mg /kg b. wt in mice. Hence doses ranging between 1/5th,

1/10th acute toxicity dose was chosen for the sub-acute studies. Here the doses selected were 50 mg /kg b. wt, 75 mg /kg b. wt and 100 mg /kg b. wt. The animals did not show any significant change in the body weight and organ weight upon administration of CZAgNPs at these over 28 day period. Contradictory to the results of Sulaiman *et al*., and Heydrnejad *et al*., the green synthesized CZAgNPs did not exhibit any symptoms of toxicity (Heydrnejad, Samani, & Aghaeivanda, 2015; Sulaiman *et al*., 2015).

Biochemical parameters are useful for tracking the clinical symptoms caused by a toxicant. Enzyme assays are also important in toxicological evaluation (Adeyemi & Akanji, 2011). The hematological parameters namely Hb, RBC, PLT and TC analyzed did not show any significant changes with regard to the control group. A marginal increase in platelet count was observed in high dose treated groups compared to the other treatment groups and control. This result was contradictory to the already reported data, in which a significant decrease in platelets were noticed accounting cellular toxicity (Tiwari, Jin, & Behari, 2011). In contrast to the control group, the total count in all the CZAgNP treated groups was high. This might be due to the immunological response detected by the immune system, due to the entry of any foreign particle. The contradiction observed might also be because of the low LD 50 based doses selected for the study and the nature of the synthesized silver nanoparticles.

The biochemical parameters including bilirubin, AST, ALT, ALP, urea, creatinine and lipid profiling did not show any significant alterations in comparison with the control group. The amount of bilirubin was kept to near normal in all the groups treated with CZAgNPs. Bilirubin, being the degraded product of haemoglobin,

is a liver function marker. However, unlike the study by Tiwari *et al*., (Tiwari *et al*., 2011), the value of bilirubin did not increase significantly but was near to normal indicating the healthy functioning of the liver. AST, ALT and ALP are the indicators of hepatocellular damage. The study of hepatic toxicity is of major interest because, the studies liver is the major target organ of localization and accumulation of nanoparticles (Heydrnejad *et al*., 2015). The increase in activity of AST and ALT can be correlated to cellular damage (Oluyomi Stephen Adeyemi & Adewumi, 2014). However, the ALT levels in both males and females were comparatively decreased in animals administered with CZAgNPs. Whereas, in males with an exception of low dose treated animals, there was a decline in the level of ALT. The AST levels of females were also low when compared with normal group. But this trend was absent in males in which they showed a marginal increase in AST level in all the treatment groups. But the level of ALP was declined in both females and males. Therefore the changes in the enzyme levels could reflect adaptive mechanism used in the animals to cope with the stress caused by CZAgNPs. All the changes reflected in the liver function test were non-significant and it is likely that the enzyme's thiol group attracted AgNPs, thus resulting in the formation of complexes and subsequent regulation of enzyme activity similar to the opinion by Oluyomi and Adewumi (Oluyomi Stephen Adeyemi & Adewumi, 2014).

The renal function parameters, urea and creatinine were evaluated and no significant changes were observed when compared to normal ones indicating no renal toxicity. The lipid profile of males and female swiss albino mice treated with 3 doses of CZAgNPs did not show any significant changes in any of the lipid parameters (cholesterol, TG, HDL, LDL and VLDL) studied. However, the HDL level in all the

treatment groups was found to be near normal, indicating the lower risk of cardiovascular diseases at these administered doses.

The histological study of the vital organs did not reveal any evident anatomical lesions except for the mild congestion noted in the liver, kidney and lungs of all the groups including the normal untreated group. The observed congestion might be a spontaneous one that might not be related to the drug treatment. Earlier study reported that in comparison to control, silver nanoparticle delivery altered the cellular architecture of renal, cardiac and hepatic tissue (Sulaiman *et al*., 2015). In contrary to the above mention study, the green synthesized silver nanoparticles exhibited no remarkable histological changes which was corroborated with the results of Nakkala *et al*., (Nakkala *et al*., 2018). This manifests that the green synthesized CZAgNPs were relatively non-toxic and safe for further applications at these administered doses.

4.11 Protective effect of Silver Nanoparticles on Sodium Fluoride Induced Oxidative Stress

4.11.1 In Vivo Antioxidant enzyme analysis

The antioxidant status in the blood and liver tissue of the male mice treated with three different doses (low dose – 25 mg / kg b. wt; medium dose – 50 mg / kg b. wt and high dose 75 mg / kg b. wt) of CZAgNPs followed by intoxication with sodium fluoride was evaluated. The activity of intracellular antioxidant enzymes (SOD, CAT, GST, GR and GPx) and non-enzymatic antioxidant GSH was estimated and the oxidative stress was measured by means of lipid peroxidation. The results revealed that the repression of the activities of enzymes in NaF intoxicated groups was alleviated by the treatment with the synthesized silver nanoparticles. Moreover,

the lipid peroxidation was high in the NaF given groups when compared to the CZAgNPs treated groups. The results are summarized as follows.

4.11.1.1 Estimation of superoxide dismutase (SOD)

Figure 4.26a depicts the SOD activity in the blood of experimental animals. The activity of blood SOD showed a significant increase in animals given with CZAgNPs compared to untreated normal animals. The activity of SOD in blood was 3.4 ± 0.45 U / Hb in high dose, 3.56 ± 0.51 U / Hb in medium dose and 4.02 ± 0.22 U / Hb in low dose administered animals, whereas, the normal group animals documented SOD activity of 2.79 ± 0.24 U / Hb. The SOD activity in the groups given standard and NaF was 3.68 ± 0.49 U / Hb and 3.07 ± 0.5 U / Hb respectively. In the hepatic tissue, the SOD activity was 15.65 ± 1.79 U / mg protein in low dose, 15.07 ± 1.83 U / mg protein in medium dose and 12.23 ± 1.38 U / mg protein in high dose treated animals. SOD activity of 11.8 ± 1.01 U / mg protein was observed in the normal group, whereas 11.13 ± 2.17 U / mg protein was showed in NaF intoxicated group. The activity of SOD was found to be significantly high for the low dose treated group when compared with the standard (Vitamin C) administered group (14.36 ± 0.93 U / mg protein). Therefore, the animals treated with CZAgNPs showed improved levels of these parameters. The SOD levels were higher when compared with the normal group, indicating the ameliorative effect of CZAgNPs (Table 4.31, Fig. 4.26b)

Table 4.31 Antioxidant enzyme status in liver tissues of untreated and treated mice with various doses of CZAgNPs and standard Vitamin C

Groups	SOD U / mg protein	CAT U / mg protein	GPx U / mg protein	GSH U / mg protein	GR U / mg protein	GST U / mg protein	TBARS nmol / mg protein
Normal	11.8 ± 1.01	4.27 ± 0.47	0.14 ± 0.02	7.17 ± 0.38	11.9 ± 1.33	11.46 ± 0.99	2.21 ± 0.55
NaF	11.13 ± 2.17	2.75 ± 0.45	0.11 ± 0.02	7.67 ± 0.22	8.97 ± 0.52	10.32 ± 0.7	2.6 ± 0.2
Low dose	15.65±1.79*	2.93 ± 0.35	0.11 ± 0	9.62 ± 1*	10.95± 0.59	11.58 ± 0.2	2.28 ± 0.25
Medium dose	15.07 ± 1.83	2.91 ± 0.73	0.12 ± 0.03	8.30 ± 1.3	12.88± 1.33	12.16± 0.94	2.26 ± 0.35
High dose	12.23 ± 1.38	3.54± 0.54*	0.13 ± 0.04	8.11 ± 0.27	10.94± 1.33	13.62± 0.14	2.25 ± 0.4
Standard	14.23 ± 0.93	2.59 ± 0.99	0.13 ± 0.02	10.44±1.15*	11.61± 1.14	12.78± 0.85	2.2 ± 0.36

Values are expressed as mean ± SEM (n=5) by one way ANOVA followed by Bonferroni's multiple comparisons test. *$p < 0.05$ as significance
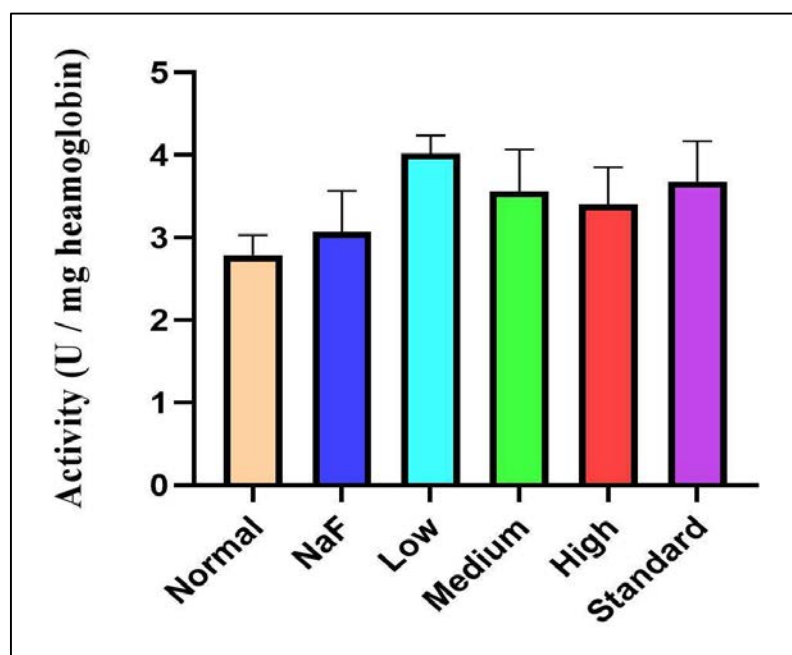
Fig. 4.26a SOD activity in blood of the untreated and animals treated with different doses of CZAgNPs, Vitamin C. Values are expressed as mean ± SEM (n=5) by one way ANOVA followed by Bonferroni's multiple comparisons test. *p<0.05 as significance
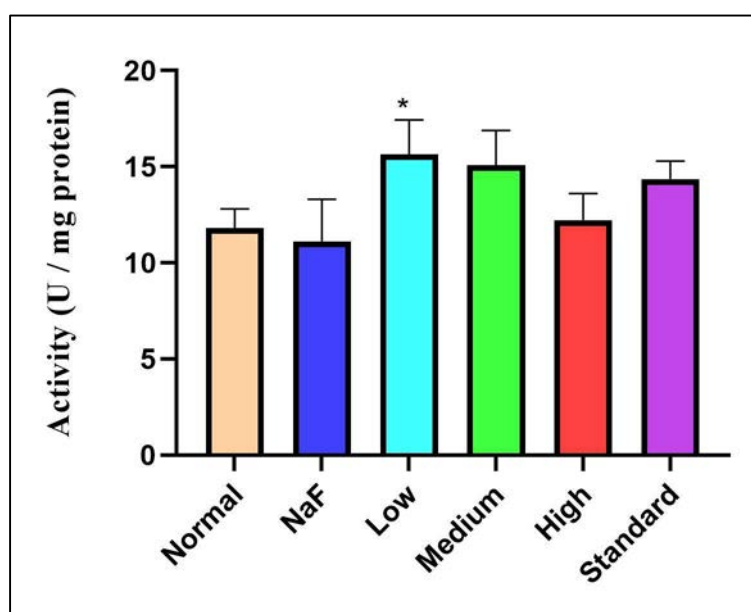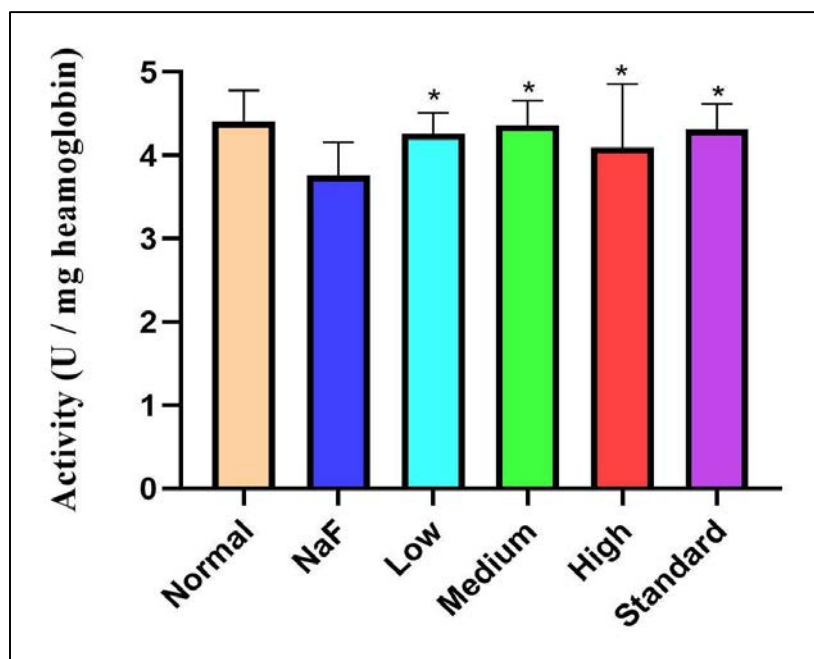

Fig. 4.26b SOD activity in tissue of the untreated and animals treated with different doses of CZAgNPs, Vitamin C. Values are expressed as mean ± SEM (n=5) by one way ANOVA followed by Bonferroni's multiple comparisons test. *p<0.05 as significance

4.11.1.2 Estimation of catalase (CAT)

The CAT activity in NaF intoxicated group animals was 3.76 ± 0.40 U / mg Hb. The CAT activity was significantly increased ($p > 0.05$) in high dose (4.10 ± 0.76 U / mg Hb), medium dose (4.36 ± 0.30 U / mg Hb) and low dose (4.26 ± 0.25 U / mg Hb) CZAgNPs given animals. The CAT activity in all CZAgNPs treated group was restored to near normal (4.40 ± 0.38 mg U / Hb) in blood. The CAT activity in liver tissue was monitored. The CAT activity in normal group of animals was 4.27 ± 0.47 U / mg protein (Fig. 4.27 a). In the hepatic tissue the CAT activity was significantly increased ($p > 0.05$) in high dose (3.84 ± 0.54 U / mg protein) treated animals. With respect to standard group (2.59 ± 0.99 U / mg protein), all the CZAgNPs treated group showed increase in CAT activity. The catalase levels were restored to the value of near normal group indicating the protective effect of the synthesized silver nanoparticles (Table 4.31, Fig. 4.27b)

Fig. 4.27a Catalase activity in blood of the untreated and animals treated with different doses of CZAgNPs, Vitamin C. Values are expressed as mean $\pm$ SEM (n=5) by one way ANOVA followed by Bonferroni's multiple comparisons test. *$p < 0.05$ as significance
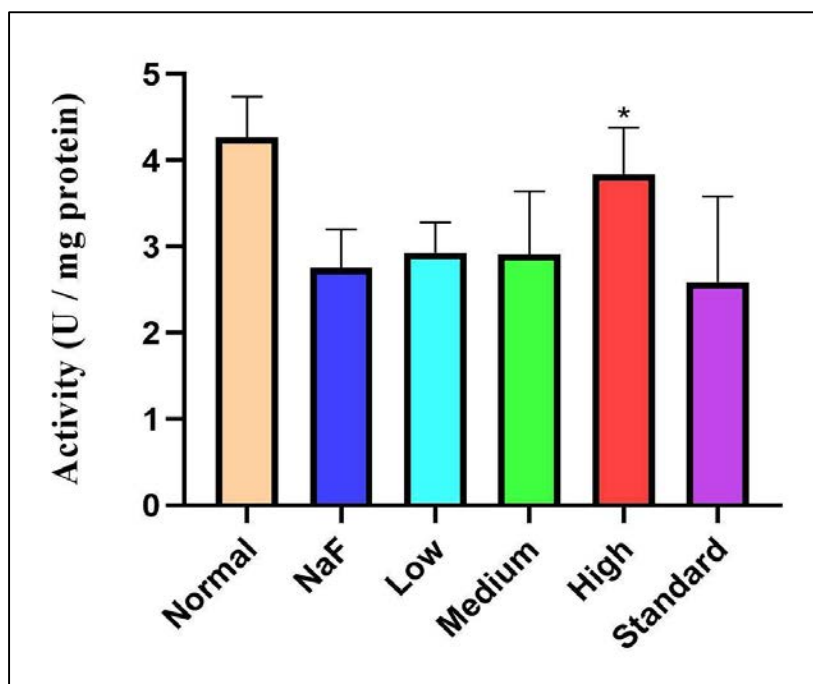
Fig. 4.27b Catalase activity in tissue of the untreated and animals treated with different doses of CZAgNPs, Vitamin C. Values are expressed as mean ± SEM (n=5) by one way ANOVA followed by Bonferroni's multiple comparisons test. *p <0.05 as significance

4.11.1.3 Estimation of reduced glutathione (GSH)

Reduced glutathione (GSH) was found to be 7.17 ± 0.38 n moles / mg protein in normal animals. The level was significantly high in low dose (9.62 ± 1 n moles / mg protein) CZAgNPs given animals when compared to medium dose (8.30 ± 1.3 n moles / mg protein), high dose (8.11 ± 0.27 n moles / mg protein) CZAgNPs and NaF (7.67 ± 0.22 n moles / mg protein) given animals. The highest activity of GSH (10.44 ± 1.15 n moles / mg protein) was seen in Vitamin C treated groups. The GSH was found to be high in CZAgNPs treated groups when compared to NaF intoxicated animals, proving its protective effect in mice. The values are shown in (Table 4.31, Fig. 4.28).
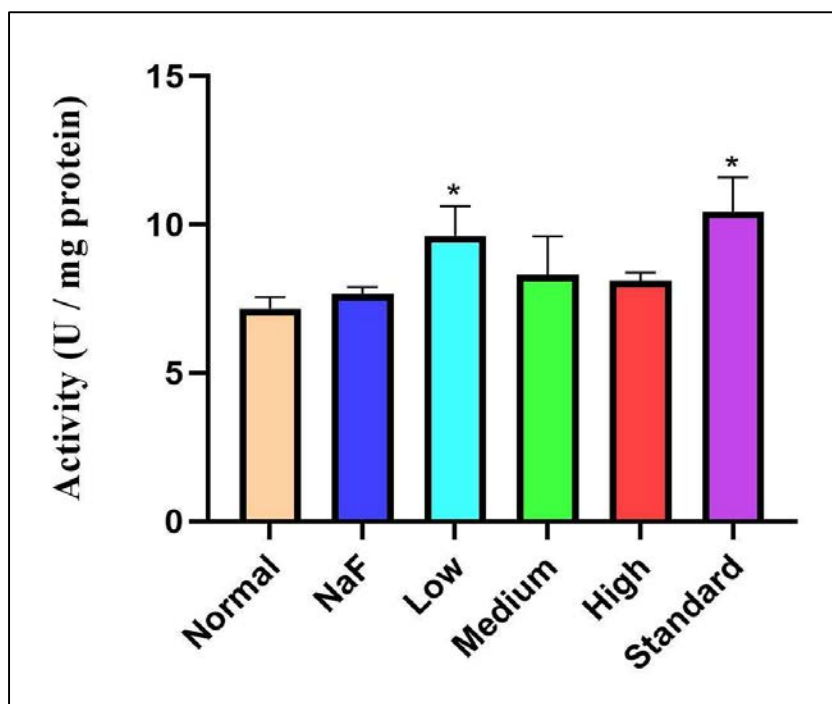
Fig. 4.28 GSH activity in tissue of the untreated and animals treated with different doses of CZAgNPs, Vitamin C. Values are expressed as mean ± SEM (n=5) by one way ANOVA followed by Bonferroni's multiple comparisons test. *p <0.05 as significance

4.11.1.4 Estimation of glutathione – s – transferase (GST)

The GST activity was found to be 11.46 ± 0.99 U / mg protein in the hepatic tissues of normal group. A gradual increase in GST was observed in low to high groups treated with CZAgNPs. The GST activity was 11.58 ± 0.2 U / mg protein, 12.16 ± 0.94 U / mg protein and 13.62 ± 0.14 U / mg protein in low dose, medium dose and high dose of CZAgNPs given groups respectively. The standard group showed 12.78 ± 0.85 U / mg protein of GST activity. The lowest activity of GST (10.32 ± 0.7 U / mg protein) was observed in NaF intoxicated group. Therefore the results show GST activity was found to high in CZAgNPs treated groups when compared to the normal, standard groups (Table 4.31, Fig. 4.29). The decreased amount of GST activity observed in NaF intoxicated groups was ameliorated with the administration of the synthesized silver nanoparticles.
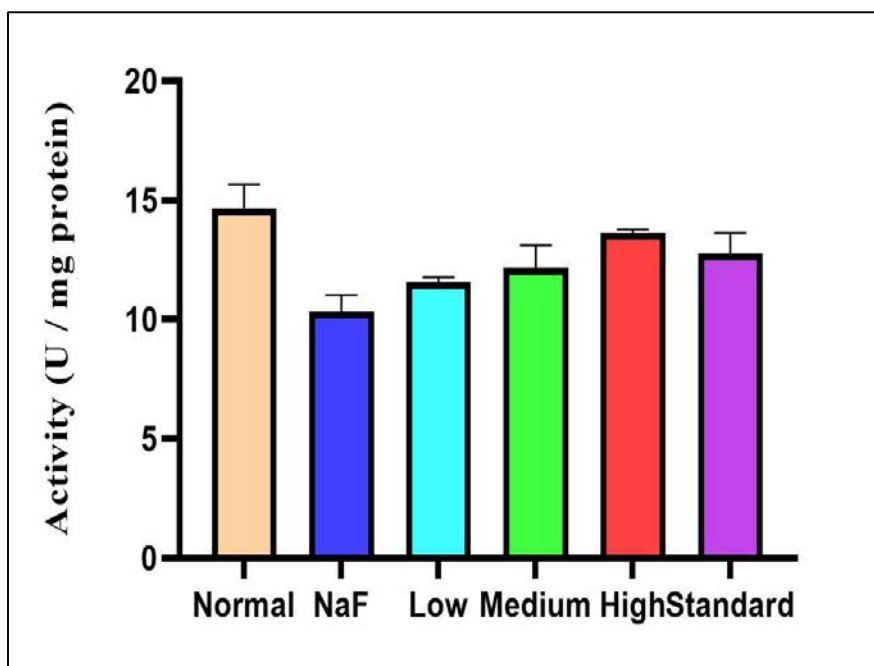
Fig. 4.29 GST activity in tissue of the untreated and animals treated with different doses of CZAgNPs, Vitamin C. Values are expressed as mean ± SEM (n=5) by one way ANOVA followed by Bonferroni's multiple comparisons test. *p <0.05 as significance

4.11.1.5 Estimation of glutathione reductase (GR)

Glutathione reductase activity (GR) in the normal animals was 11.9 ± 1.33 U / mg protein. There was an increase in activity observed in medium dose (12.88 ± 1.33 U / mg protein), low dose (10.95 ± 0.59 U / mg protein) and high dose (10.94 ± 1.33 U / mg protein) CZAgNP given animals compared to normal group. The increase was at maximum in medium dose CZAgNPs given animals. The NaF intoxicated group had the least GR activity (8.97 ± 0.52 U / mg protein, whereas the in the standard group the GR activity was 11.61 ± 1.14 U / mg protein. The results are given in (Table 4.31, Fig. 4.30). Therefore the depleted activity of GR in NaF treated animals was almost restored with the administration of the synthesized silver nanoparticles.
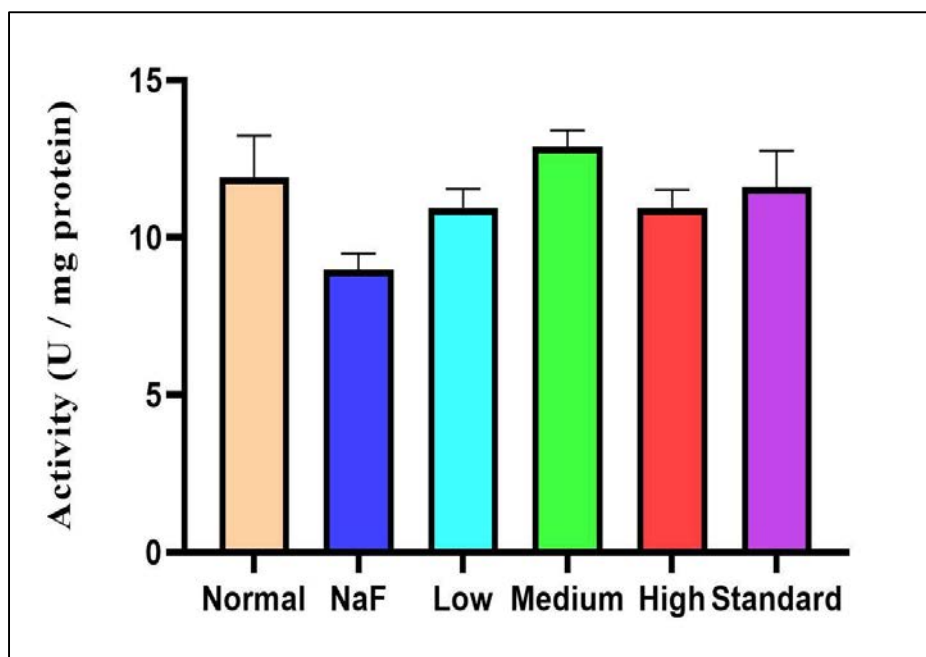
Fig. 4.30 GR activity in tissue of the untreated and animals treated with different doses of CZAgNPs, Vitamin C. Values are expressed as mean ± SEM (n=5) by one way ANOVA followed by Bonferroni's multiple comparisons test. *p <0.05 as significance

4.11.1.6 Estimation of glutathione peroxidase (GPx)

The activity of GPx was 0.14 ± 0.02 U / mg protein in normal group. In the Vitamin C and high dose of CZAgNPs treated groups the activity of GPx was 0.13 ± 0.02 U / mg protein and 0.13 ± 0.04 U / mg protein respectively. The medium dose had 0.12 ± 0.03 U / mg protein GPx activity. The activity of GPx in NaF intoxicated group was 0.11 ± 0.02 U / mg protein. Therefore the results showed that in the mice treated with CZAgNPs the activity of GPx was restored to near the control group, when compared to that of the NaF given group (Table 4.31, Fig. 4.31).
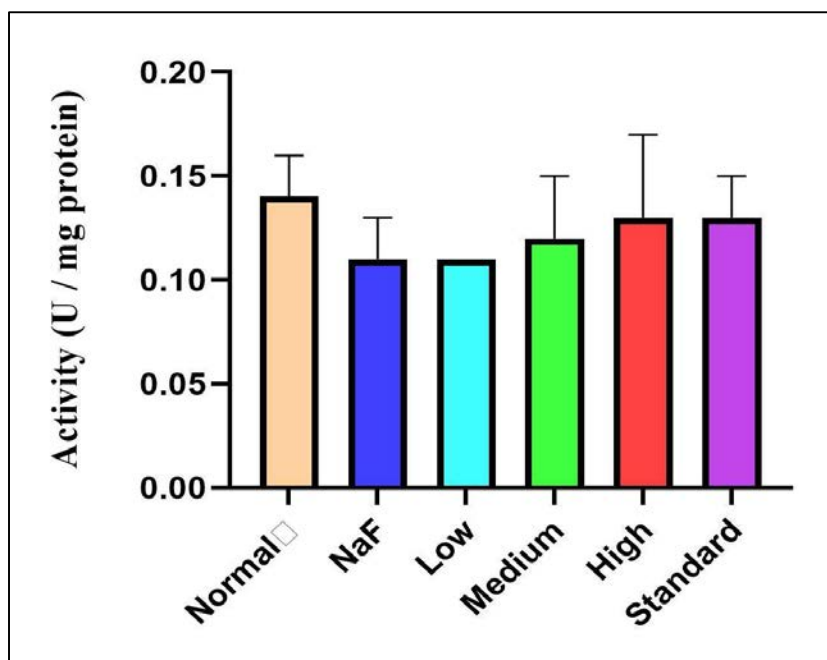
Fig. 4.31 GPx activity in tissue of the untreated and animals treated with different doses of CZAgNPs, Vitamin C. Values are expressed as mean ± SEM (n=5) by one way ANOVA followed by Bonferroni's multiple comparisons test. *p <0.05 as significance

4.11.1.7 Determination of Lipid peroxidation (TBARs)

Hepatic TBARs formed as result of lipid peroxidation was documented. In normal group, the observed TBARs content was 2.21 ± 0.55 nmol / mg protein. When compared to the normal level, there was a negligible increase in TBARs content in low dose (2.28 ± 0.25 nmol / mg protein), medium dose (2.26 ± 0.35 nmol / mg protein) and high dose (2.25 ± 0.4 nmol / mg protein) of CZAgNPs administrated animals. The least TBARs content was seen in the Vitamin C treated groups (2.2 ± 0.36 nmol / mg protein). The TBARs content observed in CZAgNPs treated groups were very near to that of the standard and normal group. The highest TBARS activity confirming greater lipid peroxidation was observed in NaF intoxicated group (2.6 ± 0.2 nmol / mg protein). The values are shown in the (Table 4.31, Fig. 4.32).
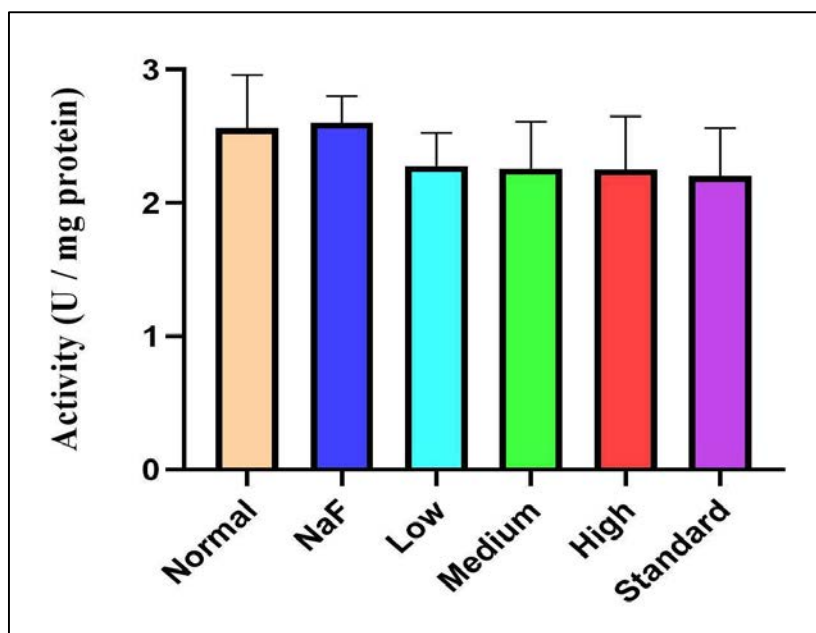
Fig. 4.32 Hepatic TBARs level in the untreated and animals treated with different doses of CZAgNPs, Vitamin C. Values are expressed as mean ± SEM (n=5) by one way ANOVA followed by Bonferroni's multiple comparisons test. *p <0.05 as significance

4.11.8 Histological analysis of liver tissue

The histological analysis of the liver tissue was carried out in order to evaluate the potency of CZAgNPs to prevent the liver damage. The results obtained revealed the protective effect of CZAgNPs over the liver damage caused at NaF intoxicated conditions (Fig. 4.33). The liver sections of the normal mice showed liver parenchyma with preserved morphology. The portal triads were intact along with central veins. In NaF intoxicated liver tissues, similar characteristics were seen. But, the NaF given liver tissue showed marked congestion in the central vein. The sections of the standard group showed preserved morphology of liver parenchyma, along the central veins, the portal triads were seen to be intact. The CZAgNPs treated mice also showed normal liver parenchyma with preserved morphology. The portal triads were found to be intact along with the central vein. Except for high dose treated CZAgNPs, the medium dose, low dose and also the standard (Vitamin C) group contained sparse inflammation.
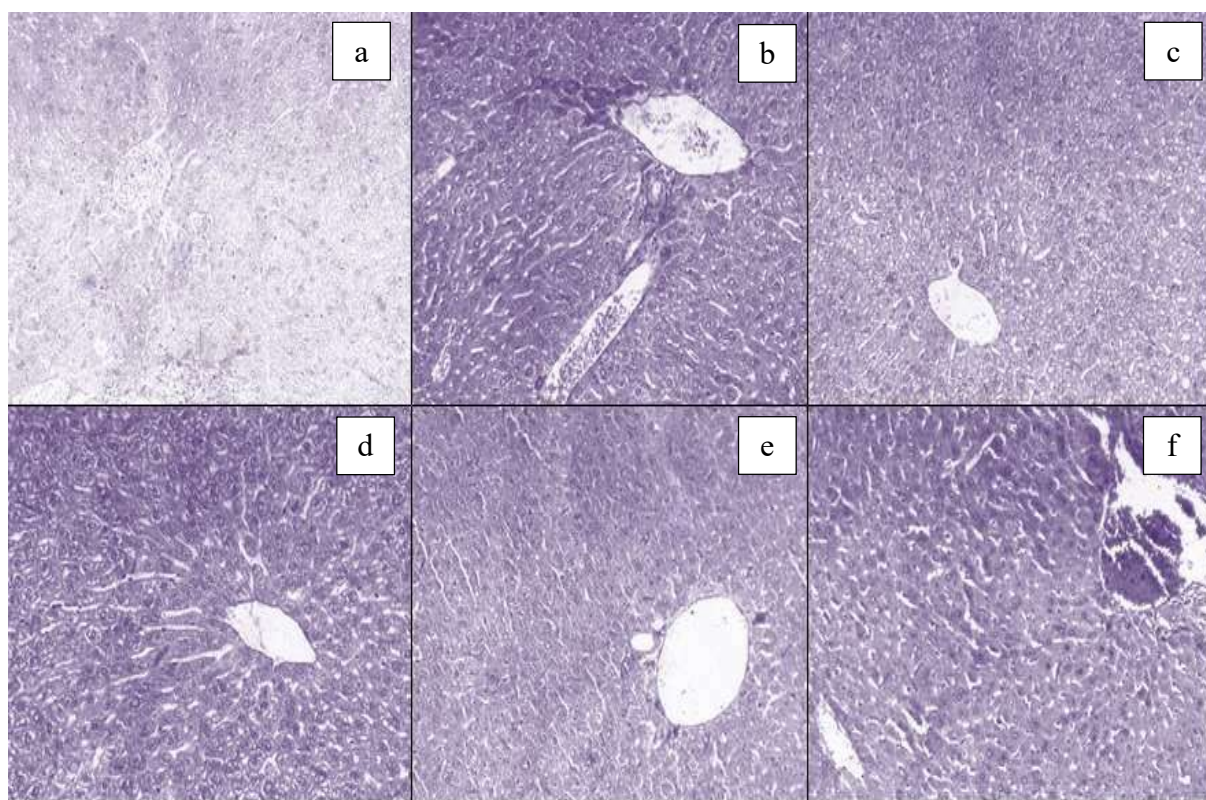
Fig. 4.33 Histology of liver tissues (a) Normal, (b) Low dose, (c) Medium dose, (d) High dose, (e) Standard and (f) NaF treatments

Fluoride is known to exhibit diverse toxicological effects in both animals and human beings. Studies have shown that fluoride inhibit the function of Na^+ / K^+ ATPase leading to ATP depletion, inactivate the function of various key enzymes involved in glycolysis and Krebs cycle (Mitta *et al.*, 2021). In biological systems the fluoride toxicity is related to the production of free radicals. The excessive production of free radicals leads to the decrease in the activities of catalase, superoxide dismutase, glutathione peroxidase and xanthine oxidase which play a major role in elimination of free radicals. Fluoride not only impairs the activities of enzymes like alkaline phosphatase, choline esterase, and adenylate cyclase but also interferes with carbohydrate and lipid metabolism (Hassan & Yousef, 2009).

The toxicity against fluoride intoxication can be eliminated with the help of chelating agents and antioxidants. The protective effect of green synthesized CZAgNPS on NaF intoxicated mice was investigated. The study revealed alterations in the level of antioxidant markers in the liver as a result of sodium fluoride exposure. The level of SOD, CAT, GPx, GR, GSH and GST was reduced whereas; the extent of lipid peroxidation as measured by TBARS was enhanced with NaF intoxication. The primary antioxidant enzymes, SOD, CAT, GST and GPx all have transition metals as cofactors. The interaction of NaF with these enzymes' metals could explain the observed inhibition in their activity. Exogenous substances that can reverse the NaF binding to metal ions thus restores the endogenous enzymatic and non-enzymatic antioxidant status, which can be an effective technique for preventing NaF induced toxicity (Abdel-Wahab, 2013).

From the study it was observed that the level of antioxidant enzyme status was brought back to near normal in the groups administered with different doses of CZAgNPs. In the low dose treated animals, the elevated level of SOD was observed denoting the generation of hydrogen peroxides in the hepatic tissues. The peroxides were acted upon by both catalase and GPx. Supporting this the GSH level is found increased in the CZAgNP treated animals with higher increase observed in low dose of CZAgNPs administered mice. Reduced glutathione (GSH) is important to redox balance all the cells. GSH is primarily involved in peroxide and lipid aldehyde detoxification. Also the increased TG in low dose improves mitochondrial respiration due to fatty acid oxidation, which could result in increased superoxide leakage in mitochondria. This cause leaching of superoxide anions into the cytoplasm where, SOD enzyme act to convert it into hydrogen peroxides. The subsequent action by GSH might augment the removal of this peroxide. Moreover GR which is involved in

the formation of GSH is found to be comparatively high, which indicates low dose of CZAgNPs increase GSH synthesis through salvage pathway. Further, decrease in GST and lower TBARS levels indicate that GSH is not utilized in the detoxification of lipid carbonyls.

In animals treated with high dose of CZAgNPs, the highest level of catalase and GPx were observed which further substantiated the presence of hydrogen peroxides that might be possibly generated in lipid metabolic route. Here the peroxidative reaction been opposed by catalase and GPx. At the same time, the highest activity of GPx shows the reduction of GSH to GSSG, which is evident from the low levels of GSH in high dose treated animals.

Compared to both high and low dose administered animals, the medium dose had increased amount of GR indicating the replenishment of GSH in the hepatic tissues. All the other enzyme activities were found to be within the range of low and high dose treated animals. In the group treated with the standard, ascorbic acid, except for catalase activity all other enzyme levels were high. This indicates that the radicals formed due to the sodium fluoride intoxication were augmented by the enzymes SOD, GST and GPx. Further, GR involved in the conversion of oxidized glutathione to GSH was found high indicating the replantation of GSH. This is corroborated with the findings that TBARs is found to be reduced in both CZAgNPs and standard drug administered groups (Jasper, Locatelli, Pilati, & Locatelli, 2012).

Our findings were in line with Shakila and Gino (Vasanth & Kurian, 2017) which shows the green synthesized silver nanoparticles caused considerably less oxidative stress in the renal tissue than chemically synthesized silver nanoparticles. Therefore, the CZAgNP administration normalized the measured antioxidants in NaF intoxicated mice, showing its potential to restore antioxidant homeostasis.

4.12 In vivo antitumor activity of the AgNPs

4.12.1 Evaluation of the effect of CZAgNPs on Ascites Tumor model

     The lifespan of ascites tumor bearing animals induced by EAC cells was found to be increased by the CZAgNPs treatment. The control animals survived for a period of 23 days and all the animals were dead within 30th day. In the low dose treated groups the life span was increased to 41 days. In medium dose and high dose treated groups the life span was increased to 42 and 45 days. The standard drug cyclophosphamide treated group increased the life span to 43 days (Fig. 4.34). The percentage increase in life span of high dose, medium dose, low dose and standard was 95.65 %, 82.6 %, 78.26 %, 86.95 % respectively (Table 4.32).

Table 4.32 The inhibitory effect of CZAgNPs on ascites tumor development

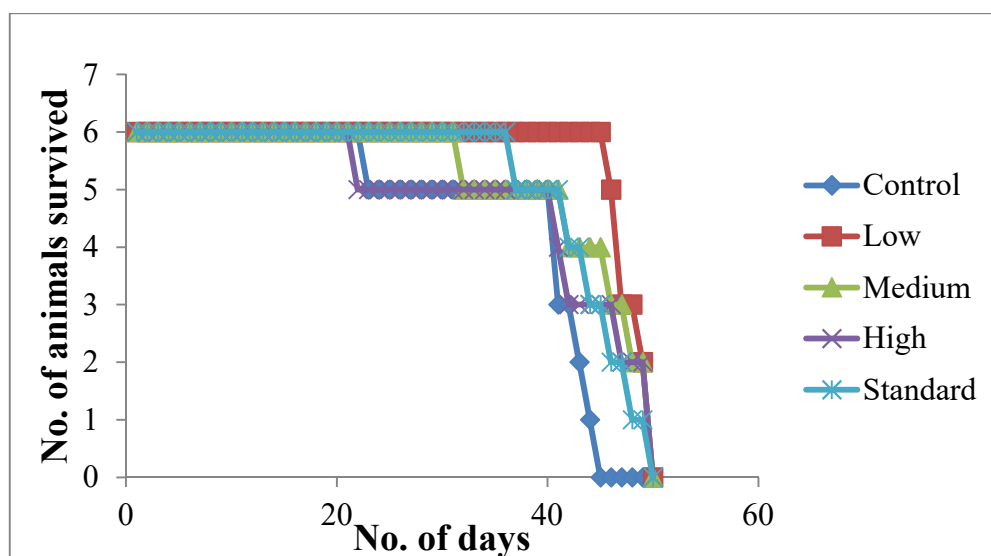| Group	Mean survival days	% ILS
Control	23	-------
Low	41	78.26
Medium	42	82.6
High	45	95.65
Standard	43	86.95

Fig. 4.34 Effect of CZAgNPs on EAC induced solid tumor development in Swiss albino mice

4.12.2 Evaluation of the effect of CZAgNPs on Solid Tumor model

A significant reduction in the volume of solid tumor was found in the group treated with high dose of CZAgNPs, when compared to the normal group. On the 30th day, the tumor volume of the control animals without any drug treatment (normal) was found to be 6.01 ± 3.3 cm^3. While in the high dose (75 mg / kg b. wt) of CZAgNPs treated animals, a significant ($p < 0.05$) reduction in volume (1.13 ± 1.57 cm^3) was observed. A percentage reduction of 81.26 % in the tumor volume was noticed in the group treated with high dose of CZAgNPs. The tumor volume of the medium and low dose was also found to be reduced, when compared to the control. The tumor volume observed was 1.65 ± 2.17 cm^3 and 1.30 ± 1.53 cm^3 respectively. The inhibition of tumor volume in the medium dose was 78.30 % and 72.60 % in the low dose treated groups. In cyclophosphamide (100 mg / kg b. wt) treated group the tumor volume was found to be 2.66 ± 1.96 cm^3 (Table 4.33). The observed results confirmed that the synthesized silver nanoparticles were comparatively more effective in reducing the solid tumor volume when compared to the standard drug cyclophosphamide (Fig. 4.35a, 4.35b, 4.35c).

Table 4.33 The inhibitory effect of CZAgNPs on solid tumor development

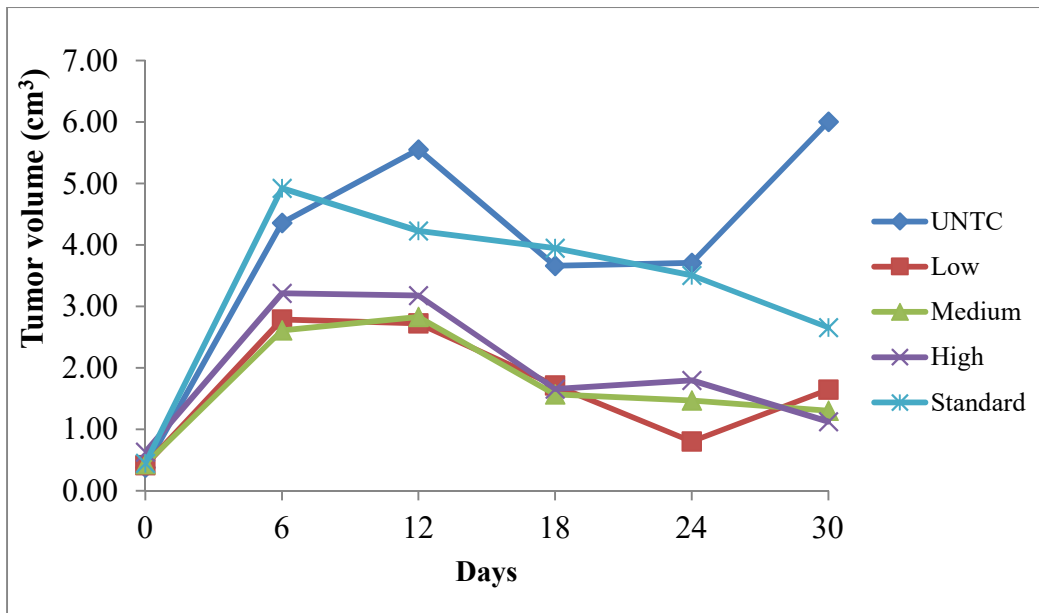| Group	Tumor volume on 30 th day (cm^3)	% inhibition
Control	6.01 ± 3.33	0
Low	1.65 ± 2.17*	72.60
Medium	1.30 ± 1.53**	78.30
High	1.13 ± 1.57**	81.26
Standard	2.66 ± 1.96	55.78

Fig. 4.35a Effect of CZAgNPs on DLA induced solid tumor development in Swiss albino mice (UNTC- untreated group)
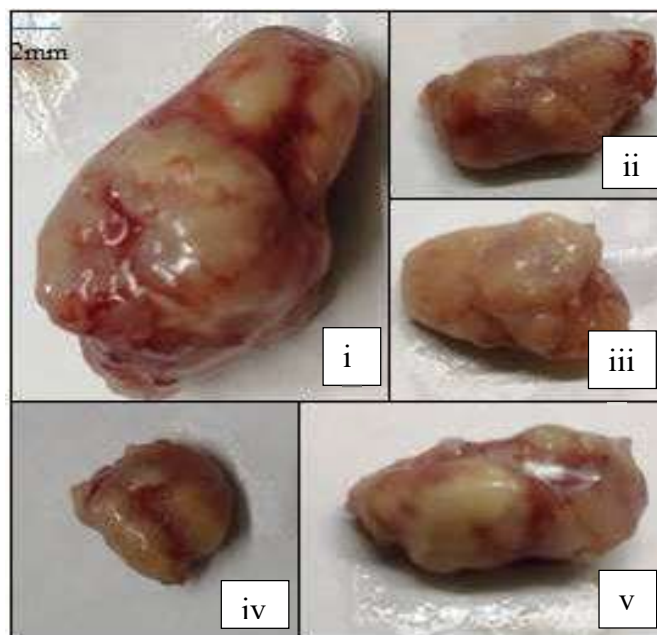

Fig. 4.35b Solid tumor excised from the mice treated with CZAgNPs (i) control, (ii) low dose, (iii) medium dose, (iv) high dose, (v) standard
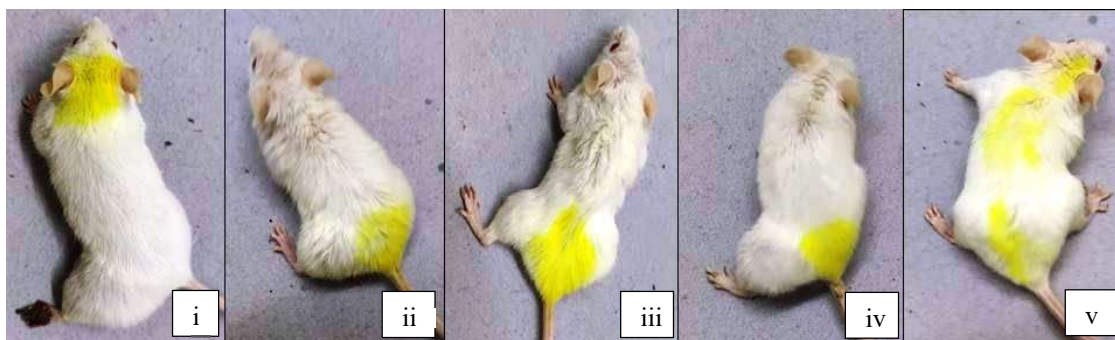
Fig. 4.35c Tumor development (Left limb) in DLA induced solid tumor in (i) control group animals, CZAgNPs administered animals (ii) low dose, (iii) medium dose, (iv) high dose and (v) standard

Antiangiogenic compounds are known for their ability to block the activity of abnormally expressed signaling proteins like Ras as well as cytokine based therapies, DNA-or protein based vaccines against specific tumor markers, and tyrosine kinase inhibitors with a consistent antitumor effect. AgNPs have been demonstrated to have angiogenic properties rendering them capable for research into their anticancer potential (Sriram, Barath, Kanth, Kalishwaralal, & Gurunathan, 2010).

In this study the potential of CZAgNPs in reducing the rapid growth and proliferation of both DLA and EAC tumor models were studied. EAC resembles human tumors, due to their rapid growth and aggressive behavior; they are more sensitive to chemotherapy. Ascitic fluid, constitutes the direct source of nutrition for tumor growth (Anand, Sumithira, Chinna Raja, Muthukumar, & Vidhya, 2013). In the present study, the untreated EAC tumor bearing mice showed increased ascites tumor volume and reduced survival (only for a period of 23 days) and all the animals in the group was found to be dead by the end of the experiment (30 days). While animals treated with CZAgNPs exhibited a dose dependent increase in the lifespan of EAC tumor bearing mice. The percentage of increase in the life span of EAC tumor bearing mice were 40 % (low dose), 56.66 % (medium dose) and 66.66 % (high dose). Animals in cyclophosphamide treated groups however lived up to 45 days with 50 % increase in lifespan of the tumor bearing animal. As per NCI criteria, the drug is

considered to be a potential antitumor candidate if the ILS exceeds 25 %. In the present study, all the CZAgNPs treated groups including low dose showed an ILS exceeding 25 % with the highest for high dose followed by medium dose and standard. The activity shown by the CZAgNPs at its higher dose executed higher efficacy than that of the standard cyclophosphamide treated animals which strongly suggests its anticancer potential.

A similar mode, an extent of antitumor efficacy was observed in DLA induced solid tumor model. DLA are poorly differentiated, malignant transplantable tumors originally seen in mouse as lymphocytes. The treatment with CZAgNPs decreased the volume of solid tumor in DLA bearing mice in a dose dependent manner. Following implantation of DLA cells to the left hind limb of mice, a dose dependent decrease in tumor volume by 72.60 %, 78.30 % and 81.26 % was observed respectively when administered CZAgNPs orally at concentrations 25 mg / kg b. wt, 50 mg / kg b. wt and 75 mg / kg b. wt in mice. The CZAgNPs exhibited strong antitumor potential which was evident from the comparison with cyclophosphamide administered animals in which the tumor volume was reduced only by 55.78 %.

The obtained results were corroborated with the previous reports suggesting the role of CZAgNPs as potential antitumor candidates (Ferreira *et al*., 2020; Jiang *et al*., 2021; Munawer *et al*., 2020). The criteria to be considered for any proposed anticancer drug is its efficiency in prolonging the life span of individuals and reducing the tumor volume and viable tumor cell count (Sriram *et al*., 2010). The silver nanoparticles serve as antitumor drugs by slowing down the progression of tumor cells. This could be owing to their inhibitory actions in numerous signaling cascades and by inducing apoptosis by activating the caspases 3 and 9 (Ullah *et al*., 2020).

Hence our findings demonstrate that the CZAgNPs can cause toxic effects in DLA and EAC tumor models, halting tumor formation and successfully managing disease progression without damage to normal cells.